

# Spin and helicity in structured waves for light and electrons

DISSERTATION

zur Erlangung des akademischen Grads  
Doctor rerum naturalium (Dr. rer. nat.)

dem Bereich der Mathematik und Naturwissenschaften der  
Technischen Universität Dresden vorgelegt

von

Koen Corstiaan van Kruining

geboren am 14.05.1988 in Amsterdam

Eingereicht am 29.10.2018

Eingereicht am 29.10.2018

Verteidigt am 17.05.2019

**Gutachter:**

Prof. Dr. M. Dennis  
(University of Birmingham)  
Prof. Dr. J-M. Rost  
(Max Planck Institut für Physik komplexer Systeme)  
Prof. Dr. W. Strunz  
(Technische Universität Dresden)

**Promotionskommission:**

Prof. Dr. K. Leo  
(Vorsitzender, Technische Universität Dresden)  
Prof. Dr. M. Dennis  
(University of Birmingham)  
Prof. Dr. H. Kantz  
(Max Planck Institut für Physik komplexer Systeme)  
Prof. Dr. J-M. Rost  
(Max Planck Institut für Physik komplexer Systeme)  
Prof. Dr. W. Strunz  
(Technische Universität Dresden)

Voor Lucas van Kruining (1953-2016), die mijn vroege interesse in de wetenschap heeft aangewakkerd en gekoesterd.



# Erklärung

Hiermit versichere ich daß ich die vorliegende Arbeit ohne unzulässige Hilfe Dritter und ohne Nutzung anderer als der angegebenen Hilfsmittel habe angefertigt. Die aus fremden Quellen direkt oder indirekt übernommene Gedanken sind als solche kenntlich gemacht. Die Arbeit wurde weder im Inland noch im Ausland in einer ähnlicher Form einer anderen Prüfungsbehörde vorgelegt.

Die Arbeit wurde am Max Planck Institut für Physik komplexer Systeme in der Abteilung 'endliche Systeme' unter Betreuung von Prof. Dr. Jan-Michael Rost angefertigt.

Ich erkenne die Promotionsordnung der Fakultät Mathematik und Naturwissenschaften der technische Universität Dresden von 23.02.2011 an.

Ort,                      Datum,                      Unterschrift  
Dresden



# Contents

<b>List of publications</b>	<b>3</b>
<b>Abstract</b>	<b>5</b>
<b>Introduction</b>	<b>7</b>
<b>I</b>	<b>13</b>
<b>1 Duality in media</b>	<b>15</b>
1.1 Vacuum Maxwell equations . . . . .	15
1.2 Duality symmetry in matter . . . . .	18
1.3 Properties of duality symmetric media . . . . .	21
1.4 Left- and right handed fields . . . . .	23
1.5 The feasibility of duality symmetric optics . . . . .	24
<b>2 Noninterfering superpositions</b>	<b>27</b>
2.1 Introduction . . . . .	27
2.2 Construction of noninterfering superpositions and their helicity properties	28
2.2.1 Interference cancellation . . . . .	28
2.2.2 Optical helicity and helicity lattices . . . . .	29
2.3 Explicit examples . . . . .	29
2.3.1 Two waves . . . . .	30
2.3.2 Three waves . . . . .	30
2.3.3 Four waves . . . . .	33
2.3.4 Five waves . . . . .	35
2.3.5 Six waves . . . . .	37
2.4 Small deviations . . . . .	39
2.4.1 Deviations in amplitude, phase and polarisation. . . . .	39
2.4.2 Deviations in the propagation direction . . . . .	40
2.4.3 Partially coherent light . . . . .	40
2.5 Recording helicity patterns with liquid crystals . . . . .	42
2.6 Mathematical remarks . . . . .	43
2.7 Conclusion . . . . .	43

<b>II</b>	<b>45</b>
<b>3 Electron vortices in a magnetic field</b>	<b>49</b>
3.1 Introduction . . . . .	49
3.2 Electron beams in a magnetic field . . . . .	52
3.3 Detailed analysis of the current structure . . . . .	55
3.4 Nonuniform spin . . . . .	59
3.5 The kinetic angular momentum operator . . . . .	60
3.6 Conclusion . . . . .	62
<b>4 Radiative spin polarisation</b>	<b>65</b>
4.1 Introduction . . . . .	65
4.2 Quantisation of the fields . . . . .	66
4.3 Analytical computation of the transition rates . . . . .	67
4.4 Numerical results . . . . .	71
4.5 Discussion . . . . .	75
4.6 Outlook . . . . .	77
<b>A Optical coherence and correlation functions</b>	<b>79</b>
A.1 Temporal coherence . . . . .	79
A.2 Spatial coherence . . . . .	82
<b>B Laguerre Gauß functions</b>	<b>85</b>
B.1 Associated Laguerre polynomials. . . . .	85
B.2 Laguerre-Gauß functions. . . . .	88
<b>C Integrating complex exponentials</b>	<b>93</b>
<b>D Kinematics of two-particle decay</b>	<b>95</b>
<b>E A two-population model for equilibration times</b>	<b>97</b>
<b>Summaries</b>	<b>99</b>
<b>Acknowledgements</b>	<b>109</b>
<b>Bibliography</b>	<b>111</b>



# List of publications

K. van Kruining & J. B. Götze; The conditions for the preservation of duality symmetry in a linear medium; *J. Opt* **18** 085601; 2016.

K. van Kruining, A. G. Hayrapetyan & J. B. Götze; Nonuniform currents and spins of relativistic electron vortices in a magnetic field; *Phys. Rev. Lett.* **119** 030401; 2017.

K. van Kruining, R. P. Cameron & J. B. Götze; Superpositions of up to six plane waves without electric-field interference; *Optica* **9** 1091-1098; 2018.

K. van Kruining, F. Mackenroth & J. B. Götze; Radiative spin polarization of twisted electrons in an ultrastrong magnetic field; submitted; arXiv:1809.02133; 2018.



# Abstract

This dissertation consists of two parts, connected by the overarching theme of the dynamics of structured waves with internal degrees of freedom. Part I concerns light, whose internal degree of freedom is polarisation. We investigate the helicity, or handedness of light, which is a good quantum number for massless fields in general and light in particular. In free space it is always possible to describe the light field in a basis left- and right handed helicity modes which are solutions of Maxwell's equations, regardless what spatial structure is chosen. This is useful for bases of highly inhomogeneous waves, such as Bessel waves, for which the spin cannot be unambiguously defined.

In chapter 1 we study the conservation of helicity and the preservation of its underlying symmetry, electric-magnetic duality symmetry when light travels through inhomogeneous and/or anisotropic media. We will discuss some of the unique properties of duality symmetric media and reformulate Maxwell's equations in such a way that the decoupling of different helicities for duality symmetric media becomes apparent. The feasibility of constructing duality symmetric media is discussed at the end of the chapter.

In chapter 2 we consider superpositions of plane electromagnetic waves in free space. Such superpositions typically interfere. We present superpositions of up to six plane waves which defy this expectation by having a perfectly homogeneous mean square of the electric field. Because most matter interacts much stronger with the electric than with the magnetic field, these superpositions can be considered noninterfering. Our superpositions show complex patterns in their helicity densities, of which we will show many examples. We study the effects on our helicity patterns of imperfections that may occur in a realistic experiment: deviations from the optimal amplitudes, phases and polarisations of the superposed waves, small misalignments and partially coherent light. Our superpositions can be used to write chiral patterns in light sensitive liquid crystals. Conversely, these liquid crystals can be used for an 'optical helicity camera' which records spatial variations in helicity. In the final paragraph of chapter 2 we discuss some mathematical questions concerning noninterfering superpositions.

Part II concerns electrons, whose internal degree of freedom is spin. In chapter 3 we will present analytical solutions of the Dirac equation for an electron vortex beam in a homogeneous magnetic field. Including spin from the beginning reveals that spin polarised electron vortex beams have a complicated azimuthal current structure, containing small rings of counterrotating current between rings of stronger corotating current. Contrary to many other problems in relativistic quantum mechanics, there exist vortex beam solutions with exactly zero spin-orbit mixing in the highly relativistic and nonparaxial regime.

Chapter 4 treats the interaction between electron vortex states in a homogeneous magnetic field and light, where we expand and quantise the radiation field in a basis of Bessel modes with definite helicity. Our results apply for magnetic field strength beyond the crit-

ical field strength at which the spin contributes as much to the electron's energy as its rest mass. We are able to compute spin flip rates for low lying states, finding a much higher degree of equilibrium spin polarisation than approximations for high lying electron states suggested.

# Introduction

This dissertation is concerned, in various ways, with the angular momentum of light and electrons. Although the concept of angular momentum dates back to Kepler's second law and is fairly familiar in Newtonian mechanics, for its use on classical and quantum fields, some less familiar concepts have to be introduced which I will do first here, along with some historical background.

Just as momentum can be considered 'the amount of motion in a certain direction', angular momentum can be considered 'the amount of rotation around a certain axis'. When considering a planet rotating around a star, a planet rotating around its axis or a molecule rotating around its axis, this colloquial definition can be quantified by introducing the moment of inertia. These are all examples of extrinsic or orbital angular momentum, that is, angular momentum due to the rotation of a scalar quantity. In all of the above cases, the rotation of mass. As all-encompassing as this definition for orbital angular momentum seems, it is not the only kind possible.

It was in 1909 that Poynting noticed that circularly polarised light could transfer angular momentum [1]. This is the first mention of an intrinsic angular momentum or spin, an angular momentum that stems from the rotation of an internal degree of freedom, for light polarisation. Thus the concept of spin is older than the quantisation of angular momentum. Poynting deduced the existence of light's spin from an analogy with a spinning shaft, but it can be understood better with a simple thought experiment. Electric dipoles tend to align themselves with the local electric field. As a circularly polarised light wave passes by, a dipole will try to follow the electric field which rotates, thus the electric dipole will start to rotate along with the field. Since a rotating dipole clearly possesses angular momentum this shows that a rotating electric field, and thereby circularly polarised light, can transfer angular momentum. By replacing the electric dipole by a magnetic dipole it follows that the spin of circularly polarised light can be transferred by the magnetic as well as the electric field, but because magnetic dipole moments are typically smaller than electric dipole moments, the electric transfer usually dominates.

The spin of light was first measured in 1936 by Richard Beth [2], using a birefringent plate hanging from a quartz fibre. The birefringent plate changes the polarisation of the light passing through it and the corresponding transfer of angular momentum results in a slight rotation of the plate.

The magnitude of the spin of light cannot exceed the magnitude of the spin of perfectly circularly polarised light. For monochromatic light this bound is  $\frac{\mathcal{E}}{\omega}$ . Quantising the light in photons with energy  $\mathcal{E}_\gamma = \hbar\omega$  this corresponds to a maximum spin of  $\hbar$  per photon.

Although orbital angular momentum is the older and more familiar concept and the existence of the spin of light was already proposed in 1909, it took until 1992 before the world came to know that a beam of light can carry orbital angular momentum [3]. It is open

for debate whether this discovery could have been made much earlier but had been overlooked or that only by the early '90s knowledge of physics and mathematics had evolved to the point where exploring this aspect of light was possible. There are arguments for both viewpoints. On the one hand, the separation of light's angular momentum into spin and orbital parts had been achieved in 1932 [4] and after observing the mechanical effect of spin in 1936 [2] it would have made sense to try to separately observe the orbital part as well. In 1974 Nye and Berry realised that any wave, including light, could have vortex like dislocations in its wave structure [5]. Around these vortices the momentum flows in circles. But since these vortices were seen as random defects in waves reflected off rough surfaces, the connection with orbital angular momentum was not made. Another opportunity for noticing the angular momentum of light arose in 1986 when Durnin introduced Bessel beams as diffraction free solutions of Helmholtz equation [6, 7]. By constructing a complete set of solutions rather than restricting himself to the physically more easily realisable zero angular momentum solutions and recognising that all solutions are physically relevant, he could have discovered the orbital angular momentum of light five years before anyone else.

There are also some relevant facts to nuance these missed opportunities. First, whereas the angular momentum of light is undoubtedly important in its emission, be it visible light emitted by an atom or radio waves emitted by an antenna, at the point of reception, approximating the light field as a plane wave usually suffices. Then there is the fact that two light beams carrying equal but opposite orbital angular momentum differ only in the phase structure of the light field, not in the intensity pattern, so they cannot be distinguished visually and laser cavities do not preferentially operate in one mode over the other.<sup>1</sup> But the most important argument against orbital angular momentum of light being discovered much earlier is that some essential parts of the 1992 article were at the time surprisingly novel. The mode converter, consisting of two cylindrical lenses, proposed to make light with orbital angular momentum was only described two years before in a peer reviewed publication [9] and the theoretical description of the mode converter for arbitrary modes requires a mathematical relation between Hermite-Gauß and Laguerre-Gauß functions that was only derived one year before [10].

Since their inception, orbital angular momentum light beams have been used for a wide range of purposes. There are optical spanners, devices similar to optical tweezers which can twist small transparent objects in addition to pulling them [11–14]. They can also be used to measure the rotation speed of an object via the Doppler shift of the scattered light [15–17]. STED Microscopes use them because the dark spot in the centre is well-suited for deexciting all but a few fluorescent molecules [18, 19] (First mention of the idea [20]), thereby beating the diffraction limit. When not beating the diffraction limit, vortex beams can be used for picturing the relief of microscopic samples [21–23]. In astronomy, adding a vortex to the light passing through a telescope can be used to eliminate the light from a bright star to see the dimmer objects around it [24, 25] and the angular momentum composition of the light from the accretion disc of a rotating black hole can be analysed to infer the black hole's rotation rate [26]. They have been proposed for high bandwidth communication, because every orbital angular momentum state adds an additional communication channel [27–36]. Finally, different angular momentum beams can be entangled and used to test Bell's and Leggett's inequality [37–40].

The above overview shows that different applications use different properties. Some

---

<sup>1</sup>Now that light with orbital angular momentum is a big research field, there are custom made laser cavities that do [8].

applications exploit the orbital angular momentum, whereas others exploit the fact that any beam with nonzero orbital angular momentum has a perfectly dark spot in its centre and others use the large number of different orbital angular momentum modes that exist.

The angular momentum beam is a generic feature of wave phenomena and is not restricted to light. The results achieved with laser beams can therefore be reproduced in other kinds of waves, often with similar methods. The second kind of wave that got used for making orbital angular momentum beams was ultrasound in water [41], with a transducer that functioned similar to a spiral phase plate for light (compare to [42]). After sound, electron beams gained orbital angular momentum. These beams are one of the main interests of this thesis.

Electrons are in many ways different from photons, they have mass, so they move slower than the speed of light and disperse as a consequence of a spread in momenta, they have an electric charge, so they are deflected by static electric and magnetic fields, whereas photons pass straight through, their number (minus the number of anti-electrons) is conserved whereas photons can be created and annihilated freely and no more than one electron can occupy the same quantum state whereas an arbitrary number of photons can. This last property rules out the possibility of an electron laser<sup>2</sup>.

Yet electrons obey a wave equation similar to the one light obeys, making it straightforward to infer the existence of electron beams carrying orbital angular momentum from this similarity [43]. In recent years, electron vortex beams were realised in the lab [44, 45] and the technology for making them has matured [46–53]. Uses for electron vortices have been proposed in nuclear and high energy physics [54–59], but any applications actually carried out are in the domain of electron microscopy [60–63] since a transmission electron microscope is the device used to make them.

Interestingly enough, solutions that can be considered electron vortex beams date back almost to the discovery of the Schrödinger and Dirac equations, although no relevance or use of their orbital angular momentum and central dark spot was recognised. The electron vortex beam in a magnetic field was one of the first exact solutions of the Dirac equation [64]. Landau obtained vortex solutions in a magnetic field when explaining diamagnetism [65].

Just as photons, electrons carry spin. Their spin is  $\frac{1}{2}\hbar$ , half the photon value. The internal degree of freedom associated with electron spin is called a spinor and it allows for four orthogonal states. Dirac recognised that because not all four states are physically allowed for electrons, spin and orbital angular momentum can only approximately separated. The reason is that when you have specified the electrons wave function, you are not free to choose the spin to be the same at every point due to the constraints [66]. For light something analogous occurs. Because light's polarisation is transverse, that is orthogonal to the local propagation direction, it is impossible to choose the same polarisation everywhere for an light field with an inhomogeneous intensity profile.

For light, it is possible to describe the polarisation in a way that is independent of the spatial structure using the helicity. Helicity is the spin along the local propagation direction and can be assigned independently of the spatial structure. It is only well defined for massless particles. The problem with the helicity of massive particles is that an observer moving faster than the particle observes the opposite helicity from an observer moving slower than the particle. This makes the helicity of a massive particle ambiguous. Since no observer can overtake a massless particle, this ambiguity does not occur in the massless

---

<sup>2</sup>A device that uses stimulated emission to produce a coherent beam of electrons, not to be confused with a free electron laser, a device that produces light from an electron beam.

case.

Fields having nonzero optical helicity are chiral, that is, not identical to their mirror images and the helicity is a measure for their ‘chirality’. When shone on molecules that are chiral as well, and many complex molecules including most building blocks of life are, the absorption rates and refractive indices can be different for the left and right handed helicity. The simplest light waves having nonzero helicity are circularly polarised waves and they have been a tool in chemical analysis since the nineteenth century [67]. Using light waves having a more complicated helicity structure has allowed more possibilities in this area of research, such as improved chirally selective absorption [68–70] and exerting chirally selective forces on molecules [71–73]. In spite of their usefulness light fields with a shaped helicity profile are a little explored area of research compared to light beams carrying orbital angular momentum.

This thesis is divided into two parts. Part I deals with the helicity of light and the symmetry responsible for its conservation. Part II focuses on electron vortex beams in a magnetic field. Light beams carrying orbital angular momentum play a small role in this part as a useful basis for expanding the electromagnetic field when studying the quantum electrodynamics of electron vortex beams.

## Used notation

Throughout this thesis a lot of different symbols will appear. Most have agreed upon meanings that can usually be inferred from their contexts, but for reference here a complete overview.

$\hat{a}^\dagger, \hat{a}$	Bosonic ladder operators
$A_\mu, A_0, \mathbf{A}, \tilde{\mathbf{A}}$	Four vector potential, its zeroth component (scalar potential), its spatial part, the complex vector potential.
$\mathbf{B}, \tilde{\mathbf{B}}$	Magnetic induction, the complex magnetic induction.
$c$	Speed of light, often set to 1
$c_\theta$	$\cos \theta$
$C_\mu, C_0, \mathbf{C}, \tilde{\mathbf{C}}$	Dual four vector potential, its zeroth component, its spatial part, the complex dual vector potential.
$\mathbf{D}, \tilde{\mathbf{D}}$	Electric displacement, The complex electric displacement.
$\mathcal{D}_\alpha$	Six component displacement vector $[\mathbf{D}, \mathbf{B}]$
$\delta(p - p')$	Dirac delta function
$\delta_{ij}$	Kronecker delta symbol
$\mathbf{E}, \tilde{\mathbf{E}}$	Electric field, the complex electric field.
$ e $	Magnitude of the electron charge
$\mathcal{E}$	Total energy of an electron or energy density
$\mathcal{E}_L$	Landau energy of the electron
$\mathcal{E}_Z$	Zeeman energy of the electron
$\eta_{\mu\nu}$	Minkowski metric
$\epsilon_0 \epsilon$	Vacuum permittivity, effective permittivity
$\mathbf{F}$	Force
$F_{\mu\nu}$	Electromagnetic field tensor
$\mathcal{F}_\alpha$	Six component field vector $[\mathbf{E}, \mathbf{H}]$



$G$	Chiral response
$\gamma$	Diracmatrix or Tellegen response (depending on context)
$\Gamma$	Decay rate
$g_t^{(1)}, g_s^{(1)}$	First order temporal and spatial autocorrelation functions
$\mathbf{H}, \tilde{\mathbf{H}}$	Magnetic field, the complex magnetic field.
$\mathcal{H}$	Helicity density
$\hbar$	Reduced Planck constant, often set to 1
$I_{nn'}^{ll'}(\boldsymbol{\kappa})$	$\int_0^\infty LG_n^l(\tilde{r}) LG_{n'}^{l'}(\tilde{r}) J_{l-l'}(\boldsymbol{\kappa}r) r dr$
$j$	Angular momentum quantum number
$j_\mu, j_0$ or $\rho, \mathbf{j}$	Four current, its zeroth component or (charge) density, current
$J_j$	Bessel function of the $j$ th order
$k$	Photon momentum along the z-axis
$\boldsymbol{\kappa}$	Transverse photon momentum. Can be seen as an effective mass.
$l$	orbital angular momentum quantum number.
$\ell$	Coherence length, $c\tau_c$
$L$	Length of normalisation volume
$L_n^{ l }$	Laguerre polynomial of order $n$ of the $ l $ th kind.
$LG_n^l(r, \phi)$	Laguerre-Gauß function $r^{ l } e^{-\frac{r^2}{2}} L_n^{ l }(r^2) e^{il\phi}$ .
$Lg_n^l(r)$	Radial part of the Laguerre-Gauß function $r^{ l } e^{-\frac{r^2}{2}} L_n^{ l }(r^2)$ .
$m$	Electron mass
$\mu_0, \mu$	Vacuum permeability, effective permeability
$\mu$	Effective electron mass $\mu = \sqrt{m^2 + \mathcal{E}_L^2 + \mathcal{E}_Z^2}$
$\mathcal{M}$	Transition matrix element
$n$	Radial quantum number
$N$	Landau level $N = \frac{1}{2}(2n +  l  + l + 1 + 2\sigma)$
$\mathcal{N}$	Transverse normalisation
$\omega$	Frequency or photon energy (when using $\hbar = 1$ )
$p$	Momentum of electron along the z-axis
$\hat{\pi}^\dagger, \hat{\pi}$	Fermionic ladder operators
$P_\mu$	gauge covariant four momentum, $P_\mu = p_\mu - eA_\mu$
$\phi$	azimuthal coordinate
$\vec{\Phi}_{\mathcal{H}}$	Helicity flux
$\psi$	Scalar wave function
$\Psi$	Bispinor wave function
$r$	Radial coordinate
$\tilde{r}$	Rescaled radial coordinate $\tilde{r} = \sqrt{ e B/2}r$
$R$	Radius of normalisation volume
$S$	Scattering matrix
$\mathbf{S}$	Poynting vector
$s_\theta$	$\sin \theta$
$\sigma_{ij}$	Maxwell stress tensor
$\sigma$	Spin quantum number
$t$	Time coordinate
$\tau$	Time interval

$\tau_c$	Coherence time
$u$	Constant Bispinor
$V_{\mu\nu\rho\sigma}, V_{ijkl}$	Indices running from 0 to 3, indices running from 1 to 3
$V_{[\mu\nu]}, V_{\{\mu\nu\}}$	Antisymmetrised indices $V_{[\mu\nu]} = V_{\mu\nu} - V_{\nu\mu}$ , symmetrised indices $V_{\{\mu\nu\}} = V_{\mu\nu} + V_{\nu\mu}$
$Z$	Optical impedance, $\sqrt{\epsilon^{-1}\mu}$

# **Part I**



# Chapter 1

## Electric-magnetic duality symmetry in linear media.

### 1.1 Duality symmetry, helicity and spin for the source free Maxwell equations.

All of classical optics follows from only four coupled partial differential equations [74, 75]:

$$\begin{aligned}\nabla \cdot \epsilon_0 \mathbf{E} &= \rho & \nabla \times \mathbf{E} &= -\mu_0 \dot{\mathbf{H}}, \\ \nabla \cdot \mu_0 \mathbf{H} &= 0 & \nabla \times \mathbf{H} &= \epsilon_0 \dot{\mathbf{E}} + \mathbf{j}.\end{aligned}\quad (1.1)$$

These are Maxwell's equations. In these equations  $\mathbf{E}$  is the electric field,  $\mathbf{H}$  is the magnetic field,  $\rho$  and  $\mathbf{j}$  are the electric charge density and current and  $\epsilon_0$  and  $\mu_0$  are the vacuum permittivity and permeability, coupling constants that indicate how strong the interaction between electric charges and the electromagnetic field is. The speed of light is determined by the vacuum permittivity and permeability as  $\sqrt{\epsilon_0 \mu_0} = \frac{1}{c}$ . Together with the Lorentz force law  $\mathbf{F} = q(\mathbf{E} + \mathbf{v} \times \mathbf{B})$  Maxwell's equations also describe all of classical electromagnetism.

If one assumes an absence of any electric charges and currents, the first pair of Maxwell's equations has the same form as the second pair, suggesting there exists an interchangeability between the electric and the magnetic field. This interchangeability has been studied in quite some detail [76–81]. The source free Maxwell equations are invariant under a continuous rotation of the electric and magnetic fields among each other [76] (using shorthands for the sines and cosines).

$$\mathbf{E} \rightarrow c_\theta \mathbf{E} + s_\theta \sqrt{\frac{\mu_0}{\epsilon_0}} \mathbf{H}, \quad \mathbf{H} \rightarrow c_\theta \mathbf{H} - s_\theta \sqrt{\frac{\epsilon_0}{\mu_0}} \mathbf{E} \quad (1.2)$$

Applying this transformation to a light wave amounts to an actual rotation of the electric and magnetic fields around an axis locally perpendicular to both, hence it is called the electric magnetic duality rotation or shortly duality rotation. The energy density of the electric field is invariant under duality transformations, as are the momentum given by the

Poynting vector and the momentum flux given by the Maxwell stress tensor

$$\begin{aligned}
\mathcal{E} &= \frac{\varepsilon_0 \mathbf{E} \cdot \mathbf{E} + \mu_0 \mathbf{H} \cdot \mathbf{H}}{2} \rightarrow \\
&\quad \frac{\varepsilon_0}{2} \left( c_\theta \mathbf{E} + s_\theta \sqrt{\frac{\mu_0}{\varepsilon_0}} \mathbf{H} \right) \cdot \left( c_\theta \mathbf{E} + s_\theta \sqrt{\frac{\mu_0}{\varepsilon_0}} \mathbf{H} \right) \\
&\quad + \frac{\mu_0}{2} \left( c_\theta \mathbf{H} - s_\theta \sqrt{\frac{\varepsilon_0}{\mu_0}} \mathbf{E} \right) \cdot \left( c_\theta \mathbf{H} - s_\theta \sqrt{\frac{\varepsilon_0}{\mu_0}} \mathbf{E} \right) \\
&= \frac{c_\theta^2 + s_\theta^2}{2} (\varepsilon_0 \mathbf{E} \cdot \mathbf{E} + \mu_0 \mathbf{H} \cdot \mathbf{H}) + s_\theta c_\theta \sqrt{\varepsilon_0 \mu_0} (\mathbf{E} \cdot \mathbf{H} - \mathbf{E} \cdot \mathbf{H}) = \frac{\varepsilon_0 \mathbf{E} \cdot \mathbf{E} + \mu_0 \mathbf{H} \cdot \mathbf{H}}{2}, \quad (1.3)
\end{aligned}$$

$$\begin{aligned}
\mathbf{S} &= \mathbf{E} \times \mathbf{H} \rightarrow \left( c_\theta \mathbf{E} + s_\theta \sqrt{\frac{\mu_0}{\varepsilon_0}} \mathbf{H} \right) \times \left( c_\theta \mathbf{H} - s_\theta \sqrt{\frac{\varepsilon_0}{\mu_0}} \mathbf{E} \right) \\
&= c_\theta^2 \mathbf{E} \times \mathbf{H} - s_\theta^2 \mathbf{H} \times \mathbf{E} + c_\theta s_\theta \left( \sqrt{\frac{\mu_0}{\varepsilon_0}} \mathbf{H} \times \mathbf{H} - \sqrt{\frac{\varepsilon_0}{\mu_0}} \mathbf{E} \times \mathbf{E} \right) = \mathbf{E} \times \mathbf{H}, \quad (1.4)
\end{aligned}$$

$$\begin{aligned}
\sigma_{ij} &= \varepsilon_0 E_i E_j + \mu_0 H_i H_j - \delta_{ij} \mathcal{E} \rightarrow \\
&\quad \varepsilon_0 \left( c_\theta E_i + s_\theta \sqrt{\frac{\mu_0}{\varepsilon_0}} H_i \right) \left( c_\theta E_j + s_\theta \sqrt{\frac{\mu_0}{\varepsilon_0}} H_j \right) \\
&\quad + \mu_0 \left( c_\theta H_i - s_\theta \sqrt{\frac{\varepsilon_0}{\mu_0}} E_i \right) \left( c_\theta H_j - s_\theta \sqrt{\frac{\varepsilon_0}{\mu_0}} E_j \right) - \delta_{ij} \mathcal{E} \\
&= (c_\theta^2 + s_\theta^2) (\varepsilon_0 E_i E_j + \mu_0 H_i H_j) + c_\theta s_\theta \sqrt{\varepsilon_0 \mu_0} (E_i H_j + H_i E_j - H_i E_j - E_i H_j) - \delta_{ij} \mathcal{E} \\
&\quad = \varepsilon_0 E_i E_j + \mu_0 H_i H_j - \delta_{ij} \mathcal{E}. \quad (1.5)
\end{aligned}$$

The angular momentum density of the electromagnetic field is duality invariant too because it is a part of the angular momentum tensor  $M_{\mu\nu\rho} = x_{[\mu} T_{\nu]\rho}$  [82] with  $T_{\nu\rho}$  the energy momentum tensor whose elements are the energy density, Poynting vector and Maxwell stress tensor, all of which are duality invariant.

Noethers theorem [83, 84] states that the existence of a continuous symmetry implies the existence of a conserved quantity. The conserved quantity implied by duality symmetry cannot be constructed from their field strengths, the coordinate four vector and partial derivatives with respect to the coordinates. Instead it contains the vector potential  $(A_0, \mathbf{A})$  and the dual vector potential  $(C_0, \mathbf{C})$ . It is well known that electrodynamics can alternatively be described using the vector potential and the definitions  $\mathbf{E} = -\nabla A_0 - \dot{\mathbf{A}}$  and  $\mu_0 \mathbf{H} = \nabla \times \mathbf{A}$ . From these definitions one obtains two of Maxwell's equations

$$\nabla \cdot \mu_0 \mathbf{H} = \nabla \cdot \nabla \times \mathbf{A} = 0 \quad \text{and} \quad \nabla \times \mathbf{E} = -\nabla \times (\nabla A_0 + \dot{\mathbf{A}}) = -\mu_0 \dot{\mathbf{H}}. \quad (1.6)$$

In the absence of electric charges and currents it is possible to use the dual vector potential defining  $\mathbf{H} = -\nabla C_0 - \dot{\mathbf{C}}$  and  $\varepsilon_0 \mathbf{E} = -\nabla \times \mathbf{C}$ . These definitions yield the other two Maxwell equations. With these vector potentials, the helicity density  $\mathcal{H}$  and flux  $\vec{\Phi}_{\mathcal{H}}$  are [77, 78, 80, 81]

$$\begin{aligned}
\mathcal{H} &= \frac{1}{2} \sqrt{\varepsilon_0 \mu_0} (\mathbf{A} \cdot \mathbf{H} - \mathbf{C} \cdot \mathbf{E}), \\
\vec{\Phi}_{\mathcal{H}} &= \frac{1}{2} \left( \sqrt{\frac{\varepsilon_0}{\mu_0}} \mathbf{E} \times \mathbf{A} + \sqrt{\varepsilon_0 \mu_0} \mathbf{H} A_0 + \sqrt{\frac{\mu_0}{\varepsilon_0}} \mathbf{H} \times \mathbf{C} - \sqrt{\varepsilon_0 \mu_0} \mathbf{E} C_0 \right). \quad (1.7)
\end{aligned}$$

Together they obey the conservation law  $\dot{\mathcal{H}} + \nabla \cdot \vec{\Phi}_{\mathcal{H}} = 0$ .

$$\begin{aligned}\dot{\mathcal{H}} &= \frac{1}{2} \sqrt{\varepsilon_0 \mu_0} \left( (-\mathbf{E} - \nabla A_0) \cdot \mathbf{H} + \mathbf{A} \cdot \dot{\mathbf{H}} + (\mathbf{H} + \nabla C_0) \cdot \mathbf{E} - \mathbf{C} \cdot \dot{\mathbf{E}} \right), \\ \nabla \cdot \vec{\Phi}_{\mathcal{H}} &= \frac{1}{2} \left( \sqrt{\frac{\varepsilon_0}{\mu_0}} (\mathbf{A} \cdot \nabla \times \mathbf{E} - \mathbf{E} \cdot \nabla \times \mathbf{A}) + \sqrt{\varepsilon_0 \mu_0} \mathbf{E} \cdot \nabla A_0 \right) \\ &\quad + \frac{1}{2} \left( \sqrt{\frac{\mu_0}{\varepsilon_0}} (\mathbf{C} \cdot \nabla \times \mathbf{H} - \mathbf{H} \cdot \nabla \times \mathbf{C}) - \sqrt{\varepsilon_0 \mu_0} \mathbf{E} \cdot \nabla C_0 \right) \\ &= \frac{1}{2} \sqrt{\varepsilon_0 \mu_0} (-\mathbf{A} \cdot \dot{\mathbf{H}} - \mathbf{E} \cdot \mathbf{H} + \mathbf{E} \cdot \nabla A_0 + \mathbf{C} \cdot \dot{\mathbf{E}} + \mathbf{H} \cdot \mathbf{E} - \mathbf{E} \cdot \nabla C_0).\end{aligned}\tag{1.8}$$

Due to the explicit appearance of the vector potentials the helicity density is not locally gauge invariant. The total helicity is however if one assumes that the field strength goes to zero at infinity. The helicity as stated above is related to the magnetic helicity  $\mathbf{A} \cdot \mathbf{B}$  [85–87], which looks like a non duality symmetric version of the optical helicity. The magnetic helicity is also a conserved quantity, but under completely different assumptions, namely assuming perfect conductivity. It is an irony of scientific history that of all conserved quantities of charge and current free electrodynamics helicity is the one that was formulated in a duality violating form first and quite a miracle that two completely different assumptions (perfect conductivity vs. no electric currents and charges) can lead to such similar conservation laws.

The helicity density is a measure for the local handedness of light. It is a time even, parity odd scalar density<sup>1</sup>. For linearly polarised light the helicity density is zero and it is, for a given energy density  $\mathcal{E}$  extremal for circularly polarised light. For monochromatic light there is an upper limit to the time averaged helicity density if one chooses the gauge  $A_0 = C_0 = \nabla \cdot \mathbf{A} = \nabla \cdot \mathbf{C} = 0$  wherein there is a direct proportionality between the vector potentials and the fields. This upper limit can best be shown a complex representation for monochromatic light  $\mathbf{E} = \text{Re}(\tilde{\mathbf{E}}e^{-i\omega t})$  (and likewise for other fields and vector potentials). The time average of any quantity quadratic in the fields is one half of the scalar product of the complex amplitudes, because the mean square of the cosine is  $\frac{1}{2}$ . Using the complex representation we find:

$$\begin{aligned}|\mathcal{H}| &= \frac{\sqrt{\varepsilon_0 \mu_0}}{4} |\tilde{\mathbf{A}}^* \cdot \tilde{\mathbf{H}} - \tilde{\mathbf{C}}^* \cdot \tilde{\mathbf{E}}| = \frac{\sqrt{\varepsilon_0 \mu_0}}{4\omega} |i(\tilde{\mathbf{E}}^* \cdot \tilde{\mathbf{H}} - \tilde{\mathbf{H}}^* \cdot \tilde{\mathbf{E}})| = \frac{\sqrt{\varepsilon_0 \mu_0}}{2\omega} |\text{Im}(\tilde{\mathbf{E}}^* \cdot \tilde{\mathbf{H}})| \\ &\leq \frac{\varepsilon_0 \tilde{\mathbf{E}} \cdot \tilde{\mathbf{E}}^* + \mu_0 \tilde{\mathbf{H}} \cdot \tilde{\mathbf{H}}^*}{4\omega} = \frac{\mathcal{E}}{\omega},\end{aligned}\tag{1.9}$$

where in the last step I used  $(\sqrt{\varepsilon_0} \tilde{\mathbf{E}} + \sqrt{\mu_0} \tilde{\mathbf{H}}) \cdot (\sqrt{\varepsilon_0} \tilde{\mathbf{E}} + \sqrt{\mu_0} \tilde{\mathbf{H}})^* \geq 0$ . Considering the light field to consist of photons with energy  $\hbar\omega$ , this amounts to light having a helicity between  $\pm\hbar$  per photon, allowing the helicity to be written as  $\hbar$  times the difference between the number of right and left handed circularly polarised photons, the form in which it was first recognised in optics [76].

For a plane wave, the helicity is equivalent to the spin along the propagation direction and both can be used to describe the degree of circular polarisation of the light. For nonparaxial light fields, that are, light fields built up from plane wave components pointing in wildly different directions, helicity has the advantage that it can be unambiguously

<sup>1</sup> Compare: your left hand remains the same under time reversal, but turns into a different object (your right hand) under parity.

defined whereas it may not be possible to find a useful axis along which to define spin. This advantage becomes useful when when expanding the electromagnetic field in a set of basis modes other than plane waves. Regardless what modes one can in free space always choose left handed helicity and right handed helicity as basis polarisations. I will use this advantage in part II.

## 1.2 Continuum electrodynamics and duality symmetry in matter

The presence of a single electron suffices to break duality symmetry. This is unfortunate because for nearly every application in optics light has to pass through some form of matter, even when one discounts the presence Earths atmosphere, and duality symmetry is fundamentally violated. The transfer of helicity from the electromagnetic field to matter has been studied [88], but for matter there exists no conserved helicity, so it is impossible to construct a total helicity.

But typically free charges do not occur and for nonconductive materials, free currents do not exist either and charges tend to get only redistributed within a single molecule. For visible light (and electromagnetic radiation of lower frequencies) the wavelength is much longer than the size of a molecule and the small scale charge and current distribution can be well described by a space averaged polarisation and magnetisation. This allows the microscopic Maxwell equations to be approximated well by an effective continuum theory that is well understood [74, 75, 89, 90]. Then similar to the vacuum Maxwell equations, the invariance of the continuum theory under (a modified) duality symmetry can be investigated. Fernandez-Corbaton et. al. found the conditions for duality symmetry in linear, isotropic, achiral media [91], but these conditions are not typically satisfied for real world materials. In this chapter we relax their constraints to derive a broader set of conditions under which duality symmetry is preserved in matter. We will start with a derivation of Maxwell's equations in matter, because we include some parameters that are usually omitted from textbooks because they are small or equal to zero for most materials.

Separating the magnetic field in a free part,  $\mathbf{H}_f$  and an induced magnetisation  $\mathbf{M}$  and writing the charges in terms of the induced polarisation  $\mathbf{P}$  gives the equations

$$\begin{aligned} \nabla \cdot \epsilon_0 \mathbf{E} &= -\nabla \cdot \mathbf{P} & \nabla \times \mathbf{E} &= -\mu_0(\dot{\mathbf{H}}_f + \dot{\mathbf{M}}), \\ \nabla \cdot \mu_0(\mathbf{H}_f + \mathbf{M}) &= 0 & \nabla \times (\mathbf{H}_f + \mathbf{M}) &= \epsilon_0 \dot{\mathbf{E}} + \dot{\mathbf{P}} + \nabla \times \mathbf{M}. \end{aligned} \quad (1.10)$$

With  $\nabla \times \mathbf{M}$  the induced magnetisation current. Introducing the magnetic flux  $\mathbf{B} \equiv \mu_0(\mathbf{H}_f + \mathbf{M})$  and the electric displacement  $\mathbf{D} \equiv \epsilon_0 \mathbf{E} + \mathbf{P}$  and dropping the  $f$ -index for simplicity yield the general form of Maxwell's equations in nonconductive matter

$$\begin{aligned} \nabla \cdot \mathbf{D} &= 0 & \nabla \times \mathbf{E} &= -\dot{\mathbf{B}}, \\ \nabla \cdot \mathbf{B} &= 0 & \nabla \times \mathbf{H} &= \dot{\mathbf{D}}. \end{aligned} \quad (1.11)$$

Within this model the vector potentials are still helpful tools and are defined via

$$\begin{aligned} -\dot{\mathbf{A}} - \nabla A_0 &= \mathbf{E} & -\dot{\mathbf{C}} - \nabla C_0 &= \mathbf{H}, \\ \nabla \times \mathbf{A} &= \mathbf{B} & -\nabla \times \mathbf{C} &= \mathbf{D}. \end{aligned} \quad (1.12)$$



The properties of the medium under consideration determine  $\mathbf{P}$  and  $\mathbf{M}$  and thereby the relation between the fields  $\mathbf{E}$  and  $\mathbf{H}$  on the one hand and the displacement and flux,  $\mathbf{D}$  and  $\mathbf{B}$  on the other hand. We will restrict ourselves to the assumption that the induced polarisation and magnetisation are linear in the fields. Under these assumptions, the most general relation between the fields is [92]:

$$\begin{bmatrix} \tilde{\mathbf{D}} \\ \tilde{\mathbf{B}} \end{bmatrix} = \hat{R} \begin{bmatrix} \tilde{\mathbf{E}} \\ \tilde{\mathbf{H}} \end{bmatrix}, \quad \hat{R} = \begin{bmatrix} \varepsilon(\mathbf{x}; \omega) & -iG(\mathbf{x}; \omega) + \gamma(\mathbf{x}; \omega) \\ iG(\mathbf{x}; \omega) + \gamma(\mathbf{x}; \omega) & \mu(\mathbf{x}; \omega) \end{bmatrix}. \quad (1.13)$$

The entries  $\varepsilon$  and  $\mu$  are the modified permittivity and permeability of the medium,  $G$  is the chiral response present in optically active media and  $\gamma$  is the magneto-electric response, proposed by Tellegen [93] when he hypothesised a new electronic circuit component and later verified to exist [94–97]. If a medium is inhomogeneous, these medium parameters are position dependent and at sharp interfaces (like an air-glass interface) they are discontinuous. For isotropic media, these four parameters are numbers, but anisotropic media can be described to by considering these parameters to be  $3 \times 3$  matrices. The only restrictions imposed on  $\hat{R}$  is that it is invertible and independent of the fields. If there is no gain or absorption,  $\hat{R}$  is hermitian. The continuum Maxwell equations are usually written using  $\tilde{\mathbf{E}}, \tilde{\mathbf{H}}, \tilde{\mathbf{D}}$  and  $\tilde{\mathbf{B}}$ , but using  $\hat{R}$ , two can be eliminated. Keeping only  $\tilde{\mathbf{D}}$  and  $\tilde{\mathbf{B}}$ , Maxwell's equations become in matrix form

$$\begin{aligned} & \begin{bmatrix} \partial_x & \partial_y & \partial_z & 0 & 0 & 0 \\ 0 & 0 & 0 & \partial_x & \partial_y & \partial_z \end{bmatrix} \begin{bmatrix} \tilde{\mathbf{D}} \\ \tilde{\mathbf{B}} \end{bmatrix} = 0, \\ & \begin{bmatrix} \nabla \times & 0 \\ 0 & \nabla \times \end{bmatrix} \begin{bmatrix} 0 & I \\ -I & 0 \end{bmatrix} \hat{R}^{-1} \begin{bmatrix} \tilde{\mathbf{D}} \\ \tilde{\mathbf{B}} \end{bmatrix} = -i\omega \begin{bmatrix} \tilde{\mathbf{D}} \\ \tilde{\mathbf{B}} \end{bmatrix}, \end{aligned} \quad (1.14)$$

It is obvious that any linear combination of  $\tilde{\mathbf{D}}$  and  $\tilde{\mathbf{B}}$  obeys the divergence laws, so a good ansatz to make for the generalised duality transformation is

$$\begin{bmatrix} \mathbf{D} \\ \mathbf{B} \end{bmatrix} \rightarrow \begin{bmatrix} c_\theta & -Z^{-1}s_\theta \\ Zs_\theta & c_\theta \end{bmatrix} \begin{bmatrix} \mathbf{D} \\ \mathbf{B} \end{bmatrix}, \quad (1.15)$$

with  $Z = \sqrt{\varepsilon^{-1}\mu}$ , the optical impedance, which we assume to be a number (this assumption will prove to be correct). The duality rotation matrix commutes with the time derivative and with the curl operator. Thus the condition for duality symmetry becomes

$$\left[ \begin{bmatrix} c_\theta & -Z^{-1}s_\theta \\ Zs_\theta & c_\theta \end{bmatrix}, \begin{bmatrix} 0 & I \\ -I & 0 \end{bmatrix} \hat{R}^{-1} \right] = 0. \quad (1.16)$$

Using the commutator identity  $[A, B^{-1}] = B^{-1}[B, A]B^{-1}$  and evaluating the commutator explicitly leads to the following conditions for duality symmetry and determines  $\alpha$

$$\begin{aligned} \gamma(\mathbf{x}; \omega) &= 0, \\ \varepsilon(\mathbf{x}; \omega) &\propto \mu(\mathbf{x}; \omega), \\ G(\mathbf{x}; \omega) &= \text{free}. \end{aligned} \quad (1.17)$$

Where the proportionality applies to both the position dependence and the matrix structure.

The commutator identity used to derive duality symmetry does not only work for  $\hat{R}$  being a matrix, it works for any linear invertible operator. This makes it possible to generalise the above result to media with a nonlocal linear response. In a nonlocal medium, the

polarisation and magnetisation at point  $\mathbf{x}$  do not only depend on the fields in  $\mathbf{x}$ , but, due to interactions between neighbouring atoms, on the fields in the surroundings of  $\mathbf{x}$  as well. A linear nonlocal medium can be described by replacing the elements of  $\hat{R}$  with integral kernels [90].

$$\mathcal{D}_\alpha(\mathbf{x}; \omega) = \int R_{\alpha\beta}(\mathbf{x}, \mathbf{x}'; \omega) \mathcal{F}_\beta(\mathbf{x}'; \omega) dV'. \quad (1.18)$$

Here  $\mathcal{D}_\alpha$  is one of the components of the six component  $(\tilde{\mathbf{D}}, \tilde{\mathbf{B}})$  vector and  $\mathcal{F}_\alpha$  is one of the components of the six component  $(\tilde{\mathbf{E}}, \tilde{\mathbf{H}})$  vector, the indices  $\alpha$  and  $\beta$  run from 1 to 6 and we adopt the usual convention of summing over doubly occurring indices. These integral transforms are linear, so as long as they are invertible as well, the same conditions for duality symmetry still apply. The caveat here is to find out if all integral kernels are invertible. If  $R_{\alpha\beta}$  only depends on  $\mathbf{x} - \mathbf{x}'$ , as is the case for homogeneous nonlocal media, invertibility can be checked by Fourier transforming.

If the medium properties vary with time, like in acoust-optic modulators, an approach similar to the one for nonlocal media can be used [90]. Working in the time domain instead of in the frequency domain, one can introduce time dependent complex fields via the Fourier transform,  $\mathcal{F}(\mathbf{x}, t) = \int \mathcal{F}(\mathbf{x}, \omega) e^{-i\omega t} d\omega$ . The elements of the response matrix for stationary media is given by

$$\mathcal{D}_\alpha(\mathbf{x}, t) = \int \int_{-\infty}^{t - \frac{|\mathbf{x} - \mathbf{x}'|}{c}} R_{\alpha\beta}(\mathbf{x}, \mathbf{x}', t - t') \mathcal{F}_\beta(\mathbf{x}', t') dt' dV'. \quad (1.19)$$

Time varying medium properties can be included by allowing for other time dependences than  $t - t'$  in the response matrix and the conditions for duality symmetry become.

$$\begin{aligned} \gamma(\mathbf{x}, \mathbf{x}', t, t') &= 0, \\ \varepsilon(\mathbf{x}, \mathbf{x}', t, t') &\propto \mu(\mathbf{x}, \mathbf{x}', t, t'), \\ G(\mathbf{x}, \mathbf{x}', t, t') &= \text{free}. \end{aligned} \quad (1.20)$$

Where each entry is a  $3 \times 3$  matrix of integral operators. An important difference between the stationary and the nonstationary case is that in the stationary case one can assume to be working with monochromatic light and require duality symmetry to hold only for the frequency of interest whereas in the nonstationary case the frequency of light can change and duality symmetry must apply broadband.

Whenever duality symmetry applies in a medium, there should exist a generalised helicity density and flux which obey the conservation law  $\dot{\mathcal{H}} + \nabla \cdot \vec{\Phi}_{\mathcal{H}} = 0$  and reduce to the vacuum helicity density and flux if all parameters in  $\hat{R}$  are set to their vacuum values. Using complex fields in the time domain, defined via  $\tilde{\mathbf{E}} = \int \tilde{\mathbf{E}}_\omega e^{-i\omega t} d\omega$  (and likewise for the other fields and vector potentials), we propose to generalise these quantities in a linear medium in the following way:

$$\begin{aligned} \mathcal{H} &= \frac{1}{4} (Z^{-1} \tilde{\mathbf{A}}^* \cdot \tilde{\mathbf{B}} - Z \tilde{\mathbf{C}}^* \cdot \tilde{\mathbf{D}}), \\ \vec{\Phi}_{\mathcal{H}} &= \frac{1}{4} (Z^{-1} \tilde{\mathbf{E}} \times \tilde{\mathbf{A}}^* + Z^{-1} A_0^* \tilde{\mathbf{B}} + Z \tilde{\mathbf{H}} \times \tilde{\mathbf{C}}^* + Z C_0^* \tilde{\mathbf{D}}). \end{aligned} \quad (1.21)$$

The only addition made compared to previous works [77–81, 98] are the prefactors  $Z^{-1}$  and  $Z$ . Substituting these expressions into the continuity equations and using Maxwell's equations yields

$$\frac{d\mathcal{H}}{dt} + \nabla \cdot \vec{\Phi}_{\mathcal{H}} = -\frac{1}{2} \text{Re}(Z^{-1} \tilde{\mathbf{E}}^* \cdot \tilde{\mathbf{B}}) + \frac{1}{2} \text{Re}(Z \tilde{\mathbf{H}}^* \cdot \tilde{\mathbf{D}}). \quad (1.22)$$

Now assuming duality symmetry,  $\tilde{\mathbf{B}} = Z^2 \varepsilon \tilde{\mathbf{H}} + iG\tilde{\mathbf{E}}$  and  $\tilde{\mathbf{D}} = \varepsilon \tilde{\mathbf{E}} - iG\tilde{\mathbf{H}}$ . Assuming hermiticity of  $\hat{K}$ ,  $\varepsilon, \mu$  and  $G$  are Hermitian operators, expanding  $\tilde{\mathbf{H}}$  in the eigenvectors of  $Z\varepsilon$  with eigenvalues  $\lambda_j$  yields

$$\frac{d\mathcal{H}}{dt} + \nabla \cdot \vec{\Phi}_{\mathcal{H}} = \text{Re} \left( \sum_j \lambda_j \tilde{\mathbf{H}}_j^* \cdot \tilde{\mathbf{E}} - \tilde{\mathbf{E}}^* \cdot \sum_j \lambda_j \tilde{\mathbf{H}}_j \right) - \text{Re}(Z^{-1} \tilde{\mathbf{E}}^* \cdot iG\tilde{\mathbf{E}} + Z\tilde{\mathbf{H}}^* \cdot iG\tilde{\mathbf{H}}) = 0. \quad (1.23)$$

This shows that our helicity is indeed locally conserved if the medium is duality symmetric and if there is no gain or absorption. If one is interested in quasi-monochromatic light it is useful to separate the fields in a rapidly oscillating phase and a slowly varying envelope:  $\tilde{\mathbf{E}}(t)e^{-i\omega_0 t}$  etc., and to write the helicity density in terms of the envelope only.

### 1.3 Properties of duality symmetry preserving interfaces and media

Duality symmetric media interact in a unique way with light. An achiral duality symmetric optical element can (if it exists) manipulate light without affecting its polarisation. To illustrate this property, we will give two simple examples: reflection off and transmission through a duality symmetric flat interface and the propagation of light through a duality symmetric uniaxial crystal.

Consider the interface between two achiral media. The Fresnel coefficients are [67]

$$\begin{aligned} r_{\perp} &= \frac{\sqrt{\frac{\varepsilon_i}{\mu_i}} \cos(\theta_i) - \sqrt{\frac{\varepsilon_t}{\mu_t}} \cos(\theta_t)}{\sqrt{\frac{\varepsilon_i}{\mu_i}} \cos(\theta_i) + \sqrt{\frac{\varepsilon_t}{\mu_t}} \cos(\theta_t)}, & t_{\perp} &= \frac{2\sqrt{\frac{\varepsilon_i}{\mu_i}} \cos(\theta_i)}{\sqrt{\frac{\varepsilon_i}{\mu_i}} \cos(\theta_i) + \sqrt{\frac{\varepsilon_t}{\mu_t}} \cos(\theta_t)}, \\ r_{\parallel} &= \frac{\sqrt{\frac{\varepsilon_i}{\mu_i}} \cos \theta_i - \sqrt{\frac{\varepsilon_t}{\mu_t}} \cos \theta_t}{\sqrt{\frac{\varepsilon_i}{\mu_i}} \cos \theta_i + \sqrt{\frac{\varepsilon_t}{\mu_t}} \cos \theta_t}, & t_{\parallel} &= \frac{2\sqrt{\frac{\varepsilon_t}{\mu_t}} \cos \theta_t}{\sqrt{\frac{\varepsilon_i}{\mu_i}} \cos \theta_i + \sqrt{\frac{\varepsilon_t}{\mu_t}} \cos \theta_t}. \end{aligned} \quad (1.24)$$

Duality symmetry implies that the Fresnel coefficients are the same for both polarisations on the interface under consideration. Filling in  $\varepsilon$  and  $\mu$  for the media under consideration shows this and also simplifies the Fresnel coefficients:

$$r_{\perp, \parallel} = \frac{\cos \theta_i - \cos \theta_t}{\cos \theta_i + \cos \theta_t}, \quad t_{\perp, \parallel} = \frac{2 \cos \theta_i}{\cos \theta_i + \cos \theta_t}. \quad (1.25)$$

The refractive index appears only implicitly via Snels law.

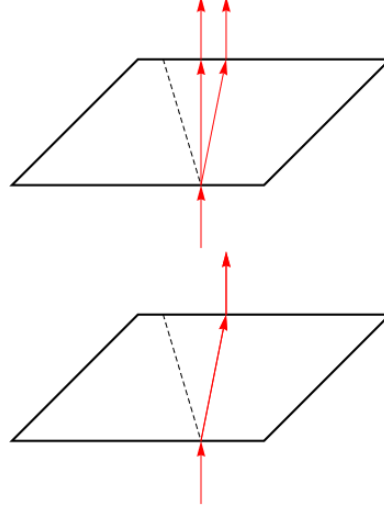
These expressions can also be generalised to chiral duality symmetric interfaces. In that case it is useful to consider circularly rather than linearly polarised light. The Fresnel coefficients follow from the following continuity equations [99]

$$\begin{aligned} \cos \theta_i \hat{x} + i\hat{y} &= t_R (\cos \theta_t \hat{x} + i\hat{y}) + r_R (-\cos \theta_t \hat{x} + i\hat{y}), \\ \cos \theta_i \hat{x} - i\hat{y} &= t_L (\cos \theta_t \hat{x} - i\hat{y}) + r_L (-\cos \theta_t \hat{x} - i\hat{y}). \end{aligned} \quad (1.26)$$

Here,  $\hat{x}$  and  $\hat{y}$  are the respective unit vectors in the  $x$  and  $y$  direction. From the continuity equations one obtains

$$r_R = \frac{\cos \theta_i - \cos \theta_t}{\cos \theta_i + \cos \theta_t}, \quad t_R = \frac{2 \cos \theta_i}{\cos \theta_i + \cos \theta_t} \quad (1.27)$$

Figure 1.1: Comparison between the passage of rays through an ordinary dielectric uniaxial crystal (top) and a duality symmetric uniaxial crystal (bottom). In an ordinary uniaxial crystal an incident unpolarised light ray gets separated into two linear orthogonally polarised rays, one of which is shifted relative to the incident ray. In a duality symmetric crystal this separation does not occur and both rays get shifted by the same amount.



and identical expressions for the left handed polarisation, the only difference being that  $\theta_r$  assumes a different value for left and right handed polarisations. It is interesting to note that for normal incidence  $r = 0$  and both polarisations are transmitted perfectly. This can be understood by noting that due to rotational symmetry the angular momentum component perpendicular to the interface is conserved. Reflection of circularly polarised light at normal incidence flips the spin angular momentum and therefore may not occur. Alternatively, the perfect transmission can be understood using the optical impedance [100]. Interpreting  $\frac{E_{\parallel}}{H_{\parallel}}$  as an impedance, one obtains the laws for transmission of an electric signal through an electronic circuit, with transmission being perfect if the impedances of both media are equal. By virtue of the duality symmetry condition  $\epsilon \propto \mu$  this impedance matching condition is automatically satisfied for light at normal incidence.

Another interesting situation to study is the propagation of light through a uniaxial duality symmetric crystal. In most uniaxial crystals, light is separated into an ordinary ray, for which the wave vector is the propagation direction, and an extraordinary ray for which the propagation direction is different from the wave vector. In a duality symmetric crystal, both rays propagate in the same direction, which is different from the wave vector. Both rays can be viewed as ‘equally extraordinary’. This can be shown as follows. Choose your coordinate system such that the optic axis lies along the z-axis and the wave vector of the light ray under consideration in the xz-plane. The permittivity and permeability can now be written as  $\epsilon = \alpha^{-1} \text{diag}(c_{\perp}^{-1}, c_{\perp}^{-1}, c_{\parallel}^{-1})$  and  $\mu = \alpha \text{diag}(c_{\perp}^{-1}, c_{\perp}^{-1}, c_{\parallel}^{-1})$ , where  $\alpha$  is chosen such that the common factor among  $\epsilon$  and  $\mu$  has the dimension of inverse velocity. One can find two sets of plane wave solutions, the first one for which  $\mathbf{E}_1$  points in the y-direction and the second one for which  $\mathbf{H}_2$  points in the y-direction.

$$\mathbf{E}_1 = Z^{\frac{1}{2}} e^{i(\mathbf{k}\cdot\mathbf{x} - \omega t)} \begin{bmatrix} 0 \\ 1 \\ 0 \end{bmatrix}, \quad \mathbf{H}_2 = Z^{-\frac{1}{2}} e^{i(\mathbf{k}\cdot\mathbf{x} - \omega t)} \begin{bmatrix} 0 \\ 1 \\ 0 \end{bmatrix}. \quad (1.28)$$

From Maxwell’s equations, one has  $\mathbf{D}_j = -\frac{1}{\omega} \mathbf{k} \times \mathbf{H}_j$  and  $\mathbf{B}_j = \frac{1}{\omega} \mathbf{k} \times \mathbf{E}_j$ . Using these

expressions and  $\varepsilon$  and  $\mu$ , one can compute  $\mathbf{H}_1$  and  $\mathbf{E}_2$ .

$$\mathbf{H}_1 = \frac{Z^{-\frac{1}{2}}}{\omega} e^{i(\mathbf{k}\cdot\mathbf{x}-\omega t)} \begin{bmatrix} -k_z c_\perp \\ 0 \\ k_x c_\parallel \end{bmatrix}, \quad \mathbf{E}_2 = \frac{Z^{\frac{1}{2}}}{\omega} e^{i(\mathbf{k}\cdot\mathbf{x}-\omega t)} \begin{bmatrix} k_z c_\perp \\ 0 \\ -k_x c_\parallel \end{bmatrix}. \quad (1.29)$$

Now the light rays propagate along the (time averaged) Poynting vector, which is  $\mathbf{S}_j = \frac{1}{2} \mathbf{E}_j \times \mathbf{H}_j^*$ . Computing the Poynting vector for both polarisations gives

$$\mathbf{S}_1 = \mathbf{S}_2 = \frac{1}{\omega} \begin{bmatrix} k_x c_\parallel \\ 0 \\ k_z c_\perp \end{bmatrix}. \quad (1.30)$$

So rays of both polarisations propagate in the same direction which differs from the direction of the wave vector, as depicted in Fig. 1.1

## 1.4 The separation of the electromagnetic field in a right handed and a left handed field

For a duality symmetric medium, there exists another way to write Maxwell's equations in a simple and insightful form, which we will show now. Start by introducing the following right and left handed fields  $\mathbf{R}$  and  $\mathbf{L}$  and their corresponding refractive indices  $n_R$  and  $n_L$ :

$$\begin{aligned} \mathbf{R} &= \frac{1}{\sqrt{2}} \left( \mathbf{E} - i \sqrt{\frac{\mu}{\varepsilon}} \mathbf{H} \right), & n_R &= \sqrt{\varepsilon\mu} + G, \\ \mathbf{L} &= \frac{1}{\sqrt{2}} \left( \mathbf{E} + i \sqrt{\frac{\mu}{\varepsilon}} \mathbf{H} \right), & n_L &= \sqrt{\varepsilon\mu} - G. \end{aligned} \quad (1.31)$$

When applying these fields and refractive indices in an anisotropic medium, one can remove the ambiguity in the square root of a matrix by replacing  $\sqrt{\frac{\mu}{\varepsilon}}$  by  $\alpha^{-1}$  and  $\sqrt{\varepsilon\mu}$  by either  $\alpha\varepsilon$  or  $\alpha^{-1}\mu$ . With these fields the divergence laws take the following form

$$\begin{aligned} \nabla \cdot \left( \varepsilon(\mathbf{R} + \mathbf{L}) + G \sqrt{\frac{\varepsilon}{\mu}} (\mathbf{R} - \mathbf{L}) \right) &= 0, \\ \nabla \cdot (\sqrt{\varepsilon\mu} (\mathbf{R} - \mathbf{L}) + G(\mathbf{R} + \mathbf{L})) &= 0. \end{aligned} \quad (1.32)$$

In a duality symmetric medium,  $\sqrt{\frac{\varepsilon}{\mu}}$  can be taken in front of the divergence operator and the divergence laws can be rewritten as

$$\nabla \cdot (n_R \mathbf{R}) = 0, \quad \nabla \cdot (n_L \mathbf{L}) = 0. \quad (1.33)$$

More interesting are the curl laws, which become, after some algebra,

$$\begin{aligned} \nabla \times (\mathbf{R} + \mathbf{L}) &= -i \frac{d}{dt} (\sqrt{\varepsilon\mu} (\mathbf{R} - \mathbf{L}) + G(\mathbf{R} + \mathbf{L})), \\ \nabla \times \sqrt{\frac{\varepsilon}{\mu}} (\mathbf{R} - \mathbf{L}) &= -i \frac{d}{dt} \left( \varepsilon(\mathbf{R} + \mathbf{L}) + G \sqrt{\frac{\varepsilon}{\mu}} (\mathbf{R} - \mathbf{L}) \right). \end{aligned} \quad (1.34)$$

Again, if the medium is duality symmetric, a factor of  $\sqrt{\frac{\epsilon}{\mu}}$  can be taken in front of all differential operators and these equations simplify to

$$\nabla \times \mathbf{R} = -i \frac{d}{dt} n_R \mathbf{R}, \quad \nabla \times \mathbf{L} = i \frac{d}{dt} n_L \mathbf{L}. \quad (1.35)$$

When written in this form, it is clear that for a duality symmetric medium, right and left handed light fields are completely decoupled and obey their own field equations. Moreover, one can show that any plane wave solution has  $\mathbf{R}$  rotating counterclockwise (with the wave vector pointing toward you) and  $\mathbf{L}$  rotating clockwise, thus verifying that they indeed contain only resp. right and left handed contributions.

This separation in left and right handed components only works if one takes the fields to be complex. Only then the real part of the electric field and the imaginary part of the magnetic field (and vice versa) interfere destructively for one and constructively for the other handedness. If one treats the field as real quantities  $\mathbf{L}$  becomes the Riemann-Silberstein bivector, which contains all information about both handednesses of the light [101, 102]. Although Silberstein suggestively used the terms L- and R-quaternions in one of his articles, to the best of our knowledge no one has mentioned this non-intuitive difference between the real and complex treatments of the fields (see also the recent review articles [103, 104]).

Like the fields, the vector potentials can be rewritten in left and right handed contributions as well:

$$\begin{aligned} (\Lambda_0, \vec{\Lambda}) &= \frac{1}{\sqrt{2}} \left( (A_0, \mathbf{A}) + i \sqrt{\frac{\mu}{\epsilon}} (C_0, \mathbf{C}) \right), \\ (\Delta_0, \vec{\Delta}) &= \frac{1}{\sqrt{2}} \left( (A_0, \mathbf{A}) - i \sqrt{\frac{\mu}{\epsilon}} (C_0, \mathbf{C}) \right). \end{aligned} \quad (1.36)$$

From these definitions follow

$$\begin{aligned} \dot{\vec{\Lambda}} + \nabla \Lambda_0 &= -\mathbf{L}, & \nabla \times \vec{\Lambda} &= -in_L \mathbf{L}, \\ \dot{\vec{\Delta}} + \nabla \Delta_0 &= -\mathbf{R}, & \nabla \times \vec{\Delta} &= in_R \mathbf{R}, \end{aligned} \quad (1.37)$$

which are similar to the normal relations between vector potentials and fields. It is insightful to rewrite the helicity density and flux in terms of these new fields and potentials.

$$\begin{aligned} \mathcal{H} &= \frac{i}{4\alpha} (\vec{\Delta}^* \cdot n_R \mathbf{R} - \vec{\Lambda}^* \cdot n_L \mathbf{L}), \\ \vec{\Phi}_{\mathcal{H}} &= \frac{1}{4\alpha} (\mathbf{R} \times \vec{\Delta}^* + \mathbf{L} \times \vec{\Lambda}^*). \end{aligned} \quad (1.38)$$

These show that the helicity is the difference between left and right handed contributions, which is perfectly in line with the the definition of helicity as the difference in the number of left and right handed circularly polarised photons [79–81, 98].

## 1.5 The feasibility of duality symmetric optics

The condition  $\epsilon \propto \mu$  cannot be genercially satisfied for two different materials, because for many materials  $\mu$  is close to its vacuum value for most frequencies, whereas  $\epsilon$  varies

from material to material. Even for materials with strong magnetic responses  $\epsilon$  and  $\mu$  are not typically proportional across two materials. The reason is that any realistic material is absorbing, which means that the imaginary parts of  $\epsilon$  and  $\mu$  are nonzero. So there are four parameters<sup>2</sup> which have to be proportional to each other. One of them can be used to set the proportionality constant across the interface, leaving three constraints. If the only thing one can do is varying the frequency of the light, one constraint can be satisfied (provided all parameters vary enough with frequency), leaving two unsatisfied constraints.

Designing (superconducting [105–107]) metamaterials with the desired properties allows to satisfy all constraints within manufacturing tolerance[108–114]. In this case duality symmetry can be considered an approximate symmetry rather than an exact symmetry.

The only nontrivial case<sup>3</sup> where duality symmetry is exactly satisfied, is a system consisting of a chiral material and the same material with opposite chirality. One can expand the light field in a left handed and a right handed component, and verify that both components experience a change in refractive index as they pass from the right handed to the left handed material or vice versa, yet duality symmetry is obviously preserved here. Combining a chiral material with its opposite chirality counterpart one can imagine novel optical components like chiral waveguides that only guide light of one helicity or chiral lenses that focus one left handed light whilst defocusing right handed light (or vice versa).

In short, we have shown that electric-magnetic duality symmetry is preserved within the framework of linear optics as long as the permittivity and permeability response remain in the same proportion everywhere and there is no magneto-electric response. The proportionality of the permittivity and the permeability is typically not preserved upon going from one medium to another, making this condition hard to achieve, but using only both chiralities of a chiral material, one can satisfy all conditions.

---

<sup>2</sup>For isotropic materials; for anisotropic materials the number of parameters is even larger.

<sup>3</sup>That is, other than vacuum or a large piece of homogeneous, isotropic material.





## Chapter 2

# Superpositions of up to six plane waves without electric-field interference

### 2.1 Introduction

The experiments of Thomas Young cemented the idea that different sources of light, if sufficiently coherent, interfere with each other [115, 116]. Young's experiment confirmed the wave nature of light, which could straightforwardly explain this phenomenon, unlike the corpuscle model then commonly accepted. Bright fringes appear where two crests or two troughs overlay and dark fringes appear when a crest of one wave overlays with a trough of the other. Further interference experiments by Fresnel and Arago confirmed the transversality of light waves [117].

In modern electrodynamics, the electric and magnetic fields of a plane electromagnetic wave are orthogonal to each other and the direction of propagation. This suggests that the maximum number of waves with the same frequency that can be superposed without any interference is three. This can be done by choosing three waves travelling in mutually orthogonal directions and choosing all three polarisations orthogonal to each other.

If one is content with only the mean squared electric field being homogeneous without requiring that the mean square of the magnetic field also be homogeneous, larger superpositions are allowed. For many practical purposes, such superpositions can still be considered noninterfering, as it is the electric field that interacts most with matter, including fluorescent dyes, CCDs and the light-sensitive pigments in the human eye. The inhomogeneity in the magnetic field is relatively difficult to detect.

The helicity density, a quantity indicating the handedness of the light [77–80, 118], is in general inhomogeneous for noninterfering superpositions. It will vary in space in a pattern that is quite often, although not necessarily, periodic and resembles the intensity variations in optical lattices. There is enough freedom left in the superpositions to allow for a large variety of helicity lattices.

Some noninterfering superpositions show superchirality, an effect introduced by Tang & Cohen [68–70]. Superchiral light has regions where the helicity density is much higher than one would expect from the local mean square of the electric field. The key difference

is that other superchiral superpositions exploit interference to create a region where the mean square of the electric field is weak, but the mean square of the magnetic field is not, allowing for the helicity density to become very large compared the squared local electric field [68, 119]. The helicity is actually quite small compared to the squared electric field outside of this ‘dark region’. Alternatively plasmonic resonators have been proposed to generate high helicities close to a surface [120–124]. Noninterfering superpositions achieve superchirality in free space and in ‘bright regions’ where the mean square of the electric field is not suppressed.

The scope of this chapter is broad. We will treat the explicit construction of noninterfering superpositions and their helicity structures, the mathematically interesting question what the maximum number of noninterfering plane waves is and the possibility to use liquid crystals to record the helicity structures of our noninterfering superpositions. This chapter is structured as follows: in section 2.2 we show how to construct noninterfering superpositions. We then give several examples along with their helicity density patterns in section 2.3. In section 2.4 we estimate the residual inhomogeneity of the mean square of the electric field under small deviations from the exact required parameters and the decrease in visibility of the helicity lattices when the light is partially coherent. In section 2.5 we discuss the possibility of recording the helicity density patterns of noninterfering superpositions using chirally sensitive liquid crystals and in section 2.6 we discuss several open mathematical questions related to noninterfering superpositions.

## 2.2 Construction of noninterfering superpositions and their helicity properties

In this chapter we work in the classical domain in free space and consider non-trivial superpositions of  $N$  plane electromagnetic waves, each of which has the same angular frequency  $\omega = ck$ . For a superposition of  $N$  waves the resulting electric and magnetic fields are

$$\begin{aligned}\mathbf{E} &= \text{Re } \tilde{\mathbf{E}} = \text{Re} \left( \sum_{j=1}^N \tilde{\mathbf{E}}_j e^{i(\mathbf{k}_j \cdot \mathbf{x} - \omega t)} \right), \\ \mathbf{H} &= \text{Re } \tilde{\mathbf{H}} = \text{Re} \left( \frac{1}{\mu_0 \omega} \sum_{j=1}^N \mathbf{k}_j \times \tilde{\mathbf{E}}_j e^{i(\mathbf{k}_j \cdot \mathbf{x} - \omega t)} \right).\end{aligned}\quad (2.1)$$

By a non-trivial superposition we mean  $\mathbf{k}_i \neq \mathbf{k}_j \forall i \neq j$  and  $\tilde{\mathbf{E}}_j \neq 0 \forall j$ . The complex amplitudes  $\tilde{\mathbf{E}}_j$  define the polarisations, amplitudes and phases of the waves. Because light’s polarisation is transverse  $\tilde{\mathbf{E}}_j \cdot \mathbf{k}_j = 0 \forall j$  applies.

### 2.2.1 Interference cancellation

The mean square of the electric field is given by

$$\frac{\omega}{2\pi} \int_0^{\frac{2\pi}{\omega}} \mathbf{E} \cdot \mathbf{E} dt = \frac{1}{2} \tilde{\mathbf{E}} \cdot \tilde{\mathbf{E}}^* = \frac{1}{2} \left( \sum_{j=1}^N \tilde{\mathbf{E}}_j \cdot \tilde{\mathbf{E}}_j^* + \sum_{j=1}^N \sum_{l \neq j} \tilde{\mathbf{E}}_j \cdot \tilde{\mathbf{E}}_l^* e^{i(\mathbf{k}_j - \mathbf{k}_l) \cdot \mathbf{x}} \right). \quad (2.2)$$

If this is to be homogeneous, the second sum must vanish. The most obvious way to achieve this is to choose the constituent plane waves such that no two interfere, in which case  $\tilde{\mathbf{E}}_j \cdot \tilde{\mathbf{E}}_l^* = 0 \forall j \neq l$ . This can be done for at most three plane waves because there

are three orthogonal polarisation directions possible. We recognise that it is also possible, however, to allow multiple pairs of waves to interfere, provided the associated interference patterns cancel. To appreciate this, suppose that there exists within the superposition a pair ( $j \neq l$ ) of interfering waves, with the spatial periodicity of the associated interference pattern being dictated by the wavevector difference  $\mathbf{k}_j - \mathbf{k}_l$ . If another pair ( $j' \neq l'$ ) of interfering waves with the same wavevector difference  $\mathbf{k}_j - \mathbf{k}_l = \mathbf{k}_{j'} - \mathbf{k}_{l'}$  can be identified, giving an associated interference pattern with the same spatial periodicity, then the two interference patterns will cancel provided that  $\tilde{\mathbf{E}}_j \cdot \tilde{\mathbf{E}}_l^* + \tilde{\mathbf{E}}_{j'} \cdot \tilde{\mathbf{E}}_{l'}^* = 0$ . The same reasoning applies for more than two pairs of interfering waves with the same wavevector difference. It is this trick that allows us to superpose more than three plane waves whilst keeping the mean square of the electric field homogeneous.

### 2.2.2 Optical helicity and helicity lattices

As only monochromatic light fields in free space are considered we can simplify the expression for the helicity: eq. (1.21). Using the gauge  $A_0 = C_0 = \nabla \cdot \mathbf{A} = \nabla \cdot \mathbf{C} = 0$ , we can express the vector potentials in terms of the fields as  $\tilde{\mathbf{A}} = \tilde{\mathbf{E}}/i\omega$  and  $\tilde{\mathbf{C}} = \tilde{\mathbf{H}}/i\omega$ . Using these relations, eq. (1.21) can be rewritten in terms of the fields only as  $\mathcal{H} = \frac{1}{2} \text{Im}(\tilde{\mathbf{E}} \cdot \tilde{\mathbf{H}}^*)/c\omega$ . For a superposition of  $N$  plane waves one has

$$\mathcal{H} = \frac{-i}{4c\omega} \sum_{j,l=1}^N (\tilde{\mathbf{E}}_j \cdot \tilde{\mathbf{H}}_l^* - \tilde{\mathbf{E}}_l^* \cdot \tilde{\mathbf{H}}_j) e^{i(\mathbf{k}_j - \mathbf{k}_l) \cdot \mathbf{x}}. \quad (2.3)$$

If all waves are linearly polarised, the terms with  $i = j$  are zero and only the ‘interference terms’ remain. The vectors  $\mathbf{k}_j - \mathbf{k}_l$  of all nonzero terms determine if the helicity density forms a lattice. If they are all linear combinations with integer coefficients of  $\dim(\text{span}\{\mathbf{k}_j - \mathbf{k}_l | \tilde{\mathbf{E}}_j \cdot \tilde{\mathbf{H}}_l^* - \tilde{\mathbf{E}}_l^* \cdot \tilde{\mathbf{H}}_j \neq 0\})^1$  vectors, they form a lattice. If not, they form a less regular structure.

## 2.3 Explicit examples

Throughout this section graphics of the helicity structure will always be  $4 \times 4$  or  $4 \times 4 \times 4$  wavelengths large unless stated otherwise and blue indicates negative helicity and red indicates positive helicity.

Also, throughout this section, diagrams illustrate the superpositions for which the helicity density is plotted. In these diagrams grey arrows indicate wavevectors and electric field polarisations are indicated with yellow arrows. Green arrows to indicate the magnetic polarisations are included for reference as well. Mutually cancelling pairs of interference terms are indicated by red lines and interference terms contributing to the inhomogeneous helicity density are shown as black dashed lines.

In every example we will give of a noninterfering superposition, there is some freedom left to change the amplitudes and propagation directions of the different waves. We will use  $a_j$  to indicate free complex amplitudes which can take any nonzero value and  $\theta_j$  and  $\phi_j$  to indicate free angles where  $0 \leq \theta_j < \pi$  and  $0 \leq \phi_j < 2\pi$ , unless additional constraints are mentioned.

<sup>1</sup> $\text{span}\{ \}$  Is the space spanned by a set of vectors,  $\dim(\ )$  is the dimension.

I will check if superchirality occurs by comparing the helicity density to the mean square of the electric field, both multiplied with suitable constants to make their dimensions the same. The superchirality threshold is  $\sqrt{\epsilon_0\mu_0}|\text{Im}(\tilde{\mathbf{E}} \cdot \tilde{\mathbf{H}}^*)| > \epsilon_0\tilde{\mathbf{E}}^* \cdot \tilde{\mathbf{E}}$  [68]. Because  $\tilde{\mathbf{E}}^* \cdot \tilde{\mathbf{E}}$  is homogeneous by design for all examples we will give, the occurrence of superchirality implies a similar inequality taking the global maxima:  $\max(\sqrt{\epsilon_0\mu_0}|\text{Im}(\tilde{\mathbf{E}} \cdot \tilde{\mathbf{H}}^*)|) > \max(\epsilon_0\tilde{\mathbf{E}}^* \cdot \tilde{\mathbf{E}})$ . That is, the local helicity is large compared to the squared electric field anywhere. To the best of our knowledge, no monochromatic electromagnetic field with this property has ever been identified.

### 2.3.1 Two waves

Two plane waves can always be orthogonally polarised regardless of what their wavevectors are. One way to achieve this is to choose the polarisation of one wave to lie in the plane spanned by the wavevectors of both waves and the other one orthogonal to this plane [72, 118]. It is convenient to choose both waves to lie in the  $xy$ -plane, symmetrically with respect to the  $y$ -axis.

$j$	$\mathbf{k}_j$	$\tilde{\mathbf{E}}_j$
1	$[\sin \theta, \cos \theta, 0]$	$a_1[0, 0, 1]$
2	$[\sin \theta, \cos \theta, 0]$	$a_2[\cos \theta, \sin \theta, 0]$

For this configuration  $\tilde{\mathbf{E}} \cdot \tilde{\mathbf{E}}^*$  and  $\tilde{\mathbf{H}} \cdot \tilde{\mathbf{H}}^*$  are homogeneous. If one computes the helicity density, however, one does find a fringe structure similar to intensity interference fringes one would get if one chose the polarisations parallel, see Fig. 2.1.

$$\mathcal{H} = -\frac{\epsilon_0}{\omega} |a_1 a_2^*| \cos^2 \theta \sin(k_0 \sin(2\theta)x + \arg(a_1 a_2^*)). \quad (2.4)$$

Because of the helicity-dependent force it exerts on chiral molecules [71, 72] and birefringent microparticles [125, 126] this superposition has been studied in some detail. It has been found to act like a matter wave grating on chiral molecules [73] similar to how a standing light wave can act like a grating for molecules in general [127–129].

### 2.3.2 Three waves

Having three waves travelling in orthogonal directions and with orthogonal polarisations yields both homogeneous  $\tilde{\mathbf{E}} \cdot \tilde{\mathbf{E}}^*$  and  $\tilde{\mathbf{H}} \cdot \tilde{\mathbf{H}}^*$ . This setup already shows an interesting helicity structure, forming a triangular lattice, as is shown in Fig. 2.2. One is free to change the relative amplitudes. This will alter the shape of the positive and negative helicity regions within a unit cell, but keeps the lattice vectors fixed.

If only  $\tilde{\mathbf{E}}^* \cdot \tilde{\mathbf{E}}$  has to be constant, but  $\tilde{\mathbf{H}}^* \cdot \tilde{\mathbf{H}}$  may vary, one can construct more superpositions by rotating the wavevectors of the three waves around axes given by their polarisation directions, yielding:

$j$	$\mathbf{k}_j$	$\tilde{\mathbf{E}}_j$
1	$[\cos \phi_1, 0, -\sin \phi_1]$	$a_1[0, 1, 0]$
2	$[-\sin \phi_2, \cos \phi_2, 0]$	$a_2[0, 0, 1]$
3	$[0, -\sin \phi_3, \cos \phi_3]$	$a_3[1, 0, 0]$

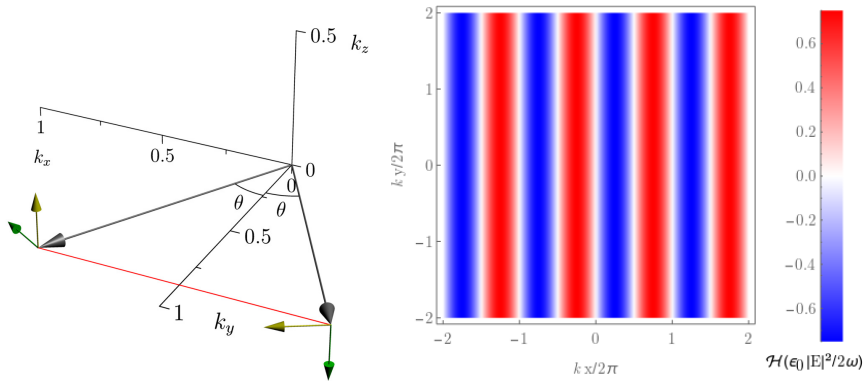


Figure 2.1: The wave- and polarisation vectors for a noninterfering two-wave superposition (left) and its helicity pattern (right)

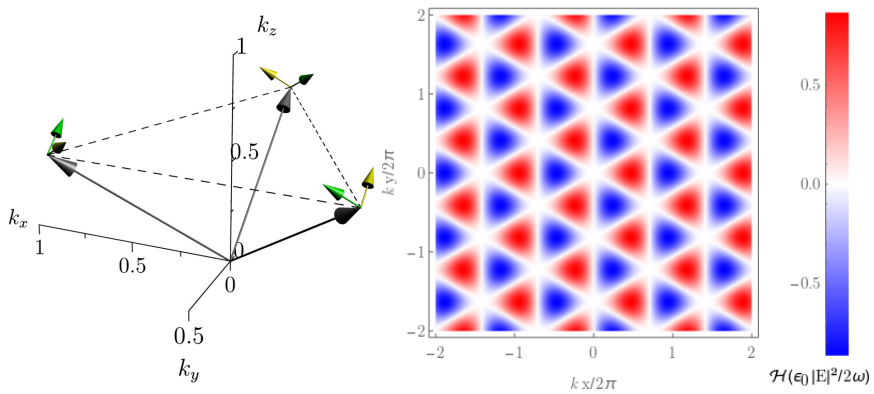


Figure 2.2: The wave- and polarisation vectors for three noninterfering orthogonal waves, all amplitudes taken equal (left) and their helicity structure (right). For three plane waves the helicity interference terms always lie in a plane and thus form a two-dimensional helicity lattice.

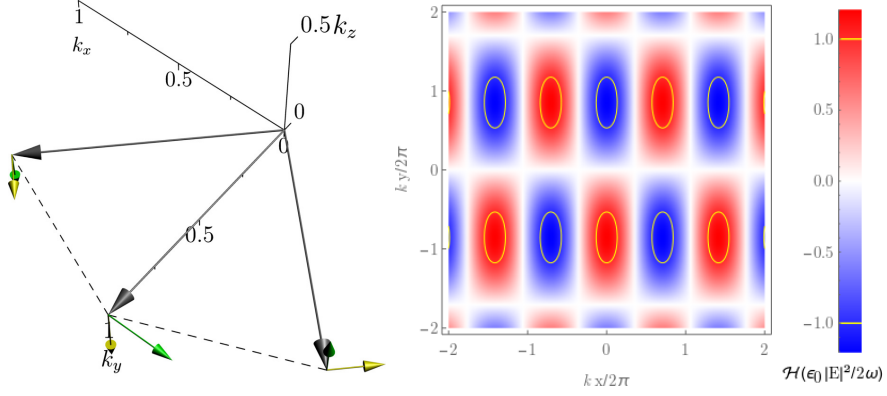


Figure 2.3: The construction of a superchiral three-wave superposition (left). The amplitude of the middle wave is  $\sqrt{2}$  times the amplitude of the other waves. The corresponding helicity structure (right) has superchiral regions (yellow ellipses) which extend for about half a wavelength in one direction and a quarter of a wavelength in the other.

with  $a_1$ ,  $a_2$  and  $a_3$  free (complex) amplitudes. The additional freedom one gets from only requiring  $\tilde{\mathbf{E}}^* \cdot \tilde{\mathbf{E}}$  to be homogeneous allows for a larger variety of helicity structures, including ones that are locally superchiral, as shown in Fig. 2.3.2.

With the above superpositions, the possibilities to superpose three plane waves whilst keeping the root-mean-square of the electric field constant are not exhausted yet. There exists another family of three-wave superpositions satisfying this requirement. It is constructed by taking two counterpropagating waves with orthogonal polarisations. Then a third wave is superposed, travelling perpendicularly to the first two waves and polarised along the propagation axis of the first two waves. Taking the first two waves travelling along the  $y$ -axis and the third wave travelling along the  $x$ -axis we get the following parametrisation:

$j$	$\mathbf{k}_j$	$\tilde{\mathbf{E}}_j$
1	$[0, 1, 0]$	$a_1 [\cos \theta, 0, \sin \theta e^{i\phi}]$
2	$[0, -1, 0]$	$a_2 [-\sin \theta, 0, \cos \theta e^{i\phi}]$
3	$[1, 0, 0]$	$a_3 [0, 1, 0]$

Unlike any other superposition we show in this chapter, the polarisations of the light waves do not have to be all linear. For waves 1 and 2 one can choose any pair of elliptic polarisations one likes, as long as they are orthogonal. For two circularly polarised light waves, to have orthogonally polarised means to have their electric field vectors rotate in opposite directions. If the waves travel in opposite directions, this is equivalent to them having the same helicity. Thus one can use this superposition to make helicity lattices that are predominantly left- or right handed, as demonstrated in Fig. 2.4. This is impossible with any of the other superpositions we will show because they have all their light waves linearly polarised which implies that the helicity density averaged over one unit cell is zero.

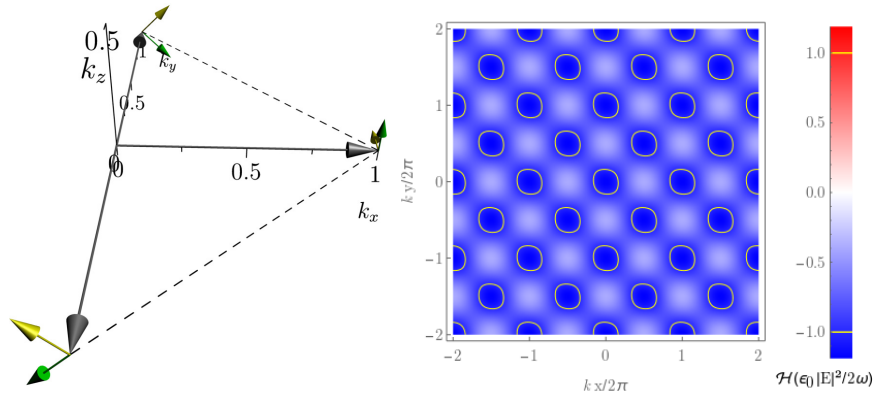


Figure 2.4: A three-wave noninterfering superposition (left), which allows for helicity lattices with a nonzero average helicity (right). The parameters chosen for the helicity plot are  $\phi = \pi/2$ ,  $\theta = \pi/4$  and  $a_1 = a_2 = \sqrt{2}a_3$ . For these parameters the helicity superposition has on average a left handed helicity density. By changing the polarisations of the two counterpropagating waves, one can tune the average helicity of the lattice.

### 2.3.3 Four waves

For superposing four waves without electric-field interference, one has to cancel a pair of interference terms against each other. One can take all wavevectors lying in a plane with their tips on the corners of a rectangle. If one takes two adjacent waves polarised out of the plane and the other two polarised in plane there is only one nonzero pair of interference terms. One can then adjust the phases and amplitudes to make this pair of interference terms cancel. Taking all wavevectors in the  $xy$ -plane one has:

$j$	$\mathbf{k}_j$	$\tilde{\mathbf{E}}_j$
1	$[\cos \theta, \sin \theta, 0]$	$a_1[0, 0, 1]$
2	$[\cos \theta, -\sin \theta, 0]$	$a_2[0, 0, 1]$
3	$[-\cos \theta, \sin \theta, 0]$	$-\frac{a_1 a_2^* \text{sgn}(\cos 2\theta)}{a_4^* \sqrt{ \cos 2\theta }} [\sin \theta, \cos \theta, 0]$
4	$[-\cos \theta, -\sin \theta, 0]$	$\frac{a_4}{\sqrt{ \cos 2\theta }} [-\sin \theta, \cos \theta, 0]$

with  $\theta$  any angle between 0 and  $\frac{\pi}{2}$  except  $\frac{\pi}{4}$ . The helicity density of this superposition is zero for  $\theta < \frac{\pi}{4}$  because both helicity terms cancel. For  $\frac{\pi}{4} < \theta < \frac{\pi}{2}$  the helicity structure consists of sinusoidal fringes along the  $x$ -axis, a pattern that can already be achieved by superposing two waves [73, 125].

One can also take two waves lying in the  $xy$ -plane and polarised in the  $z$ -direction and two waves travelling in the  $yz$ -plane polarised in the  $x$ -direction. If both pairs of waves travel at the same relative angle, one can choose the amplitudes and phases such that their interference terms cancel, yielding:

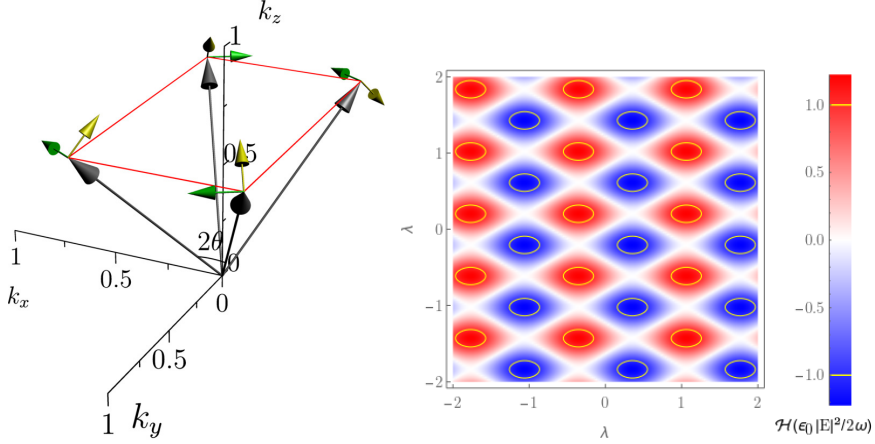


Figure 2.5: A four-wave noninterfering superposition with two pairs of cancelling interference terms (left) and its helicity structure (right). For the helicity structure shown  $a_1 = a_3$ ,  $\theta = \frac{\pi}{6}$  and  $\Delta\phi = 0$ . Superchirality is typical for superpositions of this kind and occurs over broad parameter ranges.

$j$	$\mathbf{k}_j$	$\tilde{\mathbf{E}}_j$
1	$[\cos \theta, \sin \theta, 0]$	$a_1 [0, 0, 1]$
2	$[\cos \theta, -\sin \theta, 0]$	$a_2 [0, 0, 1]$
3	$[0, \sin \theta, \cos \theta]$	$-\frac{a_1 a_2^*}{a_4^*} [1, 0, 0]$
4	$[0, -\sin \theta, \cos \theta]$	$a_4 [1, 0, 0]$

The helicity pattern of this superposition consists again of sinusoidal fringes, but this superposition allows for a fifth wave to be added whilst still keeping the mean square of the electric field constant. This five-wave superposition will be treated in the next subsection.

There exists another four-wave superposition which involves the cancellation of two pairs of interference terms. It is constructed by taking a pair of waves travelling in orthogonal directions (we take them symmetric with respect to the  $z$ -axis) polarised in the plane spanned by the wavevectors. Then add a second copy of this pair rotated around the bisector of the first pair with an additional relative phase of  $\pi$  between them yielding:

$j$	$\mathbf{k}_j$	$\tilde{\mathbf{E}}_j$
1	$\frac{1}{2}\sqrt{2}[\cos \theta, \sin \theta, 1]$	$a_1 \frac{1}{2}\sqrt{2}[-\cos \theta, -\sin \theta, 1]$
2	$\frac{1}{2}\sqrt{2}[-\cos \theta, -\sin \theta, 1]$	$a_1^* \frac{a_3}{a_3^*} e^{i\Delta\phi} \frac{1}{2}\sqrt{2}[-\cos \theta, -\sin \theta, -1]$
3	$\frac{1}{2}\sqrt{2}[-\cos \theta, \sin \theta, 1]$	$a_3 \frac{1}{2}\sqrt{2}[\sin \theta, -\cos \theta, 1]$
4	$\frac{1}{2}\sqrt{2}[\cos \theta, -\sin \theta, 1]$	$a_3 e^{i\Delta\phi} \frac{1}{2}\sqrt{2}[-\sin \theta, \cos \theta, 1]$

The helicity lattice formed by this superposition shows rhombs of positive and negative helicity arranged in a rectangular lattice, see Fig. 2.5. Superchirality occurs when  $a_1$  and  $a_3$  are of comparable magnitude.



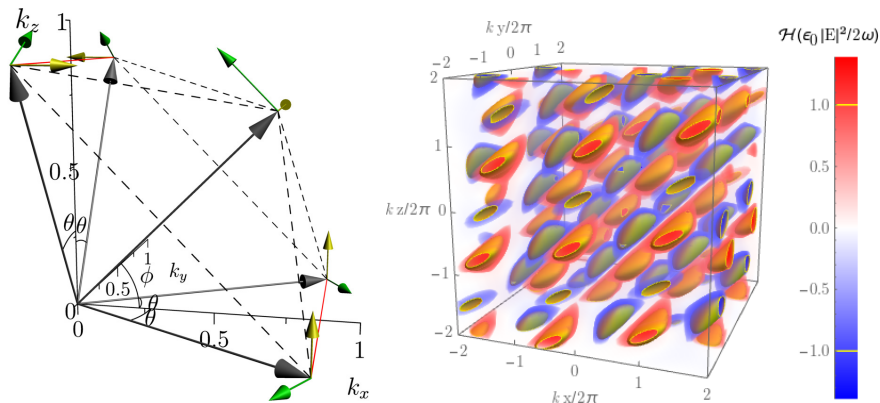


Figure 2.6: An example of a five-wave noninterfering superposition (left) yielding a three dimensional helicity lattice (right). For the helicity density  $\theta = \frac{\pi}{6}$ ,  $\phi = \frac{\pi}{4}$ ,  $a_1 = a_2 = a_4 = 1$  and  $a_5 = \sqrt[4]{8}\sqrt{\cos\pi/6}$ . The superchiral regions are enclosed by the yellow surfaces. At about half a wavelength in length they are surprisingly large.

### 2.3.4 Five waves

The five-wave superposition is the only one we know about with a genuine three-dimensional helicity structure. It is constructed the following way. Take two plane waves in propagating the  $xy$ -plane polarised in the  $z$ -direction. Take two plane waves in the  $yz$ -plane propagating at the same relative angles and polarised in the  $x$ -direction. By choosing the amplitudes and phases of these waves right, one can cancel the interference terms between these waves, as explained in the previous subsection. Then one can add a fifth wave propagating in the  $xz$ -plane polarised in the  $y$ -direction. The parameters of this superposition are the following:

$j$	$\mathbf{k}_j$	$\tilde{\mathbf{E}}_j$
1	$[\cos \theta, \sin \theta, 0]$	$a_1[0, 0, 1]$
2	$[\cos \theta, -\sin \theta, 0]$	$a_2[0, 0, 1]$
3	$[0, \sin \theta, \cos \theta]$	$-\frac{a_1 a_2^*}{a_4^*}[1, 0, 0]$
4	$[0, -\sin \theta, \cos \theta]$	$a_4[1, 0, 0]$
5	$[\cos \phi, 0, \sin \phi]$	$a_5[0, 1, 0]$

As one can see in Fig. 2.6, the wavevectors lie on the corners of a (generically skewed) pyramid. The difference vectors between them form the sides of the pyramid. One can write all these difference vectors as linear combinations with integer coefficients of only three of them, choosing two that lie in the base and one connecting the base to the apex. Therefore the helicity structure of this superposition is generically periodic. For generic parameters the helicity lattice is monoclinic, with higher lattice symmetries for special parameters. If one chooses  $\phi = \frac{\pi}{4} \vee \frac{5\pi}{4}$  the apex of the pyramid lies directly above the centre of the base, and the helicity lattice is orthorhombic. If the base of the pyramid is a square as well the helicity lattice is tetragonal. This is the case for  $\theta = \arccos \frac{2}{\sqrt{6}}$ .

For the special cases  $\phi = \frac{3\pi}{2} + \arctg(1 - \cos \theta)$  or  $\phi = \pi - \arctg(1 - \cos \theta)$  all difference vectors between the wavevectors lie in the same plane and the helicity structure is generically aperiodic, like in Fig. 2.7, except if they all are rational linear combinations of

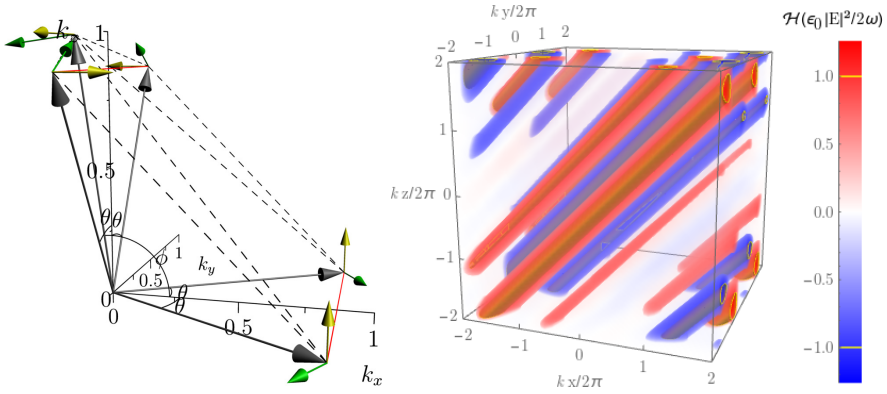


Figure 2.7: An example of a five wave superposition where all interference terms lie in the same plane. The helicity lattice becomes effectively two-dimensional and aperiodic in one direction, along a line from the upper left to the lower right corner.

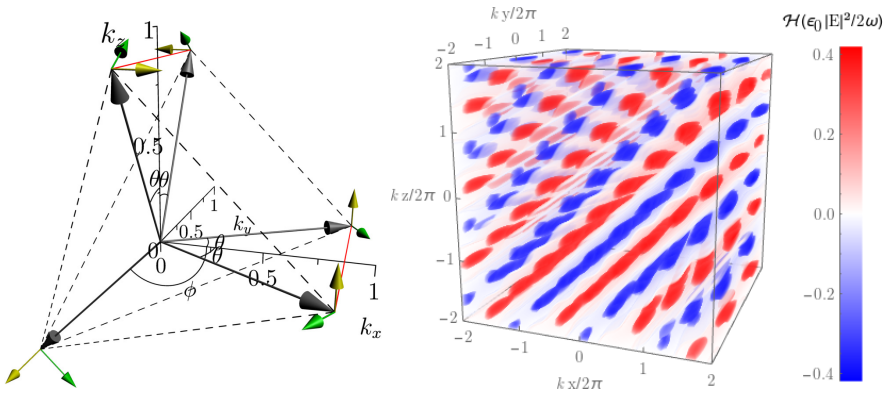


Figure 2.8: The same superposition as in Fig. 2.6, but with the direction of the fifth wave reversed. The helicity lattice is much less pronounced in this case and there is no superchirality present.

only two of them, which happens for  $\cos \theta / \sqrt{2} \sin(\arctg(1 - \cos \theta)) \in \mathbb{Q}$ . If this condition is met the helicity structure is a two-dimensional rectangular lattice, although the unit cell may be very large depending on the precise ratio.

The large number of free parameters this superposition has allows one to construct superchiral helicity lattices with surprisingly pronounced ( $\approx 1.4$  times the threshold value) and large (extending about half a wavelength in two directions) superchiral regions. The most pronounced superchirality is achieved when the fifth wave points in roughly the same direction as the total momentum of the other four whereas having it point in the opposite direction attenuates the helicity modulations to far below the superchirality threshold, which can be seen clearly by comparing Figs. 2.6 and 2.8.

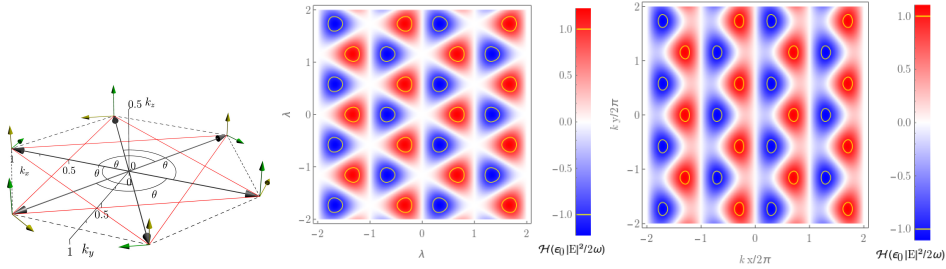


Figure 2.9: The six wave superposition with  $\theta = \frac{2\pi}{3}$  (left). This superposition requires three pairs of interference terms to cancel (red lines in the diagram). For  $\theta = \frac{2\pi}{3}$  the helicity forms a triangular lattice. Two examples are shown, one for  $a_1 = a_2 = a_3$  (centre) and one for  $a_1 = \frac{1}{2}a_2 = \frac{1}{2}a_3$  (right.)

### 2.3.5 Six waves

One can superpose six waves by having three cancelling pairs of interference terms. The superposition is constructed by putting the six wavevectors on the corners of a hexagon. Three of them are polarised in the plane of the hexagon and three perpendicular to it. In this setup, the following set of plane waves leads to cancellation of all interference terms

$j$	$\mathbf{k}_j$	$\hat{\mathbf{E}}_j$
1	$[1, 0, 0]$	$a_1 [0, 0, 1]$
2	$[\cos \theta, \sin \theta, 0]$	$a_2 [0, 0, 1]$
3	$[\cos \theta, -\sin \theta, 0]$	$a_3 [0, 0, 1]$
4	$[-1, 0, 0]$	$-\frac{a_1^* \sqrt{ \cos 2\theta }}{\cos \theta} [0, -1, 0]$
5	$[-\cos \theta, -\sin \theta, 0]$	$\frac{a_2^*}{\sqrt{ \cos 2\theta }} [\sin \theta, -\cos \theta, 0]$
6	$[-\cos \theta, \sin \theta, 0]$	$\frac{a_3^*}{\sqrt{ \cos 2\theta }} [-\sin \theta, -\cos \theta, 0]$

with  $\theta$  limited to the intervals  $\frac{\pi}{4} < \theta < \frac{\pi}{2}$  or  $\frac{\pi}{2} < \theta < \frac{3\pi}{4}$ . Because all wavevectors lie in the same plane, the helicity structure is always two dimensional and with three sets of interference terms contributing to the helicity structure (dashed lines in Fig. 2.9), it is not in general periodic, as one can see in Fig. 2.10. For the helicity structure to be periodic there have to exist two lattice vectors that have all  $\mathbf{k}_j - \mathbf{k}_l$  contributing to the helicity structure as linear combinations with integer coefficients. This condition is equivalent to all  $\mathbf{k}_j - \mathbf{k}_l$  being linear combinations with rational coefficients of two  $\mathbf{k}_j - \mathbf{k}_l$  and is satisfied if  $|\cos \theta|/(1 - |\cos \theta|) \in \mathbb{Q}$ . There exist an infinite number of angles that satisfy this condition, yielding an infinite number of different lattices, with unit cells being allowed to become arbitrarily large. In Fig. 2.11 one can see some examples of more complex helicity lattices.

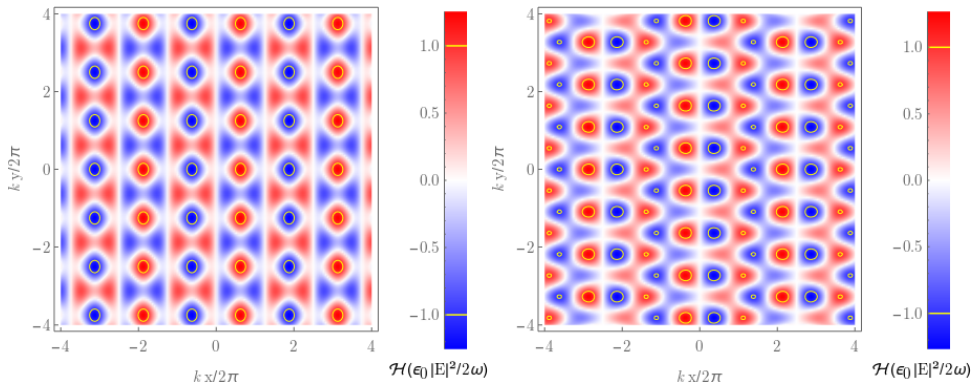
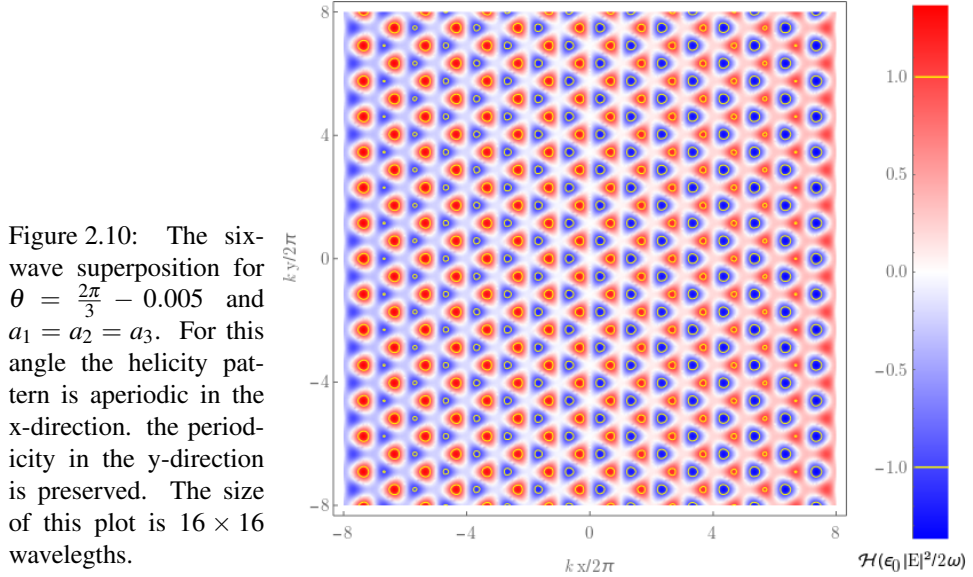


Figure 2.11: A six wave helicity lattice with  $\theta = \arccos -\frac{3}{5}$  and  $a_1 = a_2 = a_3$  (left) and with  $\theta = \arccos -\frac{2}{5}$  and  $a_1 = a_2 = a_3$  (right). The size of these plots is  $8 \times 8$  wavelengths.

## 2.4 The effects of small deviations from the exact parameters

Although the superpositions from the previous section have some parametric freedom left, the homogeneity of  $\tilde{\mathbf{E}}^* \cdot \tilde{\mathbf{E}}$  depends on the fine-tuning of at least some parameters. These parameters can be any of the parameters that specify a plane wave: amplitude, phase, polarisation or and propagation direction. In addition we assumed our light waves were perfectly coherent, which is not a realistic assumption. In this section we study the effects of imperfections of each of these properties. Amplitude, phase and polarisation errors affect small lattices as well as big ones and can be treated in a unified picture. The effects of misalignment in the propagation direction of the waves can be mitigated if the helicity lattice is of sufficiently small size and will be treated in the next subsection. The effect of limited temporally and spatially coherent waves can be mitigated if the helicity is sufficiently small too and will be treated in the last subsection.

### 2.4.1 Deviations in amplitude, phase and polarisation.

Deviations in the amplitudes, phases and polarisations of the waves constituting a noninterfering superposition from their optimal values can be treated by writing the total electric field in the following way

$$\tilde{\mathbf{E}} = \sum_{j=1}^n (\tilde{\mathbf{E}}_j + \delta\tilde{\mathbf{E}}_j) e^{i\mathbf{k}_j \cdot \mathbf{x}} \quad \text{with} \quad \delta\tilde{\mathbf{E}}_j \cdot \mathbf{k}_j = 0. \quad (2.5)$$

The different components of  $\delta\tilde{\mathbf{E}}_j$  represent the different parameters. The component parallel to and with the same complex phase as  $\tilde{\mathbf{E}}_j$  causes a deviation in the amplitude, the component parallel and  $\frac{\pi}{2}$  out of phase represents phase deviations, the component perpendicular to and with the same complex phase as  $\tilde{\mathbf{E}}_j$  represents errors in the polarisation direction and the perpendicular component  $\frac{\pi}{2}$  out of phase represents deviations in the ellipticity. Each of these components can cause residual interference in  $\tilde{\mathbf{E}}^* \cdot \tilde{\mathbf{E}}$  at first order in  $\delta\tilde{\mathbf{E}}$ . In general, the residual interference has the form:

$$\delta I_{\mathbf{k} \neq 0} = \frac{1}{4} \sum_{j \neq l}^n (\delta\tilde{\mathbf{E}}_j^* \cdot \tilde{\mathbf{E}}_l + \tilde{\mathbf{E}}_j^* \cdot \delta\tilde{\mathbf{E}}_l) e^{i(\mathbf{k}_l - \mathbf{k}_j) \cdot \mathbf{x}} + O(\delta\tilde{\mathbf{E}}^2). \quad (2.6)$$

As a measure of the quality of the superpositions we take the combined magnitude of all residual interference terms normalised by the homogeneous background field strength:

$$\frac{\sum_{j \neq l}^n \delta\tilde{\mathbf{E}}_j^* \cdot \tilde{\mathbf{E}}_l + \tilde{\mathbf{E}}_j^* \cdot \delta\tilde{\mathbf{E}}_l}{\sum_{j=1}^n \tilde{\mathbf{E}}_j^* \cdot \tilde{\mathbf{E}}_j} = \frac{(n-1) \langle |\delta\tilde{\mathbf{E}}_j^* \cdot \tilde{\mathbf{E}}_l| \rangle_{jl}}{\langle \tilde{\mathbf{E}}_j^* \cdot \tilde{\mathbf{E}}_j \rangle_j}. \quad (2.7)$$

Here  $\langle \rangle_j$  denotes averaging over all waves and  $\langle \rangle_{jl}$  denotes averaging over all pairs of different waves. The expectation value of  $|\delta\tilde{\mathbf{E}}_j|$  is assumed to be independent of its orientation. That is, all parameters have equally big errors. If this is not the case, one can set the errors in all parameters equal to the least well controlled one as a worst-case estimate. Then, as a worst-case estimate one has  $\langle |\delta\tilde{\mathbf{E}}_j^* \cdot \tilde{\mathbf{E}}_l| \rangle_{jl} \leq \langle |\delta\tilde{\mathbf{E}}_j| \rangle_j \langle |\tilde{\mathbf{E}}_l| \rangle_l \frac{1}{2\pi} \int_0^{2\pi} \cos \theta d\theta = \langle |\delta\tilde{\mathbf{E}}_j| \rangle_j \langle |\tilde{\mathbf{E}}_l| \rangle_l \frac{2}{\pi}$  giving an estimate for the residual interference of

$$\frac{2(n-1) \langle |\delta\tilde{\mathbf{E}}_j| \rangle_j \langle |\tilde{\mathbf{E}}_l| \rangle_l}{\pi \langle \tilde{\mathbf{E}}_j^* \cdot \tilde{\mathbf{E}}_j \rangle_j}. \quad (2.8)$$

From this equation one can see that the residual inhomogeneity of the helicity density is linear in polarisation, phase and polarisation errors and that superpositions of many waves are expected to have relatively larger helicity density inhomogeneities.

## 2.4.2 Deviations in the propagation direction

Deviations in the propagation direction can be described by replacing  $\mathbf{k}_j$  with  $\mathbf{k}_j + \delta\mathbf{k}_j$  where  $\mathbf{k}_j \cdot \delta\mathbf{k}_j = 0$  to keep the frequency fixed. The effects of such deviations are twofold. First, if  $\delta\mathbf{k}_j$  has a component parallel to  $\tilde{\mathbf{E}}$ , the light's polarisation must rotate accordingly to preserve transversality, introducing a change in the electric field of  $\delta\tilde{\mathbf{E}}_j = \frac{\tilde{\mathbf{E}}_j \cdot \delta\mathbf{k}_j}{|\mathbf{k}_j|}$ . Second, a pair of supposedly cancelling interference terms do not cancel exactly anymore, leading to a beating pattern in the field strength. Around the nodes the root mean square of the electric field is relatively homogeneous and one can have a finite size low-interference region of size  $L$  if

$$\delta\mathbf{k}_j < \frac{A_{\max}}{LA_{\text{int}}}, \quad (2.9)$$

with  $A_{\max}$  the maximal tolerable amplitude of  $\tilde{\mathbf{E}}^* \cdot \tilde{\mathbf{E}}$ -fluctuations and  $A_{\text{int}}$  the amplitude of a single interference term.

## 2.4.3 Partially coherent light

In order to treat partial coherence, we will make some simplifying assumptions. We assume that all superposed waves originate from the same parent wave. Once separated, each individual wave has its polarisation changed and its amplitude reduced to the required amplitude and its phase shifted by the required amount. Then we assume that all waves have traversed the same optical path length in the origin of our coordinate system, where they are also perfectly spatially coherent. If one superposes more than two waves, there is generically not one point which satisfies these conditions for all waves, but it is a useful assumption for illustrating the effects of partial coherence. Any neglected errors in traversed optical paths and spatial alignment will result in further attenuations of the helicity pattern, as will any decoherence that the waves obtain after being split off. We will furthermore illustrate the effects of partial coherence with (for a laser) exaggeratedly short coherence lengths to make the effects more visible.

Using these assumptions, a single temporal and a single spatial autocorrelation function,  $g_t^{(1)}(\tau)$  and  $g_s^{(1)}(r)$  suffice to describe the effects of partial coherence on the lattice. Details and derivations of these functions are given in appendix A. We will use autocorrelation functions with only a few phenomenological parameters:  $g_t^{(1)}(\tau) = e^{-i\omega_0\tau - \frac{\delta\omega^2\tau^2}{2} - \Gamma_c|\tau|}$  and  $g_s^{(1)}(r) = e^{-\kappa|r|}$ .

Partial coherence affects helicity interference in the same way it affects the normal electric field interference. It attenuates the interference fringes proportionally to the absolute value of the autocorrelation function. For our helicity lattices, we need to consider the effect of partial coherence on each helicity interference term separately before adding them together. The interference fringes will be attenuated differently in different directions. Along the direction  $\mathbf{k}_j \times \mathbf{k}_l$ , our simplified model predicts no attenuation of the helicity fringes. If one takes two waves with wave vectors  $\mathbf{k}_j$  and  $\mathbf{k}_l$ , then along the direction  $\mathbf{k}_j - \mathbf{k}_l$  the difference in the travelled optical paths changes and the temporal autocorrelation function determines the amplitude of the helicity fringes which become proportional

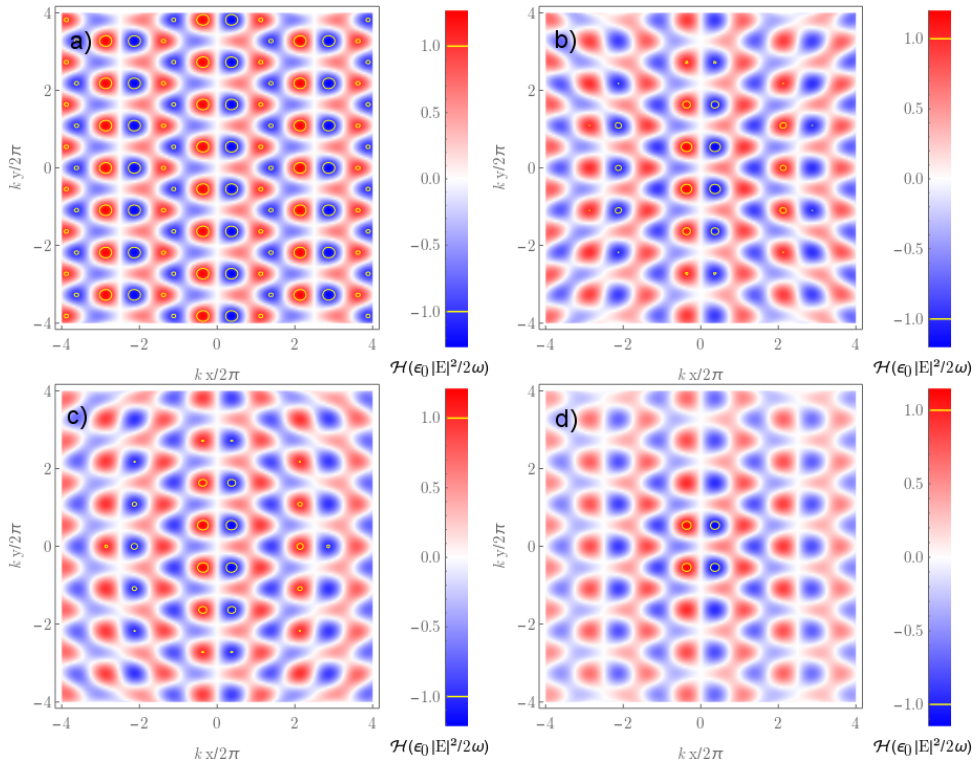


Figure 2.12: a) A six wave helicity lattice with perfectly coherent plane waves. b) Temporally incoherent waves due to collision broadening with a coherence length of eight wavelengths ( $\Gamma_c = 1/16\pi$ ). c) Spatially incoherent waves with a coherence length of eight wavelengths ( $\kappa = 1/16\pi$ ). d) The effects of b) and c) combined. In spite of choosing parameters such as to make the temporal and spatial autocorrelation functions as similar as possible, temporal and spatial partial coherence still yield different helicity structures, as can be seen by comparing b) and c). Interestingly, combining both effects with the same coherence length removes all deformation from the helicity lattice, leaving only the attenuation of the helicity maxima and -minima, as can be seen in d).

to  $g_r^{(1)}((\mathbf{k}_j - \mathbf{k}_l) \cdot \mathbf{x}/\omega)$ . Along the direction  $\mathbf{k}_j + \mathbf{k}_l$  the difference in travelled optical path lengths between the two waves remains constant, but due to the opposite components of  $\mathbf{k}_j$  and  $\mathbf{k}_l$  perpendicular to this direction, the wave fronts get shifted relative to each other and the spatial autocorrelation function will determine the attenuation of the helicity fringes. The attenuation of the helicity fringes is different in this direction, not only because of a different autocorrelation function, but also because the distance over which the waves shift parallel to their wavefronts is computed differently. We have a proportionality (appendix A) to  $g_s^{(1)}\left(2\sqrt{\frac{1}{2} - \frac{1}{2}\cos(\mathbf{k}_1 \cdot \mathbf{k}_2/c^2\omega^2)}\mathbf{x} \cdot (\mathbf{k}_1 + \mathbf{k}_2)/|\mathbf{k}_1 + \mathbf{k}_2|\right)$ . With these attenuations of a single helicity interference term, one can construct helicity lattices of superpositions of many waves. A six wave example is given in Fig 2.12. Both temporal and spatial partial coherence cause an attenuation of the helicity maxima and -minima, but on top of that they distort the helicity lattice because they do not attenuate equally strong in all directions.

## 2.5 Recording helicity patterns with liquid crystals

A inhomogeneous helicity pattern cannot be recorded on a regular photographic film or CCD, since these are only sensitive to the root-mean-square electric field strength. For recording an image of one of the helicity lattices we presented, one would need a kind of helicity sensitive film.

Over the past twenty years a rich variety of liquid crystal polymers were discovered that become chiral under illumination with circularly polarised light [130–138]. The literature on the topic is far too broad to be covered here in full, but it suffices to note that the compounds that show this behaviour are either polymers with long light-absorbing side chains that twist themselves into helices under illumination [130–132, 134, 136] or propeller shaped molecules that can stack themselves in either a left- or a right-handed helix [135, 137, 138]. The permanence of the induced chirality varies a lot between compounds. Some have their chirality erased by illumination with the opposite polarisation [132, 134] or by heating [135], others can have their chirality fixated [138]. Light intensities used to achieve this chirality are on the order of tens or hundreds of milliwatt per square centimetre and illumination takes up to an hour [132, 134, 138]. Several applications for these compounds have been tested, such as an optical polarisation switch [139] and chiral second harmonic generation [137]. So far, these compounds were only used in combination with homogeneously polarised light. Helicity lattices can imprint an inhomogeneous chirality into a polymer film, making it possible to either use the polymer as ‘chiral’ film to record the helicity structure of the light or using the light to write helicity-sensitive optical components into a polymer film. For example, the helicity patterns from Fig. 2.11 can serve as arrays of chiral waveguides that guide light of one helicity only. The kind of polymer one would want for imprinting chiral structures is one that can chirally assemble under exposure with a helicity lattice and then have its supramolecular structure fixated by a process that works equally well on both enantiomers, yielding an imprint that remains stable at high temperatures and light intensities.



## 2.6 Some remarks on the mathematics of noninterfering superpositions

I have shown superpositions with homogeneous mean squared electric field of up to six plane waves. We do not know if there is an upper bound to the number of plane waves that can be superposed in this way, but we suspect there is, because the number of interference terms increases faster than the number of free parameters available.

For every superposition of four or more plane waves shown either  $\tilde{\mathbf{E}}^* \cdot \tilde{\mathbf{E}}$  or  $\tilde{\mathbf{H}}^* \cdot \tilde{\mathbf{H}}$  is inhomogeneous. We believe there cannot exist a superposition of four or more plane waves with both of them homogeneous but this conjecture is unproven. Similarly the conjecture that when superposing three or more waves either  $\tilde{\mathbf{E}}^* \cdot \tilde{\mathbf{E}}$ ,  $\tilde{\mathbf{H}}^* \cdot \tilde{\mathbf{H}}$  or  $\tilde{\mathbf{E}}^* \cdot \tilde{\mathbf{H}}$  is inhomogeneous is unproven, although we suspect this to be the case as well.

Every noninterfering superposition of four or more waves we know about has all light waves linearly polarised and introducing elliptically polarised waves in any of them will lead to interference. This made me believe that all waves being linearly polarised is a requirement for every noninterfering superposition of three or more waves.

As far as we know, none of the above problems have been formulated before.

## 2.7 Conclusion

The examples given in this chapter show that superpositions of more than three plane waves with a homogeneous root-mean-square electric field can exist and that there exists a large variety of them. Apart from being an optics curiosity, noninterfering superpositions of more than three waves raise new mathematical challenges and provide new ways to probe and manipulate chiral matter. There is a large variety of possible helicity patterns, of which we only have shown a sample. For all helicity lattices the lattice spacing scales with the wavelength of the light and there is no size limit other than the technical ability to superpose multiple coherent beams of light at the desired wavelength. One can imagine X-ray helicity lattices with unit cells the size of atoms or radio wave lattices with unit cells bigger than a house.

The commonness of ‘bright region’ superchirality among noninterfering superpositions is surprising. We expect that it can occur as well if  $\tilde{\mathbf{E}}^* \cdot \tilde{\mathbf{E}}$  is inhomogeneous.



## **Part II**



## A note on units and conventions

The next two chapters will concern the dynamics of electrons in a homogeneous magnetic field using analytical solutions of the Dirac equation.

We will use the following conventions:  $\text{diag}(+ - - -)$  as our metric signature, energies are expressed in eV,  $c = \hbar = 1$ ,  $\epsilon_0 = \mu_0 = \frac{1}{4\pi}$ . These conventions imply  $|e| = \sqrt{\alpha} \approx 1/\sqrt{137}$ . We will use the standard representation for the Dirac matrices

$$\gamma_0 = \begin{bmatrix} \mathbb{I} & 0 \\ 0 & -\mathbb{I} \end{bmatrix}, \quad \vec{\gamma} = \begin{bmatrix} 0 & \vec{\sigma} \\ -\vec{\sigma} & 0 \end{bmatrix} \quad (2.10)$$

and use slashes to denote contractions with Dirac matrices. We designate spins and angular momenta pointing in the direction of the magnetic field lines as positive and spins and angular momenta pointing against the magnetic field lines as negative. As results for different magnetic field strengths are often related by a simple scaling law we will use the rescaled radial coordinate  $\tilde{r} = \sqrt{|B|/2}r$ , or in cartesian coordinates  $\tilde{x} = \sqrt{|e|B/2}x$ ,  $\tilde{y} = \sqrt{|e|B/2}y$  to simplify our expressions. At a field strength of one Tesla  $\tilde{r} = 1$  corresponds to 36 nanometre.



## Chapter 3

# Nonuniform currents and spins of relativistic electron vortices in a magnetic field

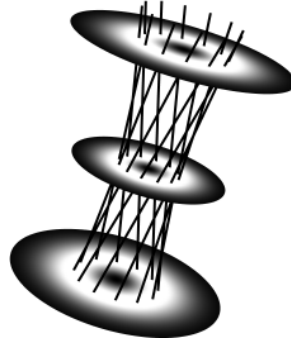
### 3.1 Introduction

All matter is quantum mechanically described by a wave function which obeys a partial differential equation similar to a wave equation. Therefore the same effects that are known to occur for light or sound waves can be seen as well for any type of matter, albeit with more effort. A well known example is interference which has been shown to occur for electrons [140, 141], neutrons, [142–144], atoms [145] molecules [127, 146], even fairly large molecules [128], and Bose-Einstein condensates containing millions of atoms [147]. In some experiments the buildup of the interference pattern could be recorded, showing that the particles of matter have a very small size compared to the spatial extent of their wave functions [148–151].

Vortex beams similarly appear for different sorts of matter. Vortex beams made from different kinds of matter have different properties, but certain features appear in all of them. These ‘vortex beam’ features are a cylindrically symmetric wave function with a well defined quantised angular momentum of  $l\hbar$  per particle along the symmetry axis (beam axis) stemming from an  $e^{il\phi}$  azimuthal phase factor in the wave function. Furthermore the wave function is zero in the centre of the beam implying a zero probability density for finding particles there (a dark spot). The size of this dark spot becomes larger and its edges become sharper with higher  $|l|$ . Neutron vortex beams do exist [152], but our main interest here are electrons.

An illustrative analogue of a vortex beam in terms of classical trajectories is a family of free particle trajectories (straight lines) which are all tilted relative to the beam axis, thus providing the angular momentum. For a charged particle in a magnetic field the classical trajectories are not straight lines, but spirals around the magnetic field lines. thus an electron vortex beam travelling along the magnetic field lines can be, using the same analogue, viewed as a collection of classical spiralling trajectories. The problem with this analogy is that the Lorentz force allows a classical particle to spiral in only one direction. When looking against the direction of the magnetic field lines, a negatively charged particle always

Figure 3.1: A free vortex beam can be pictured as a collection of classical trajectories which are tilted with respect to the beam axis.



spirals counterclockwise and a positively charged particle always spirals clockwise. Yet if one solves the Schrödinger equation one finds electron vortex beams in a magnetic field with orbital quantum numbers  $l$  of both signs suggesting that electrons can spiral in both directions [153]. A closer inspection of the electron current in the negative  $l$  vortex beams reveals that it is counterclockwise on the outside of the beam, as dictated by the Lorentz force law, but clockwise on the inside. One can say that the counterclockwise spiralling outer current shields the interior of the beam, enabling the clockwise spiralling in spite of the external magnetic field. But this current distribution persists for arbitrarily weak beam intensities for which the currents are too small to shield off the external magnetic field. Thus the negative  $l$  vortex beams in a magnetic field should be viewed as a wave mechanics phenomenon with no particle trajectory analogue.

Electron beams from a transmission electron microscope are not spin polarized and can be theoretically treated with the scalar Schrödinger equation form most vortex based electron microscopy techniques [43, 45, 48, 49, 61, 62] and many not microscopy-related processes [57, 154, 155]. There are, however, scattering processes where the spin cannot be neglected [58, 59], and even when spin polarised electron vortex beams are not experimentally feasible, assuming they can exist and studying the influence of the spin and orbital degrees of freedom on each other can give new insights in the inner dynamics of electron vortex beams [156–159].

The main topic of this chapter is the electron travelling through a magnetic field. The magnetic field breaks time reversal symmetry, causing the profile of an electron beam travelling along the field lines to rotate counterclockwise, looking against the field lines [153, 160–163], an effect that can be replicated for light only with much more difficulty [164, 165]. The magnetic field also acts as a guide for electron beams, keeping their widths constant as they travel [153, 160–163]. The main motivation for this chapter is the strong interaction between the electron's spin and the magnetic field, which thus far has been ignored for electron vortex beams.

We analytically solve the Dirac equation for an electron in a homogeneous magnetic field, a problem first considered by Rabi [64], who found an incomplete set of solutions, and studied in more detail by Landau [65, 166]. The interaction with the magnetic field confines the beam and gives rise to a set of discrete energy levels (Landau levels) [65, 153]. On top of that the Zeeman effect shifts the energy of the spin up and -down states relative to each other. The quantised Landau and Zeeman contributions to the energy determine which states undergo spin-orbit mixing with each other and completely forbid spin-orbit mixing for some of them. The inclusion of spin also leads to a (for some states large) redistribution of the azimuthal current within the beam, revealing a pattern of concentric



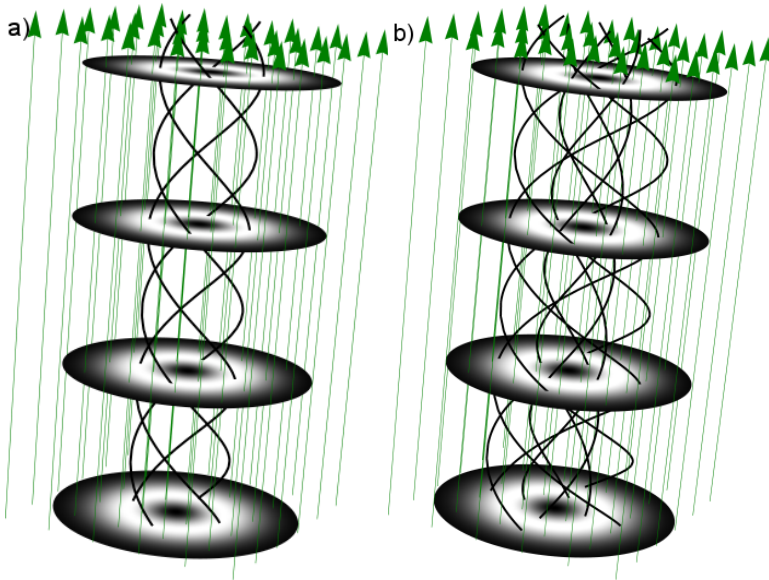


Figure 3.2: a) An electron vortex beam travelling along the magnetic field lines (green) can be intuitively understood as a particle performing a spiral motion (black curves). For an electron spiralling counterclockwise when looking against the field lines, this description makes intuitive sense. But electron vortex beams with the opposite angular momentum quantum number can exist in a magnetic field too and these require a more sophisticated picture to describe them, as shown in b). although their beam profiles look the same, the opposite angular momentum beam has a more complicated current structure with the current spiralling counterclockwise on the outside of the beam, but clockwise on the inside.

rings of clockwise and counterclockwise rotating current.

By introducing an electric quadrupole field to the homogeneous magnetic field, one obtains the field configuration of a Penning trap [167]. Penning traps are used for storing a single charged particle for a long time for high precision spectroscopy, a method that yielded, among others, the most accurate measurement of the electron's anomalous magnetic moment [168]. The Penning trap configuration is not exactly solvable for relativistic electrons, because along the magnetic field direction, the electrons experience a harmonic oscillator potential. The harmonic oscillator is nonrelativistically exactly solvable, but not relativistically. It would certainly be interesting to extend our findings to the Penning trap configuration using the nonrelativistic Pauli equation or through a suitable approximation within the relativistic formalism, but for this chapter, which focuses on exact relativistic solutions, the Penning trap configuration is not included.

## 3.2 Electron beams in a magnetic field and their spin-orbit structure

A magnetic field can be incorporated in the Dirac equation using the gauge covariant momentum operator  $P_\mu = p_\mu - eA_\mu = i\partial_\mu - eA_\mu$ , with  $A_\mu$  the vector potential and  $e$  the electron charge. Choosing the magnetic field in the positive z-direction we take the vector potential  $A_\mu = \frac{1}{2}B(0, -y, x, 0)$ , with  $B$  the magnitude of the magnetic field. Using cylindrical coordinates and first solving the 'squared' Dirac equation  $(\not{P} + m_e)(\not{P} - m_e)\Psi = 0$ , we assume a solution of the form  $\Psi = e^{i(pz - \mathcal{E}t + l\phi)}\psi(\tilde{r})u$ , with  $\mathcal{E}$  the total energy and  $u$  a constant bispinor to obtain for the radial and spin components

$$\frac{B|e|}{2} \left( \frac{1}{\tilde{r}} \partial_{\tilde{r}} \tilde{r} \partial_{\tilde{r}} - \frac{l^2}{\tilde{r}^2} - 2l - \tilde{r}^2 - 2\Sigma_z \right) \psi(\tilde{r})u = -(\mathcal{E}_L^2 + \mathcal{E}_Z^2) \psi(\tilde{r})u, \quad (3.1)$$

with  $\Sigma_i = \text{diag}(\hat{\sigma}_i, \hat{\sigma}_i)$ , and  $\hat{\sigma}_i$  the Pauli matrices. The interaction energy of the electrons spin magnetic moment is  $\mathcal{E}_Z^2 = 2\sigma_z B|e|$  (=Zeeman energy,  $\sigma_z = \pm \frac{1}{2}$ ). Here  $\mathcal{E}_L$  is the sum of the electrons orbital kinetic energy and the interaction energy of the orbital magnetic moment (Landau energy). An important field strength for this problem is the field where  $B|e| = m^2$ . This is the critical field strength where the Zeeman splitting becomes equal to the rest mass. Reinserting the factors of  $\hbar$  and  $c$  gives for the critical field  $B_c = m^2 c^2 / |e| \hbar = 4.4 \cdot 10^9$  T. The radial differential equation has the well-known solution [65, 153]

$$\psi(\tilde{r}) = Lg_n^l(\tilde{r}), \quad \mathcal{E}_L^2 = B|e|(2n + l + |l| + 1) \quad (3.2)$$

with  $Lg(\tilde{r})$  the radial part of the Laguerre-Gauß function:  $Lg_n^l(\tilde{r}) = \tilde{r}^{|l|} L_n^{|l|}(\tilde{r}^2) e^{-\frac{\tilde{r}^2}{2}}$ , with  $L_n^{|l|}$  an associated Laguerre polynomial. With this radial solution, the full solution of the squared Dirac equation can be written using a Laguerre-Gauß function,  $LG_n^l(\tilde{r}, \phi) = e^{il\phi} Lg_n^l(\tilde{r})$ . The full solution is

$$\Psi = e^{i(pz - \mathcal{E}t)} LG_n^l(\tilde{r}, \phi) \left( \begin{bmatrix} 1 \\ 0 \\ 0 \\ 0 \end{bmatrix} \vee \begin{bmatrix} 0 \\ 1 \\ 0 \\ 0 \end{bmatrix} \right), \quad \begin{aligned} \mathcal{E} &= \sqrt{m_e^2 + k^2 + \mathcal{E}_L^2 + \mathcal{E}_Z^2} \\ &= \sqrt{m_e^2 + k^2 + B|e|(2n + l + |l| + 2\sigma + 1)} \\ &= \sqrt{m_e^2 + k^2 + 2B|e|N} \\ N &\equiv n + \frac{1}{2}(l + |l|) + \sigma + \frac{1}{2} \end{aligned} \quad (3.3)$$

For negative orbital angular momentum  $\mathcal{E}_L^2$  is independent of  $l$  because the kinetic and magnetic contributions cancel. These solutions are nondiffracting Laguerre-Gauß beams, with  $p$  the radial quantum number indicating how many rings surround the central spot or ring. The solutions of the squared Dirac equation describe superpositions of positive and negative energy states. To project out the positive energy states one applies  $\not{P} + m$  to the solutions of the squared Dirac equation. The exact solutions of the first order Dirac equation can be obtained by applying  $\not{P} + m_e$  to the solutions of the squared Dirac equation using

$$\begin{aligned} (\not{P} + m) \begin{bmatrix} 1 \\ 0 \\ 0 \\ 0 \end{bmatrix} &= \begin{bmatrix} i\partial_t + m_e \\ 0 \\ -i\partial_z \\ \sqrt{\frac{|e|B}{2}}(-i\partial_{\tilde{x}} - \partial_{\tilde{y}} - (i\tilde{x} + \tilde{y})) \end{bmatrix}, \\ (\not{P} + m_e) \begin{bmatrix} 0 \\ 1 \\ 0 \\ 0 \end{bmatrix} &= \begin{bmatrix} 0 \\ i\partial_t + m \\ \sqrt{\frac{|e|B}{2}}(-i\partial_{\tilde{x}} - \partial_{\tilde{y}} - (i\tilde{x} + \tilde{y})) \\ -i\partial_z \end{bmatrix}. \end{aligned} \quad (3.4)$$

The de derivatives with respect to  $t$  and  $z$  are easy to compute and give resp.  $\mathcal{E}$  and  $p$ . The components  $\sqrt{|e|B/2}(-i\partial_{\tilde{x}} + \partial_{\tilde{y}} + (i\tilde{x} - \tilde{y}))$  and  $\sqrt{|e|B/2}(-i\partial_{\tilde{x}} - \partial_{\tilde{y}} - (i\tilde{x} + \tilde{y}))$  give rise to the spin-orbit mixing terms, whose explicit computation is rather lengthy. The following three identities will be of use

$$\begin{aligned} (\partial_{\tilde{x}} \pm i\partial_{\tilde{y}})\tilde{r}^n &= n\tilde{r}^{n-1}e^{\pm i\phi}, \\ (\partial_{\tilde{x}} \pm i\partial_{\tilde{y}})\tilde{r}^{|n|}e^{\pm i|n|\phi} &= 0, \\ (\partial_{\tilde{x}} \pm i\partial_{\tilde{y}})\tilde{r}^{|n|}e^{\mp i|n|\phi} &= 2|n|\tilde{r}^{|n|-1}e^{\pm i(|n|-1)\phi}. \end{aligned} \quad (3.5)$$

The form of the spin-orbit term depends on the signs of the spin and orbital angular momentum (OAM). We thus have to compute four different expressions for each of the four combinations of spin up and -down and positive and negative OAM.

For spin up and OAM positive, one has (using eqs. (B.15) and (B.17))

$$\begin{aligned} \sqrt{|e|B/2}(-i\partial_{\tilde{x}} + \partial_{\tilde{y}} + (i\tilde{x} - \tilde{y}))e^{i(pz - \mathcal{E}t)}LG_n^l(\tilde{r}, \phi) &= \\ i\sqrt{2|e|B} \left( e^{i(pz - \mathcal{E}t + (l+1)\phi)}\tilde{r}^{|l|+1}e^{-\frac{\tilde{r}^2}{2}} \left( L_n^{|l|}(\tilde{r}^2) - L_n^{|l|}(\tilde{r}^2) \right) \right) &= \\ = i\sqrt{2|e|B}e^{i(pz - \mathcal{E}t)}LG_n^{l+1}(\tilde{r}, \phi). \end{aligned} \quad (3.6)$$

Now for positive OAM and spin down, the spin-orbit term is (using eqs. (B.17) and (B.24))

$$\begin{aligned} \sqrt{|e|B/2}(-i\partial_{\tilde{x}} - \partial_{\tilde{y}} - (i\tilde{x} + \tilde{y}))e^{i(pz - \mathcal{E}t)}LG_n^l(\tilde{r}, \phi) &= \\ i\sqrt{2B|e|}e^{i(pz - \mathcal{E}t + (l-1)\phi)}\tilde{r}^{l-1}e^{-\frac{\tilde{r}^2}{2}} \left( -lL_n^{|l|}(\tilde{r}^2) - \tilde{r}^2L_n^{|l|}(\tilde{r}^2) \right) &= \\ = -i\sqrt{2B|e|}(n + |l|)e^{i(pz - \mathcal{E}t)}LG_n^{l-1}(\tilde{r}, \phi). \end{aligned} \quad (3.7)$$

For negative OAM and spin up, one has (using eqs. (B.23) and 9B.24))

$$\begin{aligned} \sqrt{|e|B/2}(-i\partial_{\tilde{x}} + \partial_{\tilde{y}} + (i\tilde{x} - \tilde{y}))e^{i(pz - \mathcal{E}t)}LG_n^l(\tilde{r}, \phi) = \\ i\sqrt{2|e|B}e^{i(pz - \mathcal{E}t + (l+1)\phi)}\tilde{r}^{l-1}e^{-\frac{\tilde{r}^2}{2}}\left(\tilde{r}^2L_n^{|l|}(\tilde{r}^2) - |l|L_n^{|l|}(\tilde{r}^2) - \tilde{r}^2L_n^{|l|}(\tilde{r}^2)\right) \\ = -i\sqrt{2B|e|}(n+1)e^{i(pz - \mathcal{E}t)}LG_{n+1}^{l+1}(\tilde{r}, \phi). \end{aligned} \quad (3.8)$$

The case of negative orbital angular momentum and spin is simple, one has (using eq. (B.15))

$$\sqrt{|e|B/2}(-i\partial_{\tilde{x}} - \partial_{\tilde{y}} - (i\tilde{x} + \tilde{y}))e^{i(pz - \mathcal{E}t)}LG_n^l(\tilde{r}, \phi) = i\sqrt{2|e|B}e^{i(pz - \mathcal{E}t)}LG_{n-1}^{l-1}(\tilde{r}, \phi). \quad (3.9)$$

Substituting these answers back into eq. (3.4) yields the physical solutions

$$\begin{aligned} \Psi = e^{i(pz - \mathcal{E}t)} \left( LG_n^l(\tilde{r}, \phi) \begin{bmatrix} m_e + \mathcal{E} \\ 0 \\ p \\ 0 \end{bmatrix} + iLG_n^{l+1}(\tilde{r}, \phi) \begin{bmatrix} 0 \\ 0 \\ 0 \\ \sqrt{2B|e|} \end{bmatrix} \right), \\ \text{spin} > 0, \text{ OAM} \geq 0, \end{aligned} \quad (3.10)$$

$$\begin{aligned} \Psi = e^{i(pz - \mathcal{E}t)} \left( LG_n^l(\tilde{r}, \phi) \begin{bmatrix} 0 \\ m_e + \mathcal{E} \\ 0 \\ -p \end{bmatrix} - i(n+l)e^{-i\phi}LG_n^{l-1}(\tilde{r}, \phi) \begin{bmatrix} 0 \\ 0 \\ \sqrt{2B|e|} \\ 0 \end{bmatrix} \right), \\ \text{spin} < 0, \text{ OAM} > 0, \end{aligned}$$

$$\begin{aligned} \Psi = e^{i(pz - \mathcal{E}t)} \left( LG_n^l(\tilde{r}, \phi) \begin{bmatrix} m_e + \mathcal{E} \\ 0 \\ p \\ 0 \end{bmatrix} - i(n+1)LG_{n+1}^{l+1}(\tilde{r}, \phi) \begin{bmatrix} 0 \\ 0 \\ 0 \\ \sqrt{2B|e|} \end{bmatrix} \right), \\ \text{spin} > 0, \text{ OAM} < 0, \end{aligned}$$

$$\begin{aligned} \Psi = e^{i(pz - \mathcal{E}t)} \left( LG_n^l(\tilde{r}, \phi) \begin{bmatrix} 0 \\ m_e + \mathcal{E} \\ 0 \\ -p \end{bmatrix} + iLG_{n-1}^{l-1}(\tilde{r}, \phi) \begin{bmatrix} 0 \\ 0 \\ \sqrt{2B|e|} \\ 0 \end{bmatrix} \right), \\ \text{spin} < 0, \text{ OAM} \leq 0, \end{aligned}$$

Whenever we derive an expression which is different for these four solutions, we put the corresponding expressions in the same order. The second term in the brackets is the spin-orbit mixing term, which appears because orbital angular momentum is not a good quantum number [66].

Of particular interest is the last expression (negative spin and orbital angular momentum). Rewriting  $L_{n-1}^{l+1} = -L_n^l$  (eq. (B.15)), one sees that the spin-orbit term is zero for  $n = 0$ . The lack of spin-orbit mixing for these states stems from all states having a well defined angular momentum and squared energy. The Zeeman effect shifts the squared energy upwards by  $\mathcal{E}_Z^2 = B|e|$  for the states with spin up and downwards by the same amount for the states with spin down. The Landau quantization generates a squared energy ladder with level spacing  $\Delta\mathcal{E}_Z^2 = 2B|e|$ , twice the Zeeman shift. So the spin up states are shifted upward one level compared to the spin down states (FIG. 3.3) and for the lowest lying states

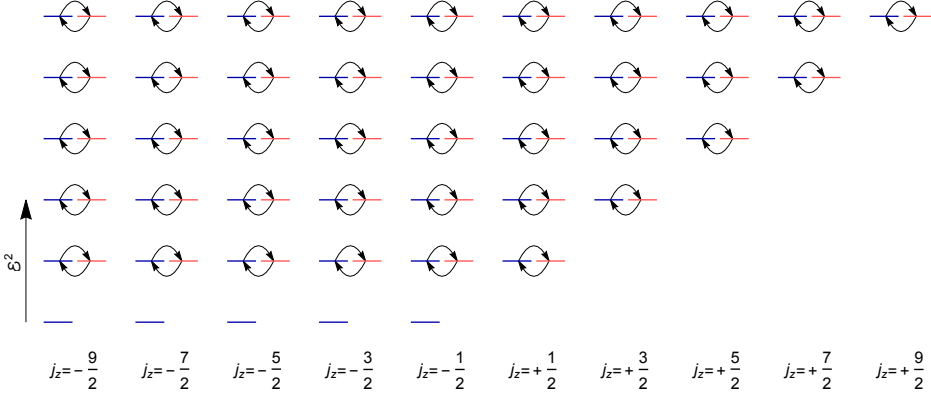


Figure 3.3: The energy levels for a fixed value of  $k$  sorted by their total angular momentum. The states with spin up (red) have one quantum of squared energy more than the states with spin down (blue). Thus the ground states are not degenerate with any opposite spin states and cannot spin-orbit mix as indicated by the arrows.

with spin down there is no spin up state with equal squared energy they can spin-orbit mix with. Without the spin-orbit mixing term, the wave function factorizes into a product state of a constant bispinor and a scalar function. Typically, both for light and electrons, such a simple separation in a spin part and a spatial part is not possible, making these negative angular momentum  $p = 0$  states quite special. This clean separation of spin and orbital angular momentum also makes the ground states perfectly spin polarized, a condition which otherwise has only been achieved with a more complicated combination of magnetic and electric fields [169, 170] high loss of beam intensity [63] or extremely high laser intensities [171, 172].

### 3.3 Detailed analysis of the current structure

The detailed charge flow within the beam can be computed using the four current  $j_\mu = \Psi^\dagger \gamma_0 \gamma_\mu \Psi$ . Integrating its zeroth component over the entire transverse plane gives a useful normalization factor. Using eq. (B.26) and  $rdr = \frac{2}{B|e|} \tilde{r} d\tilde{r}$ , the integrated probability density is evaluated to be resp.

$$\begin{aligned}
 \int j_0 &= \frac{2\pi}{B|e|} \frac{(l+n)!}{n!} (m_e^2 + \mathcal{E}^2 + 2m_e\mathcal{E} + k^2 + 2B|e|(|l| + n + 1)), \\
 \int j_0 &= \frac{2\pi}{B|e|} \frac{(l+n)!}{n!} (m_e^2 + \mathcal{E}^2 + 2m_e\mathcal{E} + k^2 + 2B|e|(|l| + n)), \\
 \int j_0 &= \frac{2\pi}{B|e|} \frac{(l+n)!}{n!} (m_e^2 + \mathcal{E}^2 + 2m_e\mathcal{E} + k^2 + 2B|e|(n + 1)), \\
 \int j_0 &= \frac{2\pi}{B|e|} \frac{(l+n)!}{n!} (m_e^2 + \mathcal{E}^2 + 2m_e\mathcal{E} + k^2 + 2B|e|n).
 \end{aligned} \tag{3.11}$$

The last term in the brackets is in each case  $\mathcal{E}_L^2 + \mathcal{E}_Z^2$ . Using  $\mathcal{E} = \sqrt{m_e^2 + k^2 + \mathcal{E}_L^2 + \mathcal{E}_Z^2}$ , the integrated probability density can in each case be written as  $\int j_0 = (4\pi/B|e|)\mathcal{E}(\mathcal{E} + m_e)(l+n)!/n!$ .

The current in the z-direction is

$$j_z = 2p(m_e + \mathcal{E})LG_n^l(\tilde{r}^2)LG_n^{l*}(\tilde{r}^2). \quad (3.12)$$

The spin-orbit term is completely absent from this expression, something which applies to beam-like solutions of the Dirac equation in general. Spin-orbit mixing has been an important motivation for treating electron vortex beams relativistically in the absence of external fields [156] and it is an important motivation for our work, too. Unfortunately most detectors measure the electron beam current through an aperture perpendicular to the beam axis and not the local electron density and they therefore cannot detect spin-orbit effects. In addition, for any realistic electron beam, spin-orbit effects will be very small. Starting from a solution of the squared Dirac equation,  $\psi$ , one can find that the magnitude of the spin-orbit term is

$$((P_x \pm iP_y)\psi)^*(P_x \pm iP_y)\psi/\int j_0 \sim \langle P_x^2 + P_y^2 \mp eB_z \rangle/\mathcal{E}(\mathcal{E} + m_e). \quad (3.13)$$

this expression becomes only nonnegligible for magnetic fields on the order of the critical field ( $4.4 \cdot 10^9$  T) or transverse momenta on the order of the reciprocal Compton wavelength of the electron. Such high transverse momenta would imply a beam focused down to a width on the order of the Compton wavelength (386 fm), which requires impractically strong focusing of high energy electron beams. The total current in the z-direction through the transverse plane is

$$\int j_z = \int j_0 \frac{p}{\mathcal{E}},$$

so the electrons have the same speed as particles with mass  $\sqrt{m^2 + \mathcal{E}_L^2 + \mathcal{E}_Z^2}$ .

For the transverse current components one can transform the Dirac matrices into

$$\begin{aligned} \gamma_r &= \cos \phi \gamma_x + \sin \phi \gamma_y = \begin{bmatrix} 0 & 0 & 0 & e^{-i\phi} \\ 0 & 0 & e^{i\phi} & 0 \\ 0 & -e^{-i\phi} & 0 & 0 \\ -e^{i\phi} & 0 & 0 & 0 \end{bmatrix}, \\ \gamma_\phi &= -\sin \phi \gamma_x + \cos \phi \gamma_y = \begin{bmatrix} 0 & 0 & 0 & -ie^{-i\phi} \\ 0 & 0 & ie^{i\phi} & 0 \\ 0 & ie^{-i\phi} & 0 & 0 \\ -ie^{i\phi} & 0 & 0 & 0 \end{bmatrix}. \end{aligned} \quad (3.14)$$

The radial component is always zero. For the azimuthal component one can compute:

$$\begin{aligned} j_\phi &= 2\sqrt{2B|e|}(\mathcal{E} + m_e)Lg_n^l(\tilde{r})Lg_n^{l+1}(\tilde{r}), \\ j_\phi &= 2\sqrt{2B|e|}(\mathcal{E} + m_e)(n+l)Lg_n^l(\tilde{r})Lg_n^{l-1}(\tilde{r}), \\ j_\phi &= -2\sqrt{2B|e|}(\mathcal{E} + m_e)(n+1)Lg_n^l(\tilde{r})Lg_{n+1}^{l+1}(\tilde{r}), \\ j_\phi &= -2\sqrt{2B|e|}(\mathcal{E} + m_e)Lg_n^l(\tilde{r})Lg_{n-1}^{l-1}(\tilde{r}). \end{aligned} \quad (3.15)$$

These expressions are quite different from the azimuthal currents for scalar vortex beams

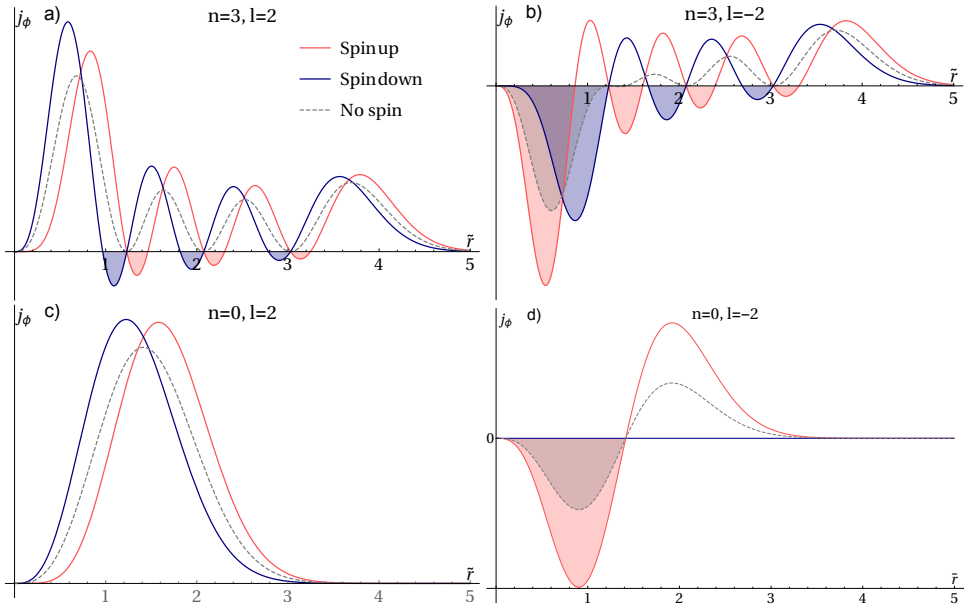


Figure 3.4:  $j_\phi$  For spin up (red), spin down (blue) and a spin 0 beam for comparison (dashed) for  $l = 2, n = 3$  (a),  $l = -2, n = 3$  (b),  $l = 2, n = 0$  (c) and  $l = -2, n = 0$  (d). The spin part of the current gives rise to a series of dips where the current flows in the opposite direction, which are absent when spin is neglected. For negative  $l$ , the azimuthal current is negative near the centre but positive on the outside due to the interaction with the magnetic field. The most striking difference from a spin 0 vortex beam occurs for negative  $l$  and  $n = 0$  where negative spin is a Landau-Zeeman ground state and the azimuthal current is exactly zero everywhere.

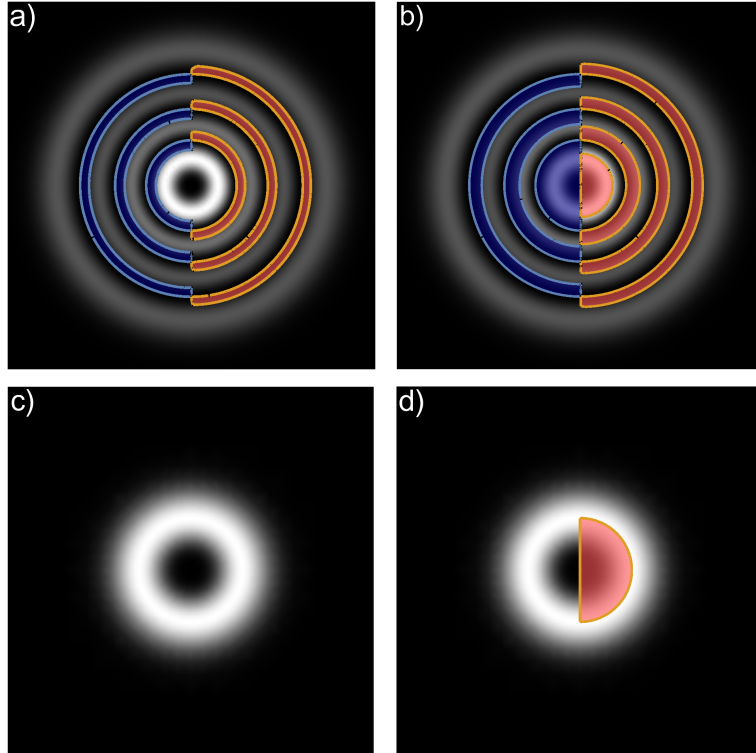


Figure 3.5: The regions of negative(=clockwise) azimuthal electron current marked for the  $n = 3, l = 2$  state (a) and  $n = 3, l = -2$  (b),  $n = 0, l = 2$  (c) and  $n = 0, l = -2$  for spin down (left side, in blue) and -up (right side, in red) superposed on the beam profiles for a magnetic field of 1 Tesla. The negative currents occur on the inner side of the dark fringes for spin up and on the outer side for spin down. Visible rearrangement of the electron density due to spin-orbit mixing only appears around the critical field of  $4.4 \cdot 10^9$  T.

in a magnetic field [153], because the spin contribution is included in them as well [173]. As can be seen in Fig. 3.4 the inclusion of the spin current reveals complicated patterns of flows and counterflows, which are absent if spin is neglected. These keep their shape even for magnetic field strengths at which there is no appreciable spin-orbit induced change in the beam profile (Fig. 3.5).

By integrating the azimuthal current, one obtains an average tangential speed of the electron. This integration is, unfortunately, difficult to perform in general. We will only consider the case  $n = 0, l \geq 0$ . In this case, the azimuthal current is clockwise everywhere (see Fig. 3.4 c). Thus these states most resemble a classical electric charge moving in a closed circle at a well-defined speed. In this case we find (upper sign for spin up, the  $\pm s$



will only appear in intermediate steps)

$$\begin{aligned} \int j_\phi dA &= \frac{4\pi(\mathcal{E} + m_e)}{B|e|} \sqrt{2B|e|} \int_0^\infty \tilde{r}^{2l+1\pm 1} e^{-\tilde{r}^2} d\tilde{r} \\ &= \frac{4\pi(\mathcal{E} + m_e)}{B|e|} \sqrt{\pi B|e|} l^{\frac{1}{2}\mp\frac{1}{2}} 2^{-l-\frac{1}{2}\mp\frac{1}{2}} (2l\pm 1)!! \end{aligned} \quad (3.16)$$

Dividing this by  $\int j_0$  we find the expectation value of the tangential speed and corresponding momentum.

$$\langle v_\phi \rangle = \frac{\sqrt{2\pi B|e|}}{\mathcal{E}} \frac{2^{-l-\frac{1}{2}\mp\frac{1}{2}} (2l\pm 1)!!}{(l-\frac{1}{2}\pm\frac{1}{2})!}, \quad \langle p_\phi \rangle = \sqrt{2\pi B|e|} \frac{2^{-l-\frac{1}{2}\mp\frac{1}{2}} (2l\pm 1)!!}{(l-\frac{1}{2}\pm\frac{1}{2})!} \quad (3.17)$$

These expressions can be rewritten using the principal quantum number  $N$ , which is  $l = \frac{1}{2} \pm \frac{1}{2}$  in our case, instead of the orbital quantum number  $l$  and making use of the Euler-gamma functions of integer and half-integer numbers,  $\Gamma(N+1) = N!$  and  $\Gamma(N+\frac{1}{2}) = \sqrt{\pi} 2^{-N} (2N-1)!!$ .

$$\langle v_\phi \rangle = \frac{\sqrt{2B|e|}}{\mathcal{E}} \frac{\Gamma(N+\frac{1}{2})}{\Gamma(N)}, \quad \langle p_\phi \rangle = \sqrt{2B|e|} \frac{\Gamma(N+\frac{1}{2})}{\Gamma(N)} \quad (3.18)$$

### 3.4 Nonuniform spin

As a consequence of spin-orbit mixing the spin polarization of an electron becomes nonuniform, similar to the nonuniform spin appearing in structured light [174–178], which is used for direction sensitive optical switching [179–189]. Its existence can be inferred decomposing the probability current in a spin and an orbital part [173, 190] and comparing the z-components of the orbital part and the total current, finding that  $\text{Re}(\Psi^* P_z/m\Psi) \neq \Psi^* \gamma_z \Psi$ . The difference has to be made up for by a spin current  $\nabla \times \vec{\sigma}$  caused by a spin component perpendicular to  $\hat{z}$ . Using

$$\begin{aligned} \Sigma_r &= \cos \phi \Sigma_x + \sin \phi \Sigma_y = \begin{bmatrix} 0 & e^{-i\phi} & 0 & 0 \\ e^{i\phi} & 0 & 0 & 0 \\ 0 & 0 & 0 & e^{-i\phi} \\ 0 & 0 & e^{i\phi} & 0 \end{bmatrix}, \\ \Sigma_\phi &= -\sin \phi \Sigma_x + \cos \phi \Sigma_y = \begin{bmatrix} 0 & -ie^{-i\phi} & 0 & 0 \\ ie^{i\phi} & 0 & 0 & 0 \\ 0 & 0 & 0 & -ie^{-i\phi} \\ 0 & 0 & ie^{i\phi} & 0 \end{bmatrix}, \end{aligned} \quad (3.19)$$

it can be shown that the radial spin is zero and the azimuthal spin is  $\pm \frac{1}{2} p/(\mathcal{E} + m) j_\phi$ , where the sign is given by the sign of the total spin in the z-direction. The ground states' spin polarization is uniform because their spin-orbit mixing is zero. This in contrast to structured light, where the nonuniformity inevitably appears in any finite width beam.

The difference between a uniformly and a nonuniformly spin polarized state is that for a uniformly polarized state one can always choose a direction along which a spin measurement will certainly give the outcome spin up whereas this is impossible for a nonuniformly

polarized state, because spin and spatial degrees of freedom are entangled. For our electron beams this entanglement can be shown by taking their density matrices and tracing out everything except the spin. The remaining mixed spin state is for spin up

$$\rho_s = \frac{((m_e + \mathcal{E})^2 + k^2)|\uparrow\rangle\langle\uparrow| + (\mathcal{E}_L^2 + \mathcal{E}_Z^2)|\downarrow\rangle\langle\downarrow|}{2\mathcal{E}(\mathcal{E} + m_e)} \quad (3.20)$$

and the same with the spins interchanged for spin down, showing that one cannot separate the spin and orbital degrees of freedom.

### 3.5 The kinetic angular momentum operator

With our choice of gauge, the exact solutions of the Dirac equation are eigenfunctions of the canonical angular momentum operator ( $\hat{J}_z = -i\partial_\phi + \frac{1}{2}\Sigma_z$ ) with eigenvalues  $l \pm \frac{1}{2}$ . The canonical momentum is not gauge invariant but can be made so by the usual minimal substitution, yielding the kinetic angular momentum operator:  $\hat{J}_z = -i\partial_\phi - erA_\phi + \frac{1}{2}\Sigma_z$ . This operator does not have any stationary solution of the Dirac equation or the ‘squared’ Dirac equation as its eigenstate, as can be verified by applying it to any (linear combination of degenerate) basis state. Its expectation value can be computed by adding  $\int \Psi^\dagger |e| r A_\phi \Psi / \int \Psi^\dagger \Psi = \int \Psi^\dagger \tilde{r}^2 \Psi / \int \Psi^\dagger \Psi$  to the canonical angular momentum. For the four different combinations of positive and negative orbital angular momentum and spin  $\int \Psi^\dagger \tilde{r}^2 \Psi$  can be shown to be resp.

$$\begin{aligned} \int \Psi^\dagger \tilde{r}^2 \Psi &= \\ \frac{4\pi}{B|e|} \int_0^\infty ((\mathcal{E} + m_e)^2 + p^2) \tilde{r}^{2|l|+2} L_n^{|l|}(\tilde{r}^2) e^{-\tilde{r}^2} + 2B|e| \tilde{r}^{2|l|+4} L_n^{|l|+1}(\tilde{r}^2) e^{-\tilde{r}^2} \tilde{r} d\tilde{r}, \\ \int \Psi^\dagger \tilde{r}^2 \Psi &= \\ \frac{4\pi}{B|e|} \int_0^\infty ((\mathcal{E} + m_e)^2 + p^2) \tilde{r}^{2|l|+2} L_n^{|l|}(\tilde{r}^2) e^{-\tilde{r}^2} + 2B|e|(n + |l|)^2 \tilde{r}^{2|l|} L_n^{|l|-1}(\tilde{r}^2) e^{-\tilde{r}^2} \tilde{r} d\tilde{r}, \\ \int \Psi^\dagger \tilde{r}^2 \Psi &= \\ \frac{4\pi}{B|e|} \int_0^\infty ((\mathcal{E} + m_e)^2 + p^2) \tilde{r}^{2|l|+2} L_n^{|l|}(\tilde{r}^2) e^{-\tilde{r}^2} + 2B|e|(n + 1)^2 \tilde{r}^{2|l|} L_{n+1}^{|l|-1}(\tilde{r}^2) e^{-\tilde{r}^2} \tilde{r} d\tilde{r}, \\ \int \Psi^\dagger \tilde{r}^2 \Psi &= \\ \frac{4\pi}{B|e|} \int_0^\infty ((\mathcal{E} + m_e)^2 + p^2) \tilde{r}^{2|l|+2} L_n^{|l|}(\tilde{r}^2) e^{-\tilde{r}^2} + 2B|e| \tilde{r}^{2|l|+4} L_{n-1}^{|l|+1}(\tilde{r}^2) e^{-\tilde{r}^2} \tilde{r} d\tilde{r}. \end{aligned} \quad (3.21)$$

Using eqs (B.12), (B.13) and (B.17), one can derive the identity

$$\int_0^\infty x^{|l|+1} L_n^{|l|}(x) e^{-x} dx = \frac{(|l| + n + 1)!}{n!} + \frac{(|l| + n)!}{(n - 1)!} = \frac{(|l| + n)!}{n!} (2n + |l| + 1), \quad (3.22)$$

which can be used to evaluate these integrals and obtain

$$\begin{aligned}
\int \Psi^\dagger \hat{r}^2 \Psi &= \frac{2\pi}{B|e|} \frac{(|l|+n)!}{n!} \left( ((\mathcal{E} + m_e)^2 + p^2) (2n+l+1) + 2B|e|(n+|l|+1)(2n+|l|+2) \right), \\
\int \Psi^\dagger \hat{r}^2 \Psi &= \frac{2\pi}{B|e|} \frac{(|l|+n)!}{n!} \left( ((\mathcal{E} + m_e)^2 + p^2) (2n+l+1) + 2B|e|(n+|l|)(2n+|l|) \right), \\
\int \Psi^\dagger \hat{r}^2 \Psi &= \frac{2\pi}{B|e|} \frac{(|l|+n)!}{n!} \left( ((\mathcal{E} + m_e)^2 + p^2) (2n+l+1) + 2B|e|(n+1)(2n+|l|+2) \right), \\
\int \Psi^\dagger \hat{r}^2 \Psi &= \frac{2\pi}{B|e|} \frac{(|l|+n)!}{n!} \left( ((\mathcal{E} + m_e)^2 + p^2) (2n+l+1) + 2B|e|n(2n+|l|) \right). \quad (3.23)
\end{aligned}$$

By noting that the last term is always proportional to  $\mathcal{E}_L^2 + \mathcal{E}_Z^2$  and rearranging one gets

$$\begin{aligned}
\int \Psi^\dagger \hat{r}^2 \Psi &= \frac{2\pi}{B|e|} \frac{(|l|+n)!}{n!} (2\mathcal{E}(\mathcal{E} + m_e)(2n+|l|+1) + \mathcal{E}_L^2 + \mathcal{E}_Z^2), \\
\int \Psi^\dagger \hat{r}^2 \Psi &= \frac{2\pi}{B|e|} \frac{(|l|+n)!}{n!} (2\mathcal{E}(\mathcal{E} + m_e)(2n+|l|+1) - \mathcal{E}_L^2 - \mathcal{E}_Z^2), \\
\int \Psi^\dagger \hat{r}^2 \Psi &= \frac{2\pi}{B|e|} \frac{(|l|+n)!}{n!} (2\mathcal{E}(\mathcal{E} + m_e)(2n+|l|+1) + \mathcal{E}_L^2 + \mathcal{E}_Z^2), \quad (3.24) \\
\int \Psi^\dagger \hat{r}^2 \Psi &= \frac{2\pi}{B|e|} \frac{(|l|+n)!}{n!} (2\mathcal{E}(\mathcal{E} + m_e)(2n+|l|+1) - \mathcal{E}_L^2 - \mathcal{E}_Z^2).
\end{aligned}$$

Dividing by  $\int \Psi^\dagger \Psi = \int j_0 = \frac{4\pi}{B|e|} \mathcal{E}(\mathcal{E} + m) \frac{(n+|l|)!}{n!}$  and adding the canonical angular momentum,  $l \pm \frac{1}{2}$ , one gets the kinetic angular momentum

$$\begin{aligned}
\mathcal{J}_z &= 2n + 2l + \frac{3}{2} + (\mathcal{E}_L^2 + \mathcal{E}_Z^2)/2\mathcal{E}(\mathcal{E} + m_e), \\
\mathcal{J}_z &= 2n + 2l + \frac{1}{2} - (\mathcal{E}_L^2 + \mathcal{E}_Z^2)/2\mathcal{E}(\mathcal{E} + m_e), \\
\mathcal{J}_z &= 2n + \frac{3}{2} + (\mathcal{E}_L^2 + \mathcal{E}_Z^2)/2\mathcal{E}(\mathcal{E} + m_e), \quad (3.25) \\
\mathcal{J}_z &= 2n + \frac{1}{2} - (\mathcal{E}_L^2 + \mathcal{E}_Z^2)/2\mathcal{E}(\mathcal{E} + m_e).
\end{aligned}$$

If one would neglect the spin-orbit term, one would always get a half-integer expectation value for the kinetic angular momentum, although the states, even without spin-orbit term are *not* eigenstates of  $\hat{J}_z$ . This fortuitous coincidence has been overlooked in the literature until now, to the best of our knowledge. The reason that the expectation value of  $\mathcal{J}_z$  is not a half integer number is that the orbital contribution changes by two quanta when  $l$  or  $n$  is changed by one whereas the spin contribution changes by the usual one quantum upon spin flip. Therefore the main term and the spin orbit term have different expectation values for  $\mathcal{J}_z$  and one takes the probability weighted average of the both terms. The quantity  $\mathcal{L}_z + 2S_z$  does have half-integer expectation values. This last quantity determines the  $z$ -component of the magnetic moment,  $M_z$ , of the electron as can be verified by computing (using eq. (B.17))

$$M_z = \int \frac{e}{2} r j_\phi = -\frac{\int j_0}{\mathcal{E}} \frac{\mathcal{E}_L^2 + \mathcal{E}_Z^2}{2B} = \frac{e}{2\mathcal{E}} \int j_0 (2n+l(1 \pm 1) + 1 + 2S) = \frac{e}{2\mathcal{E}} \int j_0 (\mathcal{L} + 2S) \quad (3.26)$$

showing that the kinetic operators are the ones determining the magnetic moment.

Apart from not having any stationary eigenfunctions, the kinetic angular momentum operators also do not generate a Lie group. These two properties can be proven more generally. To do so we change notation and write the components of the gauge covariant momenta and ‘boost’ operators as an antisymmetric tensor  $\hat{\mathcal{J}}_{\mu\nu} = \hat{\mathcal{L}}_{\mu\nu} + \frac{i}{2}\sigma_{\mu\nu}$ , with  $\sigma_{\mu\nu} = \frac{1}{2}[\gamma_\mu, \gamma_\nu]$  and  $\hat{\mathcal{L}}_{\mu\nu} = x_{[\mu}P_{\nu]}$ . The brackets on the indices indicate antisymmetrisation,  $T_{[\mu\nu]} = T_{\mu\nu} - T_{\nu\mu}$ . With this notation,  $\hat{\mathcal{J}}_{12} = \hat{\mathcal{J}}_z$ . Because  $\hat{\mathcal{L}}_{\mu\nu}$  contains no Dirac matrices, one obviously has  $[\hat{\mathcal{L}}_{\mu\nu}, \sigma_{\rho\sigma}] = 0$ , so  $[\hat{\mathcal{J}}_{\mu\nu}, \hat{\mathcal{J}}_{\rho\sigma}] = [\hat{\mathcal{L}}_{\mu\nu}, \hat{\mathcal{L}}_{\rho\sigma}] - \frac{1}{4}[\sigma_{\mu\nu}, \sigma_{\rho\sigma}]$ . Writing out the commutator for the  $\sigma$ -tensor gives

$$\begin{aligned} [\sigma_{\mu\nu}, \sigma_{\rho\sigma}] &= \frac{1}{4}((\gamma_\mu\gamma_\nu - \gamma_\nu\gamma_\mu)(\gamma_\rho\gamma_\sigma - \gamma_\sigma\gamma_\rho) - (\gamma_\rho\gamma_\sigma - \gamma_\sigma\gamma_\rho)(\gamma_\mu\gamma_\nu - \gamma_\nu\gamma_\mu)) \\ &= 2(-\eta_{\mu\rho}\sigma_{\nu\sigma} + \eta_{\mu\sigma}\sigma_{\nu\rho} + \eta_{\nu\rho}\sigma_{\mu\sigma} - \eta_{\nu\sigma}\sigma_{\mu\rho}). \end{aligned} \quad (3.27)$$

For  $[\hat{\mathcal{L}}_{\mu\nu}, \hat{\mathcal{L}}_{\rho\sigma}]$ , one can use  $[P_\mu, x_\nu] = i\eta_{\mu\nu}$  and  $[P_\mu, P_\nu] = -ieF_{\mu\nu}$  to get:

$$\begin{aligned} -i[\hat{\mathcal{L}}_{\mu\nu}, \hat{\mathcal{L}}_{\rho\sigma}] &= \eta_{\mu\rho}\hat{\mathcal{L}}_{\nu\sigma} - \eta_{\mu\sigma}\hat{\mathcal{L}}_{\nu\rho} - \eta_{\nu\rho}\hat{\mathcal{L}}_{\mu\sigma} + \eta_{\nu\sigma}\hat{\mathcal{L}}_{\mu\rho} \\ &\quad + e(x_\mu x_\rho F_{\nu\sigma} - x_\mu x_\sigma F_{\nu\rho} - x_\nu x_\rho F_{\mu\sigma} + x_\nu x_\sigma F_{\mu\rho}). \end{aligned} \quad (3.28)$$

Adding the commutators for the spin operators give for the kinetic angular momentum operators

$$\begin{aligned} -i[\hat{\mathcal{J}}_{\mu\nu}, \hat{\mathcal{J}}_{\rho\sigma}] &= \eta_{\mu\rho}\hat{\mathcal{J}}_{\nu\sigma} - \eta_{\mu\sigma}\hat{\mathcal{J}}_{\nu\rho} - \eta_{\nu\rho}\hat{\mathcal{J}}_{\mu\sigma} + \eta_{\nu\sigma}\hat{\mathcal{J}}_{\mu\rho} \\ &\quad + e(x_\mu x_\rho F_{\nu\sigma} - x_\mu x_\sigma F_{\nu\rho} - x_\nu x_\rho F_{\mu\sigma} + x_\nu x_\sigma F_{\mu\rho}). \end{aligned} \quad (3.29)$$

The proof that the kinetic orbital angular momentum operators have no stationary eigenstates goes similarly. The existence of physical states that are eigenstates of  $\hat{\mathcal{J}}_{\mu\nu}$  is only possible if the commutator  $[\not{P} - m_e, \hat{\mathcal{J}}_{\mu\nu}]$  vanishes. Again using  $\mathcal{J}_{\mu\nu} = \mathcal{L}_{\mu\nu} + \frac{i}{2}\sigma_{\mu\nu}$ , one can compute the commutators of the spin and orbital parts separately, noting that  $m$  commutes with everything:

$$\begin{aligned} [\not{P}, \sigma_{\mu\nu}] &= \frac{1}{2}P^\lambda [\gamma_\lambda, [\gamma_\mu, \gamma_\nu]] = 2P^\lambda \eta_{\lambda[\mu} \gamma_{\nu]} = 2P_{[\mu} \gamma_{\nu]} = -2\gamma_{[\mu} P_{\nu]}, \\ [\not{P}, x_{[\mu} P_{\nu]}] &= i\gamma^\lambda \eta_{\lambda[\mu} P_{\nu]} + iex_{[\mu} F_{\nu]\lambda} \gamma^\lambda = i\gamma_{[\mu} P_{\nu]} + iex_{[\mu} F_{\nu]\lambda} \gamma^\lambda, \\ [\not{P}, x_{[\mu} P_{\nu]} + \frac{i}{2}\sigma_{\mu\nu}] &= [\not{P} - m_e, \hat{\mathcal{J}}_{\mu\nu}] = iex_{[\mu} F_{\nu]\lambda} \gamma^\lambda. \end{aligned} \quad (3.30)$$

which vanishes only for an extremely restricted class of possible fields. Taking  $\hat{\mathcal{J}}_{12}$  and writing out the field components explicitly, we have

$$[\not{P} - m_e, \hat{\mathcal{J}}_{12}] = ie((xE_y - yE_x)\gamma_0 - B_z \mathbf{x} \cdot \vec{\gamma} + \gamma_3 \mathbf{x} \cdot \mathbf{B}). \quad (3.31)$$

So the only possible field that would allow for physical eigenstates of  $\hat{\mathcal{J}}_{12}$ , is a constant electric field in the z-direction. Moreover, there is no nonzero external field configuration for which all three components of the kinetic angular momentum simultaneously have stationary eigenstates.

### 3.6 Conclusion

The interaction between the electron’s spin and an external magnetic field causes several new effects for spin-polarised electron vortex beams in a magnetic field. For the modes

with the lowest energy, at a certain coaxial momentum, there is no spin-orbit mixing at all, leading to a very 'clean' vortex core. This clean separation of spin and orbital angular momentum is typically not possible for electrons or for light, making these modes quite special. For the modes with higher energy, including the effect of spin reveals an internal rearrangement of the azimuthal current which is quite substantial if the orbital angular momentum and magnetic field point in opposite directions. For electron vortex beams the current scales linearly with the beam intensity and the spin rearrangement of the azimuthal current can be magnified by using a strong enough electron beam. If an electron vortex beam is wide enough, a suitable test particle can probe these current rearrangements similar to how a small dielectric particle can probe the local Poynting vector of a light beam [11, 177, 178, 191].



## Chapter 4

# Radiative spin polarisation of electrons in a magnetic field

### 4.1 Introduction

The previous chapter dealt in great detail with the properties of the stationary electron states in a magnetic field. In this chapter we will explore the coupling to the quantised electromagnetic field of a single electron in a magnetic field with quantum electrodynamics (QED). The QED of electrons in strong background fields are a rich field of study, revealing many phenomena that cannot be derived from perturbation theory around the field-free vacuum. Examples are the electron's mass shift in a strong light field [192–195], pair production in strong electric fields [196–199], single photon Compton scattering [200], nonlinear Compton scattering [192, 193, 195, 201, 202], which has been observed by colliding a 46.6 GeV electron beam with a terawatt pulsed laser [203] and electrons in highly ionised atoms [204]. In strong magnetic fields there are the phenomena of vacuum birefringence [205, 206], the nonlinear magnetic self-energy of the electron [207–209] and the effect we are interested in, synchrotron radiation in a strong magnetic field [210–214].

In 1963, Sokolov & Ternov (S&T) found that an electron in a magnetic field tends to orient its spin against the magnetic field (from now on spin down). Taking  $n_{\downarrow}$  as the expectation value of the number of spin down electrons in the magnetic field and  $n_{\uparrow}$  as the expectation value of the number of spin up electrons (spin pointing along the magnetic field lines) they found the equilibrium spin polarisation  $(n_{\downarrow} - n_{\uparrow}) / (n_{\downarrow} + n_{\uparrow}) = 8\sqrt{3}/15 \approx 0.924$  [166, 212] independent of the magnetic field strength. In their calculations they approximated the Laguerre-Gauß wave functions of the electrons by Bessel functions, an approximation which breaks down at low Landau levels where the finite widths of the electron wave functions become important.

At high quantum numbers the S&T calculations [212] yield excellent approximations to the electron's actual spin polarisation. This situation occurs either when the orbital kinetic energy of the electron is high or the magnetic field is weak compared to the critical field. When the magnetic field becomes stronger, it will be more difficult to satisfy the conditions for which the S&T approximation applies. New proposals for generating short-lived magnetic fields in plasmas created by ultrashort laser pulses promise field strengths of  $10^5 - 10^6$  T [215, 216], which is three to four orders of magnitude beyond the field

strengths that are available from non-destructive magnets [217]. Even stronger magnetic fields, up to  $10^{11}$  T can be found on the surface of neutron stars [218–222].

For such strong fields, classical electrodynamics breaks down, as an electron with energy  $\mathcal{E}$  on a circular orbit in a magnetic field emits frequencies  $\omega \sim \mathcal{E}^2 |e| B / m_e^3$  where  $m_e$  is the electron mass,  $e$  its charge and  $B$  the magnetic field strength [166], from which we conclude that for relativistic energies  $\mathcal{E} \gtrsim m_e^3 / |e| B$  the emitted frequencies are larger than the electron's energy, indicating that recoil will be important and the emission needs to be described in a quantum electrodynamics (QED) formalism. For strong magnetic fields  $B \gtrsim B_{\text{cr}} = m_e^2 / |e| \approx 4.4 \cdot 10^9$  T this condition is always satisfied. Physically, a magnetic field of this strength can be interpreted as imparting a momentum change of  $\Delta p \sim |e(\vec{\beta} \times \mathbf{B})| \Delta t \sim m_e c$  onto a relativistic electron over a time interval  $\Delta t \sim \hbar / m_e c^2$ , forcing the virtual electron-positron pairs of QED onto circular orbits and hence effectively magnetizing the vacuum itself. On the other hand, ordinary perturbative QED is not applicable, as in a magnetic field of strength  $B \gtrsim m_e / ed$ , where  $d$  is the field's spatial extent, an electron's cyclotron radius becomes  $r = \beta \gamma c / eB \lesssim \beta \gamma d$ , indicating that in the non-relativistic approximation  $\gamma \equiv 1$  the electron's motion is bound and the magnetic field must be accounted for by non-perturbative QED techniques [201]. The S&T approximation breaks down in this regime too, because even low lying states  $N \lesssim 10$  already have kinetic energies in excess of the electron's rest mass and it becomes energetically prohibitive to occupy the much higher Landau levels which the S&T approximation presupposes. Thus the magnetic field must be accounted for by a non-perturbative technique. Such a non-perturbative QED scattering theory can be described in the Furry picture of quantum dynamics [223] through replacing the vacuum electron states by solutions of the Dirac equation in a magnetic field, which we derived in the previous chapter. The synchrotron radiation rate of an electron in a magnetic field has been studied in non-perturbative QED [213, 214] using the Hermite-Gauß basis, which is useful in the Landau gauge where one takes the vector potential pointing along the x-axis everywhere [224]. These studies did not distinguish the spins of the final electron states and could therefore not compute the spin polarisation of radiating electrons.

Analogous studies of radiation emission in nonlinear QED regimes were previously conducted in the interaction of relativistic electrons with ultra-intense laser fields [202, 225, 226], a regime which is complementary to the pure magnetic field case studied here. In the absence of strong fields, the scattering theory of non-plane wave states has been explored, using techniques similar to the one we use here [54–62, 227].

## 4.2 Quantisation of the fields

In the previous chapter we derived a complete set of exact solutions for a single electron in a homogeneous magnetic field (eq. (3.10)). We want to employ these solutions in the framework of strong field QED. To do so we have to treat the electron wave functions  $\Psi$  as excitations of a quantum field and do the same to the light field in a suitable basis. Using the fermionic anticommutation relations [228] and taking two excitations labelled by the sets of quantum numbers  $\{n\}$  and  $\{n'\}$

$$\{\hat{\Psi}_{\{n'\}}^{a\dagger}(x_\mu), \hat{\Psi}_{\{n\}}^b(y_\mu)\} = \delta(x_\mu - y_\mu) \delta_{ab} \Psi_{\{n'\}}^{a\dagger}(x_\mu) \Psi_{\{n\}}^b(y_\mu) = \Psi_{\{n'\}}^{a\dagger}(x_\mu) \Psi_{\{n\}}^a(x_\mu), \quad (4.1)$$



we can derive that

$$\sum_{a,b} \iint \{\hat{\Psi}_{\{n'\}}^{a\dagger}(x_\mu), \hat{\Psi}_{\{n'\}}^b(y_\mu)\} d^3x d^3y = \sum_a \int \Psi_{\{n'\}}^{a\dagger}(x_\mu) \Psi_{\{n'\}}^a(x_\mu) d^3x, \quad (4.2)$$

which is an overlap integral of two commuting spinor wave functions. In particular, if one takes any two orthogonal spinor modes, their anticommutator will vanish. Using our set of solutions, eq. (3.10) for the electron in a magnetic field and using as quantum numbers the principal quantum number  $N = n + \frac{1}{2}(l + |l|) + \sigma + 1/2$  and the total angular momentum quantum number  $j = l + \sigma$  instead of  $n$  and  $l$  we can derive, using suitable normalisations  $\mathcal{N}$

$$\sum_{a,b} \iint \{\hat{\Psi}_{p'N'j'\sigma'}^{a\dagger}(y_\mu) \hat{\Psi}_{pNj\sigma}^b(x_\mu)\} d^3x d^3y / \sqrt{\mathcal{N}'\mathcal{N}} = \delta(x_0 - x'_0) \delta(p - p') \delta_{NN'} \delta_{jj'} \delta_{\sigma\sigma'}. \quad (4.3)$$

Using this expression we can expand the field  $\hat{\Psi}_a(x_\mu)$  in products of commuting spinor functions and fermionic ladder operators obeying  $\{\hat{\pi}_{p'n'l'\sigma'}, \hat{\pi}_{pnl\sigma}^\dagger\} = \delta_{p'p} \delta_{N'N} \delta_{j'j} \delta_{\sigma'\sigma}$  and  $\{\hat{\pi}^\dagger, \hat{\pi}\} = \{\hat{\pi}, \hat{\pi}\} = 0$  as

$$\hat{\Psi}^a(x_\mu) = \int \sum_{N,j,\sigma} \Psi_{pNj\sigma}^a(x_\mu) \hat{\pi}_{pNj\sigma} dp / \sqrt{\mathcal{N}}, \quad \hat{\Psi}^{a\dagger}(x_\mu) = \int \sum_{N,j,\sigma} \Psi_{pNj\sigma}^{a\dagger}(x_\mu) \hat{\pi}_{pNj\sigma}^\dagger dp / \sqrt{\mathcal{N}}. \quad (4.4)$$

By similar means it is possible to quantise the photon field in any complete orthogonal set of basis modes. Using  $A_\mu = \text{Re}(\hat{A}_\mu)$  and the bosonic commutation relations [229]  $[\hat{A}_\mu^*(x_\lambda), \hat{A}_\nu(y_\lambda)] = \eta_{\mu\nu} \delta(x_\lambda - y_\lambda)$ . One can show that for any orthogonal set of basis states  $\{A_{\mu\{n\}}(x_\lambda)\}$

$$\hat{A}_\mu(x_\lambda) = \frac{1}{\sqrt{\mathcal{N}_\gamma}} \sum_{\{n\}} A_{\mu\{n\}}^*(x_\lambda) \hat{a}_{\{n\}}^\dagger + A_{\mu\{n\}}(x_\lambda) \hat{a}_{\{n\}}. \quad (4.5)$$

Assuming minimal coupling and the fermionic current  $j_\mu = \hat{\Psi}^\dagger \gamma_0 \gamma_\mu u \hat{\Psi}$ , the photon-electron interaction is

$$\mathcal{H}_{int} = -e j_\mu \hat{A}^\mu = -e \sum_a \hat{\Psi}^{a\dagger} \gamma_0 \hat{A}^\mu \hat{\Psi}_a \quad (4.6)$$

Using our expansions for the quantised fields, this interaction is written as

$$\mathcal{H}_{int} = \frac{-e}{\sqrt{\mathcal{N}'\mathcal{N}_\gamma\mathcal{N}}} \int \sum_a \Psi_{p'N'j'\sigma'}^{a\dagger}(x_\mu) \gamma_0 \hat{\pi}_{p'N'j'\sigma'}^\dagger \left( \hat{a}_{\{n\}}^\dagger \mathcal{A}_{\{n\}}^*(x_\mu) + \hat{a}_{\{n\}} \mathcal{A}_{\{n\}}(x_\mu) \right) \hat{\pi}_{pNl\sigma} \Psi_{pNl\sigma}^a(x_\mu) d^3x. \quad (4.7)$$

This interaction term will form the basis of QED perturbative calculations in a strong magnetic field. It describes the transitions of the electron states under the emission or absorption of photons. In this chapter we will be only interested in radiative decay and only consider perturbations of first order  $\mathcal{H}_{int}$ , thus we assume there are no photons in our initial quantum state and can drop the term proportional to  $\hat{a}_{\{n\}}$ .

### 4.3 Analytical computation of the transition rates

We want to compute the transmission from the state  $|\Psi_{pNj\sigma}(t); 0\rangle$  to  $|\Psi_{p'N'j'\sigma'}(t+dt); 1\rangle$ , where the number indicates the number of photons present. This transition rate is given by

the modulus squared of the matrix element

$$\langle \Psi_{p'N'j'\sigma'}; 1 | e^{i\mathcal{H}t} | \Psi_{pNj\sigma}; 0 \rangle \approx \langle \Psi_{p'N'j'\sigma'}; 1 | i\mathcal{H}_{int} dt | \Psi_{pNj\sigma}; 0 \rangle. \quad (4.8)$$

Where we used that the noninteracting Hamiltonian conserves photon number and thus yields zero when evaluated between states with different photon numbers. Taking all incoming and outgoing particles to lie on their respective mass shells, the transition matrix element for this situation can be computed by integrating over all time. At this point it is useful to specify a basis of photon states. The most effective way to keep track of angular momentum changes of the electron when it radiates is to expand the photon field too in a basis of eigenstates of angular momentum along the beam axis. These are the photon Bessel modes with total angular momentum  $j_\gamma$ , momentum in the z-direction  $k$ , transverse momentum  $\kappa$  and energy  $\omega = \sqrt{k^2 + \kappa^2}$ . For the photon polarisation we use a basis of left- (−) and right- (+) handed helicity. For a photon emitted in the positive z-direction positive helicity corresponds to a spin predominantly in the positive z-direction whereas for a photon emitted in the negative z-direction it corresponds to a spin predominantly in the negative z-direction, with the expectation value for the photon spin along the z-axis continuously decreasing with decreasing  $k$ . Using the Coulomb gauge these photon modes are described by the vector potential

$$\tilde{\mathbf{A}}_{k\kappa j_\gamma \pm} = \frac{e^{i(kz - \omega t)}}{2} \begin{bmatrix} (1 \pm \frac{\kappa}{\omega}) B_{j_\gamma - 1} + (1 \mp \frac{\kappa}{\omega}) B_{j_\gamma + 1} \\ i \left( (1 \pm \frac{\kappa}{\omega}) B_{j_\gamma - 1} - (1 \mp \frac{\kappa}{\omega}) B_{j_\gamma + 1} \right) \\ \mp 2i \frac{\kappa}{\omega} B_{j_\gamma} \end{bmatrix}, \quad (4.9)$$

With the shorthand  $B_j = J_j(\kappa r) e^{ij\phi}$ . Using this basis we can calculate  $\gamma_0 \mathcal{A}_{k\kappa j_\gamma \pm}^*$ , which we will use to compute the transition matrix elements later, to be

$$\gamma_0 \mathcal{A}_{k\kappa j_\gamma \pm}^* = e^{i(\omega t - kz)} \times \begin{bmatrix} 0 & 0 & \mp i \frac{\kappa}{\omega} B_{j_\gamma}^* & - (1 \mp \frac{\kappa}{\omega}) B_{j_\gamma + 1}^* \\ 0 & 0 & - (1 \pm \frac{\kappa}{\omega}) B_{j_\gamma - 1}^* & \pm i \frac{\kappa}{\omega} B_{j_\gamma}^* \\ \mp i \frac{\kappa}{\omega} B_{j_\gamma}^* & - (1 \mp \frac{\kappa}{\omega}) B_{j_\gamma + 1}^* & 0 & 0 \\ - (1 \pm \frac{\kappa}{\omega}) B_{j_\gamma - 1}^* & \pm i \frac{\kappa}{\omega} B_{j_\gamma}^* & 0 & 0 \end{bmatrix} \quad (4.10)$$

Using this expression and eqs. (3.10) the angular, z- and time integrations can be carried out straightforwardly. The angular integration will always yield  $2\pi \delta_{j, j' + j_\gamma}$  while we have chosen both the photon and the electron states to be angular momentum eigenstates. The time and z- integrations are integrals over complex exponentials which obey  $\int_{-\infty}^{\infty} e^{i(\omega - \omega')t} dt = 2\pi \delta(\omega - \omega')$ , as proven in appendix C. Using this identity the time and z-integrations yield the energy and momentum conserving delta functions  $(2\pi)^2 \delta(\mathcal{E} - \omega - \mathcal{E}') \delta(p - k - p')$ . combining these results, the time integrated transition matrix element is

$$-ie(2\pi)^3 \delta(\mathcal{E} - \omega - \mathcal{E}') \delta(p - k - p') \delta_{j, j' - \gamma} \frac{\mathcal{M}}{\sqrt{N' N_\gamma N}}, \quad (4.11)$$

with, taking  $\psi$  as the radial part of  $\Psi$ ,

$$\mathcal{M} = \int_0^\infty \psi_{p'N'j'\sigma'}^\dagger \gamma_0 \mathcal{A}_{k\kappa j_\gamma \pm}^* \psi_{pNj\sigma} r dr. \quad (4.12)$$

Unlike for plane waves, there are only three delta functions instead of four as there is no fourth conserved quantity whose operator commutes with the angular momentum operator and therefore the electron and photon states cannot be simultaneous eigenstates of four conserved quantities.

To obtain the transition probability we need to take the modulus squared of the matrix element. To do so we will change our notation somewhat. We will assume all our wave functions are confined within a cylinder of radius  $R$  and length  $L$ , which we will take to infinity in the end. We will pull the factors of  $L$  out of the normalisations for bookkeeping. Now the squares of the Dirac delta functions can be approximated as [166]

$$\begin{aligned} (\delta(\mathcal{E} - \omega - \mathcal{E}')\delta(p - k - p'))^2 &= \\ \lim_{T \rightarrow \infty} \lim_{L \rightarrow \infty} \frac{1}{(2\pi)^2} \int_{-T/2}^{T/2} \int_{-L/2}^{L/2} \delta(\mathcal{E} - \omega - \mathcal{E}')\delta(p - k - p') e^{i((p-k-p')z - (\mathcal{E} - \omega - \mathcal{E}')t)} dz dt & \\ &= \lim_{T \rightarrow \infty} \lim_{L \rightarrow \infty} \delta(\mathcal{E} - \omega - \mathcal{E}')\delta(p - k - p') \frac{TL}{(2\pi)^2} \end{aligned} \quad (4.13)$$

from which we get the transition probability

$$e^2 (2\pi)^4 \delta(\mathcal{E} - \omega - \mathcal{E}')\delta(p - k - p')\delta_{j,j'} \gamma L T \frac{|\mathcal{M}|^2}{LN'LN\gamma LN} \quad (4.14)$$

This probability exceeds 1 for sufficiently long time, which cannot be right. The reason this occurs is that this transition probability has been computed under the assumption that the occupation probability of the initial state does not decrease as the electron radiates, which is clearly non-physical. Dividing this expression by  $T$  gives the differential transition *rate* which is physically relevant. We are interested in the rate at which an electron in the state  $|Nj\sigma\rangle$  transitions to the state  $|N'j'\sigma'\rangle$ . To obtain this transition rate we must integrate the differential transition rate multiplied by the density of states over all allowed  $p'$  and all allowed  $k$  and  $\kappa$  and sum over both photon helicities and all  $j_\gamma$ . The outgoing electron's density of states is  $L/2\pi$  and for the emitted photon we have a density of states of (taking a single helicity and angular momentum)  $L/2\pi \times R/\pi$ . Putting everything together we have a transition rate of

$$\begin{aligned} \Gamma_{Nj\sigma \rightarrow N'j'\sigma'} &= \\ (2\pi)^4 e^2 \sum_{\pm} \sum_{j_\gamma} \iiint \delta(\mathcal{E} - \mathcal{E}' - \omega)\delta(p - p' - k)\delta_{j,j'+j_\gamma} L \frac{|\mathcal{M}|^2}{LN'LN\gamma LN} \frac{L dp' LR dk d\kappa}{2\pi} \frac{L R dk d\kappa}{2\pi^2}. \end{aligned} \quad (4.15)$$

The electron's transverse normalisation is  $\mathcal{N} = \int j_0 = 4\pi\mathcal{E}(m_e + \mathcal{E})(n+l)!/B|e|n!$ , which we computed in the previous chapter. For  $\mathcal{N}_\gamma$ , we use the condition  $\int \mathbf{A} \cdot \mathbf{A}^* dV = 2\pi/\omega$  [230]. As we will take the limit of  $R$  to infinity in the end we assume  $R \gg \kappa^{-1}$ , which yields  $\mathcal{N}_\gamma \approx LR\omega/2\kappa$  [54]. Substituting these transverse normalization factors,  $L$  and  $R$  disappear and the size of the cylinder can be taken to infinity, yielding

$$\Gamma_{Nj\sigma \rightarrow N'j'\sigma'} = (2\pi)^3 e^2 \sum_{\pm} \sum_{j_\gamma} \iiint \delta(\mathcal{E} - \mathcal{E}' - \omega)\delta(p - p' - k)\delta_{j,j'+j_\gamma} \frac{|\mathcal{M}|^2}{\mathcal{N}\mathcal{N}'\omega} dp' \frac{dk d\kappa d\kappa}{\pi^2}. \quad (4.16)$$

In order to obtain numerical values for the transition rates,  $\mathcal{M}$  has to be computed and the integrals over phase space have to be performed. The computation of

$\mathcal{M} = \int_0^\infty \Psi_{p'N'l'\sigma'}^\dagger \gamma_0 \mathcal{A}_{kkjy\pm} \Psi_{pNj\sigma} r dr$  has to be done on a case-by-case basis, as there are four different wave functions depending on the spin and orbital angular momentum of the electron (see eq. (3.10)). Combining four wave functions for the electron's initial state with four wave functions for the electron's final state makes sixteen cases in total. In all cases  $\mathcal{M}$  contains integrals of a Laguerre-Gauß function times a Bessel function times another Laguerre-Gauß function. We will use the shorthand

$$I_{nn'}^{l'l'}(\kappa) = \int_0^\infty Lg_n^l(\tilde{r}) Lg_{n'}^{l'}(\tilde{r}) J_{l-l'}(\kappa r) r dr, \left( \text{recall } \tilde{r} = \sqrt{B|e|/2r} \right) \quad (4.17)$$

to denote these integrals. In each case  $\mathcal{M}$  can be computed by a straightforward, albeit lengthy multiplication of a pair of states from eq (3.10) with the matrix (4.10). The results are:

$l$	$l'$	$\sigma$	$\sigma'$	$\mathcal{M}_\pm$
-	-	-	-	$\mp i \frac{\kappa}{\omega} ((\mathcal{E}' + m_e)p + (\mathcal{E} + m_e)p') I_{nn'}^{l'l'}(\kappa) -$ $i\sqrt{2B e } \left( (\mathcal{E}' + m_e) (1 \pm \frac{\kappa}{\omega}) I_{n-1n'}^{l'-1l'}(\kappa) - (\mathcal{E} + m_e) (1 \mp \frac{\kappa}{\omega}) I_{nn'+1}^{l'l'+1}(\kappa) \right)$
-	-	-	+	$(1 \mp \frac{\kappa}{\omega}) ((\mathcal{E}' + m_e)p - (\mathcal{E} + m_e)p') I_{nn'}^{l'l'}(\kappa)$ $\pm \frac{\kappa}{\omega} \sqrt{2B e } \left( (\mathcal{E}' + m_e) I_{n-1n'}^{l'-1l'}(\kappa) - (n' + 1)(\mathcal{E} + m_e) I_{nn'+1}^{l'l'+1}(\kappa) \right)$
-	-	+	-	$(1 \pm \frac{\kappa}{\omega}) ((\mathcal{E} + m_e)p' - (\mathcal{E}' + m_e)p) I_{nn'}^{l'l'}(\kappa)$ $\pm \frac{\kappa}{\omega} \sqrt{2B e } \left( (\mathcal{E}' + m_e)(n + 1) I_{n+1n'}^{l'+1l'}(\kappa) - (\mathcal{E} + m_e) I_{nn'+1}^{l'l'+1}(\kappa) \right)$
-	-	+	+	$\mp i \frac{\kappa}{\omega} ((\mathcal{E}' + m_e)p + (\mathcal{E} + m_e)p') I_{nn'}^{l'l'}(\kappa) +$ $i\sqrt{2B e } \left( (1 \mp \frac{\kappa}{\omega}) (\mathcal{E}' + m_e)(n + 1) I_{n+1n'}^{l'+1l'}(\kappa) \right) -$ $i\sqrt{2B e } \left( (1 \pm \frac{\kappa}{\omega}) (\mathcal{E} + m_e)(n' + 1) I_{nn'+1}^{l'l'+1}(\kappa) \right)$
-	+	-	-	$\mp i \frac{\kappa}{\omega} ((\mathcal{E}' + m_e)p + (\mathcal{E} + m_e)p') I_{nn'}^{l'l'}(\kappa) -$ $i\sqrt{2B e } \left( (1 \pm \frac{\kappa}{\omega}) (\mathcal{E}' + m_e) I_{n-1n'}^{l'-1l'}(\kappa) \right) +$ $i\sqrt{2B e } \left( (1 \mp \frac{\kappa}{\omega}) (\mathcal{E} + m_e)(n' +  l' ) I_{nn'+1}^{l'l'+1}(\kappa) \right)$
-	+	-	+	$(1 \mp \frac{\kappa}{\omega}) ((\mathcal{E}' + m_e)p - (\mathcal{E} + m_e)p') I_{nn'}^{l'l'}(\kappa)$ $\pm \frac{\kappa}{\omega} \sqrt{2B e } \left( (\mathcal{E}' + m_e) I_{n-1n'}^{l'-1l'}(\kappa) + (\mathcal{E} + m_e) I_{nn'+1}^{l'l'+1}(\kappa) \right)$
-	+	+	-	$(1 \pm \frac{\kappa}{\omega}) ((\mathcal{E} + m_e)p' - (\mathcal{E}' + m_e)p) I_{nn'}^{l'l'}(\kappa)$ $\pm \frac{\kappa}{\omega} \sqrt{2B e } \left( (\mathcal{E}' + m_e)(n + 1) I_{n+1n'}^{l'+1l'}(\kappa) + (\mathcal{E} + m_e)(n' +  l' ) I_{nn'+1}^{l'l'+1}(\kappa) \right)$
-	+	+	+	$\mp i \frac{\kappa}{\omega} ((\mathcal{E}' + m_e)p + (\mathcal{E} + m_e)p') I_{nn'}^{l'l'}(\kappa) +$ $i\sqrt{2B e } \left( (1 \mp \frac{\kappa}{\omega}) (\mathcal{E}' + m_e)(n + 1) I_{n+1n'}^{l'+1l'}(\kappa) \right) +$ $i\sqrt{2B e } \left( (1 \pm \frac{\kappa}{\omega}) (\mathcal{E} + m_e) I_{nn'+1}^{l'l'+1}(\kappa) \right)$
+	-	-	-	$\mp i \frac{\kappa}{\omega} ((\mathcal{E}' + m_e)p + (\mathcal{E} + m_e)p') I_{nn'}^{l'l'}(\kappa) +$ $i\sqrt{2B e } \left( (1 \pm \frac{\kappa}{\omega}) (\mathcal{E}' + m_e)(n +  l ) I_{nn'+1}^{l'l'+1}(\kappa) \right) +$ $i\sqrt{2B e } \left( (1 \mp \frac{\kappa}{\omega}) (\mathcal{E} + m_e) I_{nn'+1}^{l'l'+1}(\kappa) \right)$
+	-	-	+	$(1 \mp \frac{\kappa}{\omega}) ((\mathcal{E}' + m_e)p - (\mathcal{E} + m_e)p') I_{nn'}^{l'l'}(\kappa)$ $\mp \frac{\kappa}{\omega} \sqrt{2B e } \left( (\mathcal{E}' + m_e)(n +  l ) I_{nn'+1}^{l'l'+1}(\kappa) + (\mathcal{E} + m_e)(n' + 1) I_{nn'+1}^{l'l'+1}(\kappa) \right)$

+	-	+	-	$(1 \pm \frac{k}{\omega}) ((\mathcal{E}' + m_e)p - (\mathcal{E} + m')p) I_{nn'}^{ll'}(\boldsymbol{\kappa})$ $\mp \frac{\kappa}{\omega} \sqrt{2B e } \left( (\mathcal{E}' + m_e) I_{nn'}^{l'+1l'}(\boldsymbol{\kappa}) + (\mathcal{E} + m_e) I_{nn'-1}^{ll'-1}(\boldsymbol{\kappa}) \right)$
+	-	+	+	$\mp i \frac{\kappa}{\omega} ((\mathcal{E}' + m_e)p + (\mathcal{E} + m_e)p') I_{nn'}^{ll'}(\boldsymbol{\kappa}) -$ $i \sqrt{2B e } \left( (1 \mp \frac{k}{\omega}) (\mathcal{E}' + m_e) I_{nn'}^{l'+1l'}(\boldsymbol{\kappa}) \right) +$ $i \sqrt{2B e } \left( (1 \pm \frac{k}{\omega})(n' + 1)(\mathcal{E} + m_e) I_{nn'+1}^{ll'+1}(\boldsymbol{\kappa}) \right)$
+	+	-	-	$\mp i \frac{\kappa}{\omega} ((\mathcal{E}' + m_e)p + (\mathcal{E} + m_e)p') I_{nn'}^{ll'}(\boldsymbol{\kappa}) -$ $i \sqrt{2B e } \left( (1 \mp \frac{k}{\omega}) (\mathcal{E} + m_e)(n' +  l' ) I_{nn'}^{ll'-1}(\boldsymbol{\kappa}) \right) -$ $i \sqrt{2B e } \left( (1 \pm \frac{k}{\omega}) (\mathcal{E}' + m_e)(n +  l ) I_{nn'}^{l'-1l'}(\boldsymbol{\kappa}) \right)$
+	+	-	+	$(1 \mp \frac{k}{\omega}) ((\mathcal{E}' + m_e)p - (\mathcal{E} + m_e)p') I_{nn'}^{ll'}(\boldsymbol{\kappa})$ $\pm \frac{\kappa}{\omega} \sqrt{2B e } \left( (\mathcal{E} + m_e) I_{nn'}^{ll'+1}(\boldsymbol{\kappa}) - (\mathcal{E}' + m_e)(n +  l ) I_{nn'}^{l'-1l'}(\boldsymbol{\kappa}) \right)$
+	+	+	-	$(1 \pm \frac{k}{\omega}) ((\mathcal{E} + m_e)p' - (\mathcal{E}' + m_e)p) I_{nn'}^{ll'}(\boldsymbol{\kappa})$ $\pm \frac{\kappa}{\omega} \sqrt{2B e } \left( (\mathcal{E} + m_e)(n' +  l' ) I_{nn'}^{ll'-1}(\boldsymbol{\kappa}) - (\mathcal{E}' + m_e) I_{nn'}^{l'+1l'}(\boldsymbol{\kappa}) \right)$
+	+	+	+	$\mp i \frac{\kappa}{\omega} ((\mathcal{E}' + m_e)p + (\mathcal{E} + m_e)p') I_{nn'}^{ll'}(\boldsymbol{\kappa}) -$ $i \sqrt{2B e } \left( (1 \mp \frac{k}{\omega}) (\mathcal{E}' + m_e) I_{nn'}^{l'+1l'}(\boldsymbol{\kappa}) - (1 \pm \frac{k}{\omega}) (\mathcal{E} + m_e) I_{nn'}^{ll'+1}(\boldsymbol{\kappa}) \right)$

As for the integrals and sums over phase space, the sum over both helicities is straightforward. The  $\delta_{j,j'+j_\gamma}$  singles out only one photon angular momentum for a given transition. This leaves the three integrals over the momenta  $p'$ ,  $k$  and  $\boldsymbol{\kappa}$ . We will assume the electron's initial momentum along the z-axis is zero for simplicity. The transition rate for a moving electron can be found by a Lorentz transformation. One can then use the kinematic laws of two-particle decay, as recapitulated in appendix D. By viewing the emission of a photon as a two particle decay in one spatial dimension, one can use eqs. (D.2) and (D.5), assigning the effective masses  $m_A = \sqrt{m_e^2 + 2B|e|N}$ ,  $m_B = \sqrt{m_e^2 + 2B|e|N'}$  and  $m_C = \boldsymbol{\kappa}$ . Using these one finds  $\mathcal{E}'$ ,  $p'$  and  $k$  and one thereby has evaluated the integrals over  $k$  and  $p'$  using the energy and momentum conserving delta functions. Unfortunately the expressions for the momenta are quite complicated functions of the remaining integration parameter  $\boldsymbol{\kappa}$  and the electron's and photon's final energy depend on  $\boldsymbol{\kappa}$  too and appear also implicitly in the normalisations  $\mathcal{N}'$  and  $\mathcal{N}_\gamma$ . Therefore the remaining integral over  $\boldsymbol{\kappa}$  has to be evaluated numerically.

## 4.4 Numerical results

We numerically computed all transition rates for electron states in a magnetic field with  $N \leq 5$  and  $j \geq -9/2$  to final states with  $N' \leq 4$  and  $j' \geq -17/2$ . The highest allowable  $j$  for a given  $N$  is always  $j = N - 1/2$ . The reason to choose a lower  $j$  cutoff for the final state is that the electron tends to lose angular momentum when it emits a photon more often than it gains it. To compute the spin flip rate we take the sum  $\sum_{N'j'} \Gamma_{Nj\sigma \rightarrow N'j'\sigma'}$  over all energetically allowed final states in this data set.

To compare our results for the relative spin flip rates of twisted electrons to conventional results, we use the plane wave approximation from [166]. Here the electron is considered to be a plane wave with the time evolution  $e^{-iHt}$ , with  $H$  the Hamiltonian of the

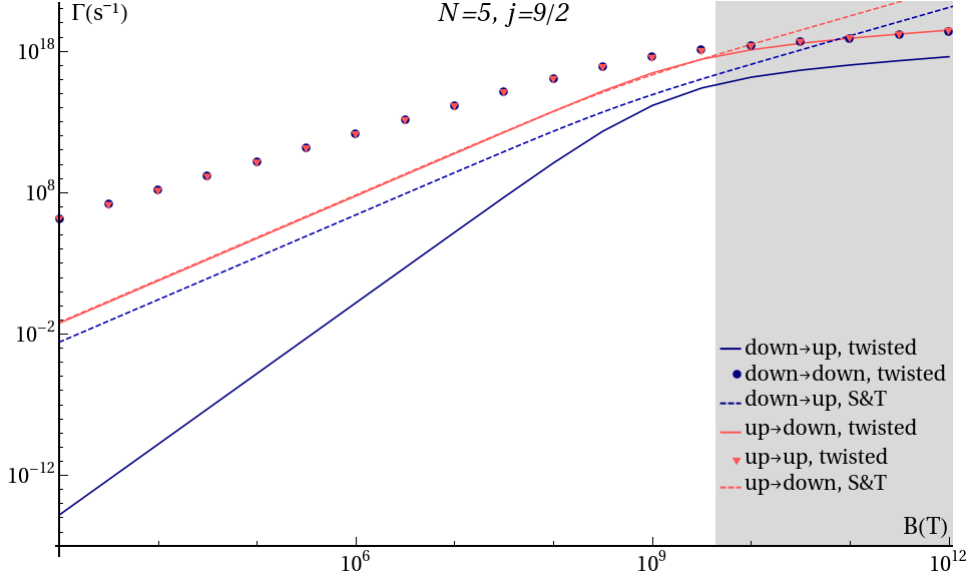


Figure 4.1: Spin flip rates compared for the twisted (continuous curves) and S&T(dashed curves) approximations for the initial quantum numbers  $N = 5$  and  $j = 9/2$ . For low magnetic fields, the transition rate from spin down to spin up is suppressed by many orders of magnitude. Spin preserving transition rates are shown for comparison (dots). Beyond the critical field (gray area), the S&T calculation becomes non-physical and the spin-flip rates obtained from it diverge from the actual rates.

problem under consideration. This approximation takes the recoil of the electron when it emits a photon into account properly and is thus an improvement over classical electrodynamics if  $\mathcal{E} \gtrsim m_e^3/|e|B$ . It reproduces the S&T spin flip rates exactly [166]. We choose a plane wave momentum equal to the expected tangential momentum of the highest  $l$  state for a given  $N$ , which is given by eq. (3.18).

$$p_{\perp} = \sqrt{2B|e|} \frac{\Gamma(N + \frac{1}{2})}{\Gamma(N)}.$$

Interestingly, taking this expression for the tangential momentum of the electron implies that in the weak field limit the change of momentum the electron gets upon emitting a photon far exceeds the emitted photon's momentum, which is  $\sim B|e|/2m_e$ . Thus upon emitting a photon, the electron always gets a 'superkick' [231], caused by the spatial extent of the (twisted) photon mode being much larger than the spatial extent of the electron's wave function. When angular momentum is transferred from one to the other, the electron's tangential momentum must change by much more than the emitted photon's tangential momentum. Because the electron's tangential momentum averaged over one orbit is zero, momentum is nonetheless conserved.

At all field strengths and all initial  $N$  and  $j$  quantum numbers we computed, we find that the spin flip rate for spin down-to-up exceeds the spin up-to-down flip rate by more than the ratio found by S&T (see Fig. 4.1). For magnetic field strength far below the critical field, the difference is many orders of magnitude and the spin-down-to-up transition rate

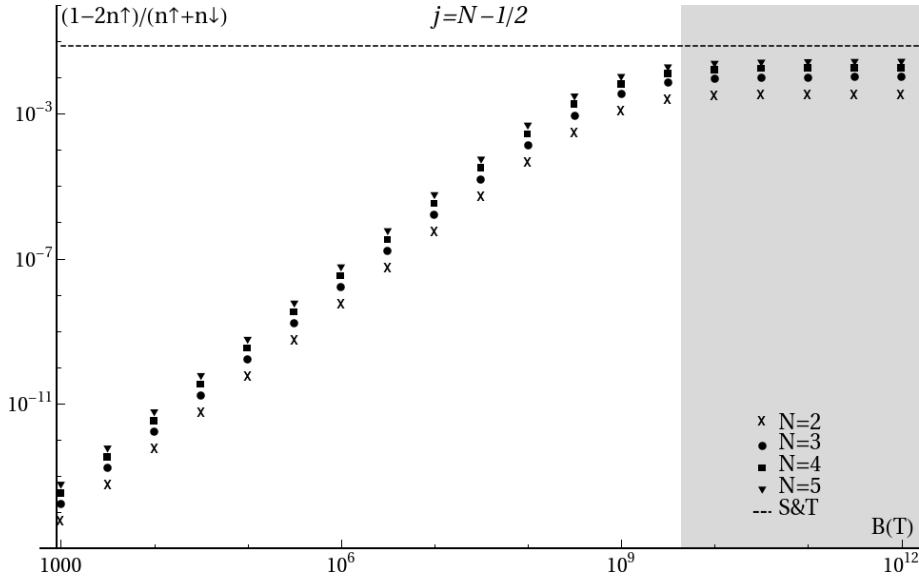


Figure 4.2: The deviations from perfect spin down polarisation for several energy levels compared to the S&T result. At all field strengths twisted electrons spin polarise better than expected from the S&T result.

scales as  $B^2$  relative to the up-to-down transition rate (see Fig. 4.1). Assuming a simple model of electrons undergoing spin flips at their respective rates, the spin polarisation of the electrons is expected to reach an equilibrium. Our results suggest that for low lying Landau levels at low magnetic field strengths, the equilibrium spin polarisation is so good as to be considered perfect for all practical purposes (see FIG. 4.2).

The large discrepancy in spin flip rates between our computations and the established results stem from the commonly made assumption to use a plane wave approximation [166] or replace the Laguerre-Gauß states by Bessel states [211, 212]. Especially for the low  $n$  states we considered, replacing a function having a finite transverse extent with a function that has an infinite transverse extent opens transitions that for the actual Laguerre-Gauß states are suppressed. This causes two kinds of overestimation of the spin flip rates.

First, at low field strength and low quantum numbers the wavelength of the emitted photon is approximately  $m_e/B|e|$  whereas the size of the electron beam is roughly  $\sqrt{2(2n+|l|+1)/B|e|}$ . This means that for  $2n+|l|+1 \ll 2m_e^2/B|e|$ , the electron only ‘probes’ the centre of the photon mode, which for a vortex mode is a dark spot. Thus the local vortex structure of the photon modes creates a set of selection rules at weak fields, dictating at what order in  $B|e|/m_e^2$  a particular transition becomes relevant. The derivation of these selection rules is beyond the scope of this dissertation, but one can see their striking effects in Fig 4.1. The up-to-down spin flip rate agrees well with the S&T result for weak magnetic fields whereas the down-to-up spin flip rate is suppressed by many orders of magnitude. A hint as to why this happens is that an electron can transition from spin up to spin down whilst keeping its  $n$  and  $l$  quantum numbers the same whereas this is energetically impossible for an down-to-up transition.

The second effect occurs because Laguerre-Gauß states with vastly different  $l$  quantum numbers and low  $n$  quantum numbers do not overlap well, as one lies in the dark spot of the

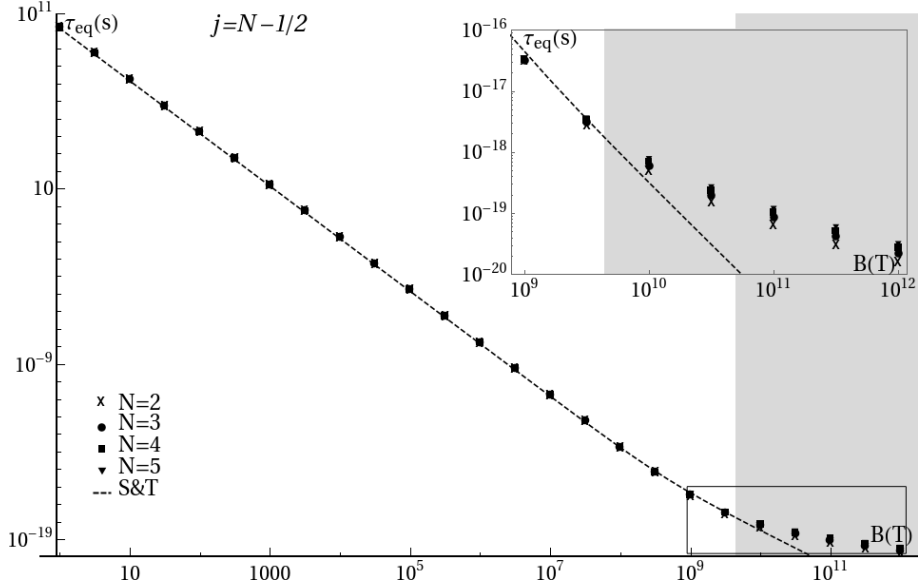


Figure 4.3: Time scale at which spin equilibrium is reached. Interestingly, beyond the critical field (grey area), lower lying states equilibrate faster. Note the diverging S&T rate beyond the critical field strength, indicating that the S&T approximation is not applicable in that regime.

other. Transitions between these states should be suppressed at all field strengths. Again, assuming the electron wave function has an infinite spatial extent overlooks this effect.

The time scale over which an electron reaches its equilibrium spin can be inferred from a simple two-state model. Assuming there is only one spin up and one spin down state with electrons transitioning back and forth between them, the equilibrium spin is approached as  $e^{-t/\tau_{eq}}$ , with  $\tau_{eq} = 1/(\Gamma_{\uparrow\downarrow} + \Gamma_{\downarrow\uparrow})$ , the reciprocal of the sum of the spin flip rates. In Fig. 4.3 we plot the spin equilibration times for several Landau levels. The equilibration time depends little on the Landau level, but decreases quadratically with  $B$  up to the critical field. At one Tesla the spin equilibration time is on the order of a millennium. The actual dynamics are more complicated, with the electron being able to transition to different Landau levels, both via spin-preserving and spin flip transitions. At low magnetic fields the time scales of spin preserving and spin flip transitions separate, as can be seen in Fig. 4.4. This separation of time scales stems from the spin preserving transitions having higher transition rates than the spin flip transitions, as one can see in Fig. 4.1. For low magnetic field strengths the electron transitions first to an  $N = 1$  spin up state before undergoing spin flip to an  $N = 0$  spin down state much later. At high field strengths both processes occur at similar rates and the electron can undergo spin flip before transitioning to an  $N = 1$  spin up state, as is signified by the lower occupation of these states at all times.

For higher  $N$  states we expect that the overestimation of transition rates due to these effects becomes smaller and the established results become more reliable.

For Figs. 4.1-4.3 we summed over the transition rates to all final states in our data set and we always used the states with the highest allowed angular momentum at their energy level as initial states ( $j = N - \frac{1}{2}$ ). To see whether it is necessary to sum over that many states



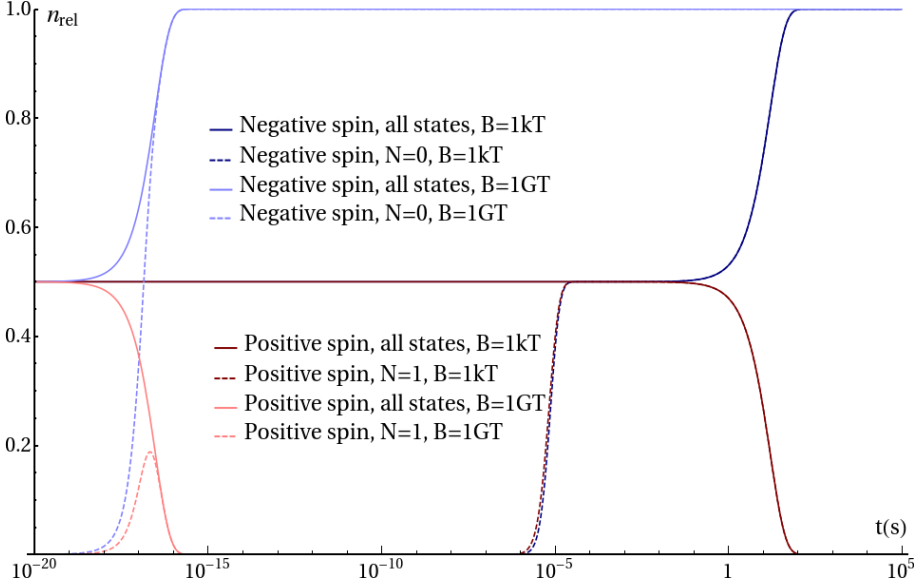


Figure 4.4: Relative occupation of different states starting out from a spin-depolarised  $N = 5$ ,  $j = 9/2$  state for different magnetic field strengths. At low field strength the electron first transitions to the lowest state allowed for its spin, before undergoing spin flip at much later times. At high fields the spin flip and spin-preserving transition rates become comparable and the lowest state for spin up ( $N = 1$ ) is less occupied at all times.

we computed the spin flip rates while progressively omitting low lying final states from the computation. The results are shown in Fig. 4.5. For the spin flip rates one can clearly see that only including the states with  $N' = N - 1$  is a very good approximation for magnetic field strengths below the critical field strength, but this approximation breaks down at the critical field strength. The same effect can be seen for spin preserving transitions, but it is much weaker.

At the lowest order perturbation theory, degenerate states with the same spin seem to have the same transition characteristics, as can be seen in Fig. 4.6. As we included only a finite number of the infinite number of electron states in our calculations, small errors are to be expected, especially for initial states with angular momentum lying close to the minimal angular momentum of final states included in the calculation. We took the precaution of taking the lowest angular momentum of the final states to be four quanta lower than the lowest angular momentum of the initial states ( $j'_{\text{min}} = -\frac{17}{2}$ ) and the data shown in Fig. 4.6 extends no further down than  $j_{\text{in}} = \frac{1}{2}$ , which makes limited data an unlikely cause for the remaining differences in transition rates. Still we have not ruled out all possible artefacts that may cause errors and have no compelling explanation why there should be a  $j$ -dependence in the transition rates.

## 4.5 Discussion

Our calculations show that for low-lying states, finite-extent effects influence the emission of synchrotron radiation. The most striking consequence is that, even in excited states, an

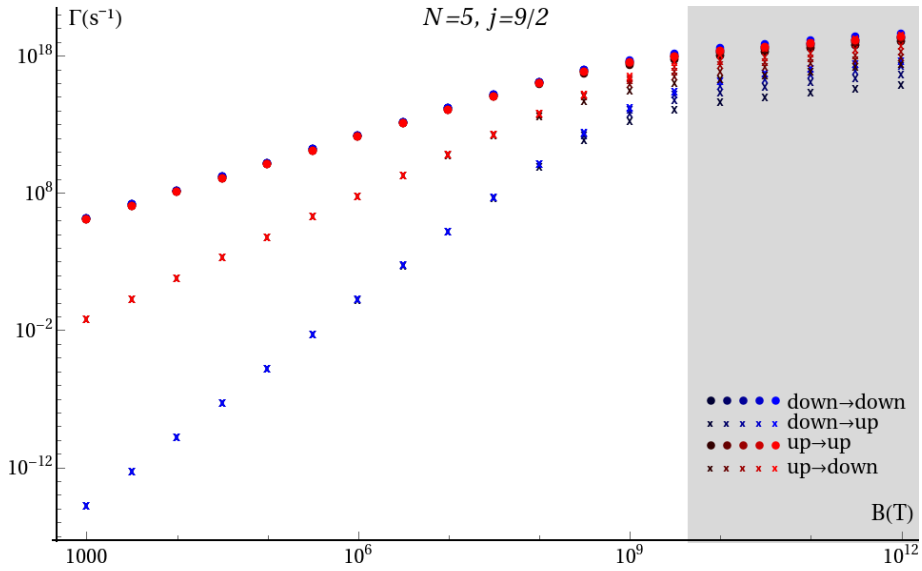


Figure 4.5: The data from Fig. 4.1 plotted using including an increasing number of energy levels. The darkest markers show the transition rates to  $N = 4$  only, the next darkest markers to  $N = 3$  and  $N = 4$  etc. As long as the magnetic field strength is far below the critical field strength, including only transitions to  $N - 1$  is a good approximation. Beyond the critical field strength even transitions directly to  $N = 0$  make a significant contribution to the spin flip rates. For spin preserving transitions, the same effect can be seen, albeit weaker.

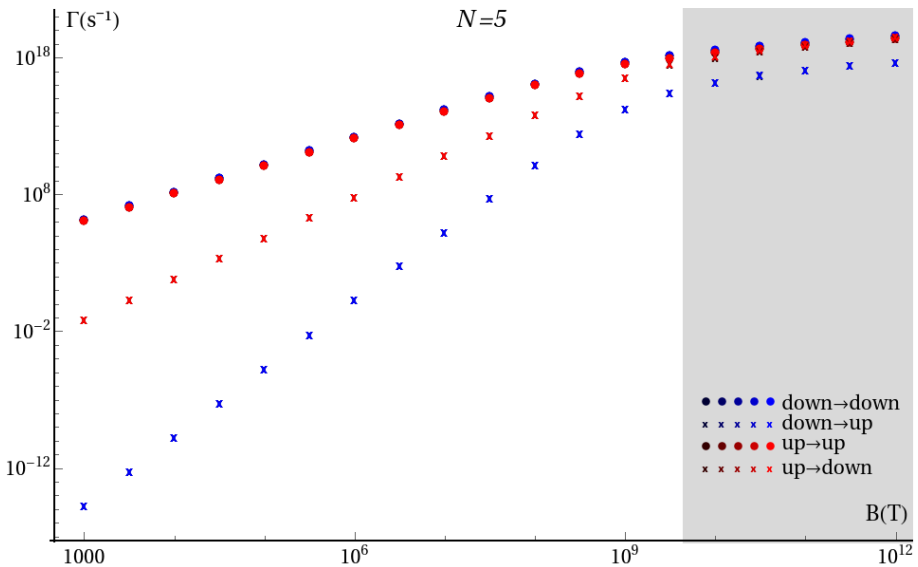


Figure 4.6: the spin preserving and spin flip transition rates for  $N = 5$  initial states with momenta ranging from  $j = \frac{1}{2}$  (darkest markers) to  $j = \frac{9}{2}$  (brightest markers). Little variation between the different angular momenta can be seen.

electron in a magnetic field can become highly spin polarised.

In our calculations we ignore level shifts due to higher order perturbations, this includes the lifting of the spin-degeneracy due to the electron's anomalous magnetic moment. For the emitted photons we ignore the effects of vacuum birefringence at strong background magnetic fields. Even at the critical field strength the magnitude of these effects is  $\sim \alpha/2\pi$  [206–209]. The main effect of the shifting of the electron's energy levels is that the available phase space for the various decay channels change. The decay rates should change proportionally to the available phase space. Therefore we expect the relative changes in the decay rates to be on the order of  $\alpha/2\pi$  too. The only qualitatively new feature that can occur due to level shifts is that it allows decays between previously degenerate states, most importantly spin up and spin down with the same  $N$ . Our method is unable to make predictions about decay rates between such near-degenerate states, but from the small available phase space we expect them to be small even at the critical field strength  $O((\alpha B/2\pi B_{\text{cr}})^2)$ . The vacuum birefringence primarily affects the propagation of the emitted photons. The changes it causes in the coupling of the photons to the electron are of second order in  $\alpha$ . Having considered these effects we believe our calculations are still fairly reliable at the critical field strength.

## 4.6 Outlook

Our numerical integration over all outgoing photon states assumed a homogeneous density of states, but it can be adapted to inhomogeneous densities as well, making it well suited for cavity QED problems in a strong magnetic field.

At low magnetic field strengths ( $\sim 1\text{T}$ ), the spin equilibration times are exceedingly long for the Landau levels we investigated. One can imagine investigating higher lying Landau levels, which we expect to trade off some equilibrium spin polarisation purity (as  $\sqrt{2(2n+|l|+1)/B|e|}$ , is larger and transition selectivity is less strict) for a faster equilibration time, finding states which combine reasonably good equilibrium spin polarisation purity with a reasonable equilibration time.

Our results were obtained using transition matrix elements obtained from first principles without making any approximation apart from ignoring higher order perturbative effects. This approach can potentially be used for many more problems including quantum corrections and scattering in a strong magnetic field. To complement our exact approach, for weak magnetic fields, the small spatial extent of the electron wave function compared to the wavelength of the radiated photons allows for constructing a simpler approximate model.



# Appendix A

## Optical coherence and correlation functions

The helicity lattices from chapter 2 are interference phenomena and therefore mutually coherent light sources are a requirement for seeing them. In order to treat light sources with partial coherence, we first note that although we are interested in interference between an electric and a magnetic field, and not in interference between two electric fields, the magnetic field of a light wave is completely determined by its electric field and thus the same correlation functions can be used to describe coherence in electric field- and helicity interference.

To construct a theoretical model for helicity lattices formed by light sources with partial coherence, we further assume that all superposed waves are split off from the same parent wave, then have their polarisation, intensity and propagation direction modified and are then recombined. This allows us to describe all coherence properties with the *autocorrelation function* of a single wave.

If one takes two plane-wave like partially coherent light fields  $\tilde{\mathbf{E}}_1 \approx e^{i\mathbf{k}\cdot\mathbf{x}-\omega t}$  then a translation along  $\mathbf{k}$  is has the same effect as a propagation in time. Thus the *spatial* correlation along this direction can be found using a *temporal* correlation function. The wave does not propagate perpendicular to  $\mathbf{k}$  and to find correlations in these directions we need to find a model for the spatial correlation function. Because we consider two- and three dimensional helicity lattices we will have to understand both the spatial and temporal coherence properties of the light waves and we will treat both here in separate sections.

### A.1 Temporal coherence and the temporal autocorrelation function

If one takes a light wave, splits off a part of it with amplitude  $\tilde{\mathbf{E}}_2$  and then superposes the split off part again with a time delay  $\tau$  on the remainder, which has amplitude  $\tilde{\mathbf{E}}_1$  (the spatial profiles of the waves are not important for this section), one obtains the following intensity

$$I = \frac{1}{2}\tilde{\mathbf{E}}_1(t) \cdot \tilde{\mathbf{E}}_1^*(t) + \frac{1}{2}\tilde{\mathbf{E}}_2(t+\tau) \cdot \tilde{\mathbf{E}}_2^*(t+\tau) + \text{Re}(\langle \tilde{\mathbf{E}}_1(t) \cdot \tilde{\mathbf{E}}_2^*(t+\tau) \rangle). \quad (\text{A.1})$$

Here  $\langle \rangle$  denotes time averaging over a time long compared to the coherence time. A time delay can be easily achieved by having both waves travel different path length and the above formula can be used to describe the interference patterns of two-slit experiments or Michelson- Mach-Zehnder- or Sagnac interferometers. If the light would be perfectly coherent the time averaging of the interference term does nothing and the interference term will persist for arbitrarily long time delays. If the light is partially coherent the interference term will average to zero for long time delays and thus the interference will disappear if the optical path difference between the two waves becomes to large.

Because the above equation can be used to describe a large variety of experiments it would be useful to separate properties of the used light source from effects that depend on the experimental setup. Making use of the fact that both waves are split off from the same parent wave, we can make the following separation [74]

$$I = \frac{1}{2} \tilde{\mathbf{E}}_1(t) \cdot \tilde{\mathbf{E}}_1^*(t) + \frac{1}{2} \tilde{\mathbf{E}}_2(t+\tau) \cdot \tilde{\mathbf{E}}_2^*(t+\tau) + \text{Re} \left( g_t^{(1)}(\tau) \tilde{\mathbf{E}}_1(t) \cdot \tilde{\mathbf{E}}_2^*(t) \right), \quad (\text{A.2})$$

where  $\tilde{\mathbf{E}}_1$  and  $\tilde{\mathbf{E}}_2$  have to be calculated from the experiment under consideration and  $g_t^{(1)}(\tau)$  is the first order autocorrelation function

$$g_t^{(1)}(\tau) = \frac{\langle \tilde{\mathbf{E}}(t) \cdot \tilde{\mathbf{E}}^*(t+\tau) \rangle}{\langle \tilde{\mathbf{E}}(t) \cdot \tilde{\mathbf{E}}^*(t) \rangle}. \quad (\text{A.3})$$

the autocorrelation function is an intrinsic property of the light source and it is the function we want to know. The interference fringes stem from the rapidly oscillating part of the first order autocorrelation function. If one is interested in the visibility, it is useful to separate out this rapidly oscillating part and focus on the slowly varying envelope only. Here using a complex representation of the fields shows its use. The fringe visibility can be written as

$$|g_t^{(1)}(\tau)| \text{Re}(\tilde{\mathbf{E}}_1(t) \tilde{\mathbf{E}}_2^*(t)). \quad (\text{A.4})$$

We will see when looking at explicit cases that the rapid oscillations are removed from  $|g^{(1)}(\tau)|$ . One can easily show the following properties of  $g_t^{(1)}(\tau)$  [230]

$$g_t^{(1)}(0) = 1, \quad g_t^{(1)}(-\tau) = g_t^{(1)*}(\tau) \text{ and for any realistic light source } \lim_{\tau \rightarrow \infty} g_t^{(1)}(\tau) = 0. \quad (\text{A.5})$$

There exist explicit forms for  $g_t^{(1)}(\tau)$  which are useful in practice for several models of quasi-monochromatic light sources. These are collision broadened sources, Doppler broadened sources and collision- and Doppler broadened sources [230].

The collision broadened model considers a collection of atoms emitting monochromatic light of frequency  $\omega_0$  which randomly collide with a collision rate  $\Gamma_c$  and after each collision have their emitted radiation undergo a phase jump to a random phase picked from the uniform distribution on  $[0, 2\pi)$  [230]. The phases of the emitted light from different atoms are completely uncorrelated and all atoms behave identically. Using this model,  $gT_t^{(1)}(\tau)$  depends only on the phase autocorrelation of a single atom

$$g_t^{(1)}(\tau) = e^{-i\omega_0\tau} \langle e^{i(\phi(t)-\phi(t+\tau))} \rangle. \quad (\text{A.6})$$

If there has been no phase jump between  $t$  and  $t+\tau$ ,  $\langle e^{i(\phi(t)-\phi(t+\tau))} \rangle = 1$ . If there has been a phase jump  $\langle e^{i(\phi(t)-\phi(t+\tau))} \rangle = 0$ . The chance of no phase jump occurring between  $t$  and  $t+\tau$  is  $e^{-\Gamma_c\tau}$ , which yields after averaging over  $t$

$$g_t^{(1)}(\tau) = e^{-i\omega_0\tau - \Gamma_c|\tau|}. \quad (\text{A.7})$$

the absolute bars follow from the time reversal properties of  $g_t^{(1)}(\tau)$ . The above autocorrelation function was derived from a collection of atoms that completely randomise their phases at random moments in time, but it can originate from other processes too. Consider a set of noncolliding uncorrelated emitters which emit light with an exponentially decaying amplitude with decay rate  $\Gamma$ . At random intervals occurring at a rate  $\Gamma_I$  the amplitude of an emitter jumps back to an initial amplitude  $E_0$ . For this model one finds an autocorrelation function with the same form:

$$g_t^{(1)}(\tau) = e^{-i\omega_0\tau - (\Gamma + \Gamma_I)|\tau|}. \quad (\text{A.8})$$

And when one reintroduces collisions one finds

$$g_t^{(1)}(\tau) = e^{-i\omega_0\tau - (\Gamma + \Gamma_I + \Gamma_c)|\tau|}. \quad (\text{A.9})$$

If considers a model of colliding atoms which undergo only small phase jumps at a collision one finds (if the phase jumps are equally likely to occur in both directions)

$$g_t^{(1)}(\tau) = e^{-i\omega_0\tau - \Gamma_c \left(1 - \cos(\sqrt{\langle \delta\phi^2 \rangle})\right) |\tau|}, \quad (\text{A.10})$$

with  $\delta\phi$  the phase jump at a collision. Thus the form of the autocorrelation function derived from the collision broadening model remains the same under a variety of assumptions.

One can also readily calculate  $g_t^{(1)}(\tau)$  for a Doppler broadened source. In this situation, one considers a collection of non-colliding, but moving atoms which emit monochromatic radiation. The frequency of the emitted radiation is Doppler shifted due to the speed of the atoms. For a thermal nonrelativistic gas the frequency distribution of the emitted light is a Gaußian centred at  $\omega_0$ . The radiation emitted by different atoms is assumed to be uncorrelated at all times. Using this model one finds [230]

$$\langle \tilde{\mathbf{E}}(t) \tilde{\mathbf{E}}^*(t + \tau) \rangle = \sum_j E_j^2 e^{-i\omega_j\tau}. \quad (\text{A.11})$$

Assuming the radiated amplitudes of all atoms to be equal and assuming the number of atoms is large, the sum can be converted to an integral over the Gaußian frequency distribution. Taking the spread in frequencies to be  $\delta\omega$  and dividing out the total radiated intensity yields

$$g_t^{(1)}(\tau) = \frac{1}{\sqrt{2\pi}\delta\omega} \int_0^\infty e^{i\omega\tau - \frac{(\omega_0 - \omega)^2}{2\delta\omega^2}} d\omega \quad (\text{A.12})$$

Assuming  $\omega_0 \gg \delta\omega$  the lower integration limit can be taken to  $-\infty$  and the integral can be evaluated

$$g_t^{(1)}(\tau) = e^{-i\omega_0\tau - \frac{\delta\omega^2\tau^2}{2}}. \quad (\text{A.13})$$

This form of the correlation function persists if one assumes that the atoms radiate with different amplitudes as long as it is not the case that a few atoms radiate almost all intensity and the assumption that the sum over emitters can be approximated by an integral does not hold.

The last case we consider is a source which displays the characteristics of both the collision- and Doppler broadening models. This will produce an autocorrelation function which contains the previous ones as special cases. We can compute the autocorrelation function by first considering the autocorrelation of the radiation emitted by a single atom

$$\langle \tilde{\mathbf{E}}_j(t) \tilde{\mathbf{E}}_j^*(t + \tau) \rangle = E_j^2 \langle e^{i(\omega_j\tau + \phi_j(t) - \phi_j(t + \tau))} \rangle = E_j^2 e^{i\omega_j\tau - \Gamma_c|\tau|}. \quad (\text{A.14})$$

The calculation of the autocorrelation function of the entire collection of atoms proceed the same way as for the solely Doppler broadened case, since the phases of the radiation contributions of different atoms are uncorrelated at all times. The end result is [230]

$$g_t^{(1)}(\tau) = e^{-i\omega_0\tau - \frac{\delta\omega^2\tau^2}{2} - \Gamma_c|\tau|}. \quad (\text{A.15})$$

The above equation can capture a lot of different physical processes using just two parameters,  $\delta\omega$  and  $\Gamma_c$ . If there would be physical processes taking place in a light source that would lead to different (that is, power law) autocorrelation function, any process giving an autocorrelation function of the form (A.15), taking place as well will make the autocorrelation function decay asymptotically exponentially. Therefore we will use eq. (A.15) as a basic model to describe the effects of partial coherence on helicity lattices.

The magnitude of  $\int_{-\infty}^{\infty} g_t^{(1)}(\tau) g_t^{(1)*}(\tau) d\tau$  is a measure for the temporal coherence of a light source. It has the dimension of time and is called the coherence time  $\tau_c$ . One can calculate that for the collision broadened model,  $\tau_c = 1/\Gamma_c$  and for the Doppler broadened model  $\tau_c = \sqrt{\pi}/\delta\omega$ . For eq. (A.15) the expression for  $\tau_c$  is more complicated. It is not the harmonic sum of the coherence times of the collision and Doppler contributions.

$$\tau_c = 2 \int_0^{\infty} e^{-\delta\omega^2\tau^2 - 2\Gamma_c^2\tau} d\tau = 2 \int_0^{\infty} e^{-(\delta\omega\tau + \frac{\Gamma_c}{\delta\omega})^2 + \frac{\Gamma_c^2}{\delta\omega^2}} d\tau = \frac{\sqrt{\pi}}{\delta\omega} e^{\frac{\Gamma_c^2}{\delta\omega^2}} \left( 1 - \operatorname{erf}\left(\frac{\Gamma_c}{\delta\omega}\right) \right). \quad (\text{A.16})$$

This expression reduces to the coherence time for the solely Doppler broadened model if  $\Gamma_c = 0$ . It also reduces to the coherence time for the radiation broadened model, as can be verified using l'Hôpital's rule

$$\lim_{\delta\omega \rightarrow 0} \frac{\sqrt{\pi} \left( 1 - \operatorname{erf}\left(\frac{\Gamma_c}{\delta\omega}\right) \right)}{\delta\omega e^{-\frac{\Gamma_c^2}{\delta\omega^2}}} = \lim_{\delta\omega \rightarrow 0} \frac{2\Gamma_c/\delta\omega^2 e^{-\frac{\Gamma_c^2}{\delta\omega^2}}}{(1 - 2\Gamma_c^2/\delta\omega^2) e^{-\frac{\Gamma_c^2}{\delta\omega^2}}} = \frac{1}{\Gamma_c}. \quad (\text{A.17})$$

As additional sanity checks, one can confirm that eq. (A.16) goes to zero if either  $\Gamma_c$  or  $\delta\omega$  goes to infinity, using l'Hôpital's rule in the case of  $\Gamma_c \rightarrow \infty$

$$\lim_{\Gamma_c \rightarrow \infty} \frac{\sqrt{\pi} \left( 1 - \operatorname{erf}\left(\frac{\Gamma_c}{\delta\omega}\right) \right)}{\delta\omega e^{-\frac{\Gamma_c^2}{\delta\omega^2}}} = \lim_{\Gamma_c \rightarrow \infty} \frac{2e^{-\frac{\Gamma_c^2}{\delta\omega^2}}/\delta\omega}{2\delta\omega\Gamma_c e^{-\frac{\Gamma_c^2}{\delta\omega^2}}/\delta\omega^2} = \lim_{\Gamma_c \rightarrow \infty} \frac{1}{\Gamma_c} = 0. \quad (\text{A.18})$$

From the coherence time, one can calculate a coherence length  $\ell = c\tau_c$  by multiplying the coherence time with the light speed. The parameter  $\ell$  will determine over which length scale the helicity lattices can remain visible.

## A.2 Spatial coherence

If one takes a plane wave, splits it in two parts with amplitudes  $\tilde{\mathbf{E}}_1$  and  $\tilde{\mathbf{E}}_2$ , sends both waves into different directions  $\mathbf{k}_1$  and  $\mathbf{k}_2$  and superposes them again, one obtains an interference pattern

$$I = \frac{1}{2} \tilde{\mathbf{E}}_1 \cdot \tilde{\mathbf{E}}_1^* + \frac{1}{2} \tilde{\mathbf{E}}_2 \cdot \tilde{\mathbf{E}}_2^* + \operatorname{Re}(\langle \tilde{\mathbf{E}}_1 \cdot \tilde{\mathbf{E}}_2^* \rangle). \quad (\text{A.19})$$

The difference in optical path lengths both waves travelled to arrive at a point  $\mathbf{x}$  translates to a difference in travel time. Taking the optical path length difference to be zero at the



origin of our coordinate system, we can find an explicit form for the interference pattern

$$I = \frac{1}{2} \tilde{\mathbf{E}}_1 \cdot \tilde{\mathbf{E}}_1^* + \frac{1}{2} \tilde{\mathbf{E}}_2 \cdot \tilde{\mathbf{E}}_2^* + |g_t^{(1)}((\mathbf{k}_1 - \mathbf{k}_2) \cdot \mathbf{x}/c)| |\tilde{\mathbf{E}}_1 \cdot \tilde{\mathbf{E}}_2^*| \cos((\mathbf{k}_1 - \mathbf{k}_2) \cdot \mathbf{x} + \arg(\tilde{\mathbf{E}}_1 \cdot \tilde{\mathbf{E}}_2^*)). \quad (\text{A.20})$$

So including limited temporal coherence causes the interference fringes to become less visible in the direction of maximally increasing optical path differences. The visibility of the interference fringes does not diminish at all in the two perpendicular directions, which is unexpected for a light source assumed to be imperfect. This indicates that a temporal autocorrelation function alone is not enough to describe the coherence properties of light. The total absence of fringe visibility loss in two directions stems from the assumption that amplitude and phase are perfectly uniform in the plane perpendicularly to the propagation direction. this is not a realistic assumption and dropping it will result in a limited spatial coherence.

Similar to the temporal autocorrelation function, one can define a spatial autocorrelation function which tells how well the electric field is correlated in the plane perpendicular to the propagation direction. it will be a function of two spatial coordinates, which can be written in either Cartesian or polar coordinates as  $g_s^{(1)}(x, t)$  or  $g_s^{(1)}(r, \varphi)$ . the spatial autocorrelation can be anisotropic, but we will only consider isotropic autocorrelation functions which can be written as  $g_s^{(1)}(r)$ . Unfortunately there is not a single autocorrelation function which captures most physics one could care about with only a few phenomenological parameters, like Eq. (A.15) does. For a faraway incoherent light source there is the van Cittert-Zernike theorem which states that [232, 233]

$$g_s^{(1)}(x, y) = \frac{\int I(X, Y) e^{i \frac{k}{R}(xX + yY)} dX dY}{\int I(X, Y) dX dY} \quad (\text{A.21})$$

With  $R$  the distance to the source,  $k$  the wave number of the light and  $I(X, Y)$  the intensity profile in the source plane. This expression is a Fourier transform, which demonstrates how an autocorrelation function can be anisotropic. Take a source that is much more extended in the Y-direction than in the X-direction, a narrow slit which is lit from behind is a good example. Upon Fourier transforming The autocorrelation function becomes wide in the x-direction and narrow in the y-direction. A commonly used intensity profile is a uniform disc, which is useful for describing, amongst others, the light from an illuminated pinhole or a star. Taking  $R_0$  as the radius of the disc and using the two dimensional vectors  $\vec{X} = (X, Y)$  and  $\vec{x} = (x, y)$  with lengths  $R'$  and  $r$  and a relative angle of  $\Phi$  between them the autocorrelation function can be written as

$$g_s^{(1)}(r) = \frac{1}{2\pi R_0^2} \int_0^{R_0} \int_0^{2\pi} e^{i \frac{k}{R} r R' \cos(\Phi)} d\Phi dR' = \frac{1}{R_0^2} \int_0^{R_0} J_0\left(\frac{kr}{R} R'\right) R' dR'. \quad (\text{A.22})$$

This integral can be evaluated as the limit of an integral over a product of Bessel functions

$$\begin{aligned} g_s^{(1)}(r) &= \lim_{\kappa \rightarrow 0} \frac{1}{R_0^2} \int_0^{R_0} J_0\left(\frac{kr}{R} R'\right) J_0(\kappa R) R' dR' \\ &= \lim_{\kappa \rightarrow 0} \frac{1}{R_0} \frac{1}{(kr/R)^2 - \kappa^2} \left( \kappa J_0\left(\frac{kr}{R} R_0\right) J_0'(\kappa R) - \frac{kr}{R} J_0'\left(\frac{kr}{R} R_0\right) J_0(\kappa R) \right) \\ &= \frac{2J_1\left(\frac{kr}{R} R_0\right)}{R_0 kr/R}. \end{aligned} \quad (\text{A.23})$$

In the last line we used the recurrence relation  $J'_0(x) = 2J_1(x)$ . This result looks similar to the  $\sin(x)/x$  function, only with the sine replaced by a Bessel function, and one can check that the limit  $r \rightarrow 0$  equals one as it should be. One can see that the autocorrelation function decays faster for short wavelengths, since a short wavelength light field can fluctuate over shorter length scales, and it decays slower if the distance between source and observer is longer, as fluctuations get ‘stretched out’ upon propagation over long distances. The oscillations of the Bessel function imply that interference fringes will disappear completely and then reappear again, something Michelson used to determine the size of a star [234, 235]. The autocorrelation function also decays more slowly if the size of the source is small, which explains why a pinhole can be used to make an incoherent light source spatially coherent.

In any realistic attempt to make helicity lattices, lasers will be used, for which the van Cittert-Zernike theorem is unfortunately not applicable and one needs other models. Assuming the laser operates perfectly in single mode, it is perfectly spatially coherent and all inhomogeneities in the wave front are picked up during propagation. Using Kolmogorov’s theory for turbulence [236, 237], one can find for turbulent media the autocorrelation function  $g_s^{(1)}(r) = e^{-(r/r_0)^{5/3}}$  [238, 239]. This is a useful model for outdoor experiments [28], but in a laboratory turbulence is less of a disturbance. We will therefore use a different model. We will assume that between two points the phase of the wavefront will make a random walk with a sufficiently small step size. The phase difference between two points a distance  $r$  part can then be described by a diffusive model where the phase difference between two points a distance  $r$  apart is drawn from the probability distribution

$$P(\Delta\phi) = e^{-\Delta\phi^2/2\kappa r}/\sqrt{2\pi\kappa r} \quad (\text{A.24})$$

with  $\kappa$  an inverse length scale related to the spatial coherence length. Using an inverse length scale as phenomenological parameter instead of a length scale will allow us to retrieve the limit of perfect spatial coherence by sending  $\kappa$  to zero. Now the expectation value of the scalar product of the electric field in two different is

$$\langle \tilde{\mathbf{E}}(0) \cdot \tilde{\mathbf{E}}^*(r) \rangle = \tilde{\mathbf{E}}(0) \cdot \tilde{\mathbf{E}}^*(0) \langle e^{-i\Delta\phi - \Delta\phi^2/2\kappa r} / \sqrt{2\pi\kappa r} \rangle = \tilde{\mathbf{E}}(0) \cdot \tilde{\mathbf{E}}^*(0) e^{-\kappa r} \implies g_s^{(1)}(r) = e^{-\kappa r}. \quad (\text{A.25})$$

With this autocorrelation function we can determine the attenuation of interference patterns due to partial spatial coherence. Along the direction  $\mathbf{k}_1 + \mathbf{k}_2$  The wavefront of wave 1 slides sideways by a distance  $\mathbf{x} \cdot (\mathbf{k}_1 + \mathbf{k}_2) / |\mathbf{k}_1 + \mathbf{k}_2| \sin \theta / 2$  with  $\theta$  the angle between  $\mathbf{k}_1$  and  $\mathbf{k}_2$ . The wavefront of wave 2 slides over an equal distance in the opposite direction. We know that  $\cos \theta = \mathbf{k}_1 \cdot \mathbf{k}_2 / c^2 \omega^2$  and using the half angle formula  $\sin(\theta/2) = \sqrt{\frac{1}{2} - \frac{1}{2} \cos \theta}$  we arrive at the following expression for the interference fringes of two partially coherent plane waves

$$|g_i^{(1)}((\mathbf{k}_1 - \mathbf{k}_2) \cdot \mathbf{x}/c)| |g_s^{(1)} \left( 2\sqrt{\frac{1}{2} - \frac{1}{2} \cos(\mathbf{k}_1 \cdot \mathbf{k}_2 / c^2 \omega^2)} \mathbf{x} \cdot (\mathbf{k}_1 + \mathbf{k}_2) / |\mathbf{k}_1 + \mathbf{k}_2| \right) \times \\ |\tilde{\mathbf{E}}_1 \cdot \tilde{\mathbf{E}}_2^*| \cos((\mathbf{k}_1 - \mathbf{k}_2) \cdot \mathbf{x} + \arg(\tilde{\mathbf{E}}_1 \cdot \tilde{\mathbf{E}}_2^*)). \quad (\text{A.26})$$

This is the form of the interference terms we will use to model helicity lattices of partially coherent light.

## Appendix B

# Associated Laguerre polynomials and Laguerre-Gauß functions.

The Laguerre-Gauß modes are important tools for the description of light- or matter wave beams. Because they occur a lot in this thesis we will here recap some of their important mathematical relations.

### B.1 Associated Laguerre polynomials.

The associated Laguerre polynomials of the  $l$ th kind  $L_n^l(x)$  are the eigenfunctions of the differential equations

$$xL_n^{l''}(x) + (l+1-x)L_n^{l'}(x) = -nL_n^l(x), \quad n, l \in \mathbb{N}_0. \quad (\text{B.1})$$

I will follow the solution strategy given in [240] for solving these differential equations. This strategy is solving the  $l = 0$  case with a Frobenius series substitution and obtaining the solutions for  $l > 0$  with induction. Substituting  $\sum_{m=0}^{\infty} a_m x^{m+\sigma}$  into the differential equation for  $l = 0$  yields

$$\sum_{m=0}^{\infty} (m+\sigma)(m+\sigma-1)a_m x^{m+\sigma-1} + (m+\sigma)(1-x)a_m x^{m+\sigma-1} = -n \sum_{m=0}^{\infty} a_m x^{m+\sigma}. \quad (\text{B.2})$$

Dividing through  $x^{\sigma-1}$  and setting  $x = 0$  shows that  $\sigma = 0$ . Therefore the solutions are simple power series. The coefficients  $a_m$  can be found by equating terms with equal powers of  $x$ . One has

$$\sum_{m=0}^{\infty} ((m+1)m a_{m+1} + (m+1)a_{m+1})x^m = \sum_{m=0}^{\infty} (m-n)a_m x^m \implies a_{m+1} = \frac{m-n}{(m+1)^2} a_m. \quad (\text{B.3})$$

The recurrence relation shows that  $L_n^0(x)$  is a polynomial of order  $n$ . Following the convention  $a_0 = 1$  the Laguerre polynomials are

$$L_n^0(x) = 1 + \sum_{m=1}^n \frac{\prod_{\mu=1}^m (\mu-n)}{\prod_{\mu=1}^m (\mu-1+1)^2} x^m = \sum_{m=1}^n \frac{(-1)^m n!}{(m!)^2 (n-m)!} x^m. \quad (\text{B.4})$$

To obtain the solutions for  $l > 0$  differentiate the differential equation

$$xL_n^{l'''}(x) + (l+2-x)L_n^{l''}(x) = -(n-1)L_n^{l'}(x) \implies L_{n-1}^{l+1}(x) \propto L_n^{l'}(x). \quad (\text{B.5})$$

Conventionally the proportionality constant is chosen to be  $-1$ , yielding  $L_n^l(x) = (-1)^l \frac{d^l}{dx^l} L_{n+l}^0(x)$ . Thus the explicit expressions for  $L_n^l(x)$  are

$$L_n^l(x) = \sum_{m=l}^{n+l} \frac{(-1)^{m-l} (n+l)! m!}{(m!)^2 (n+l-m)! (m-l)!} x^{m-l} = \sum_{m=0}^n \frac{(-1)^m (n+l)!}{(m+l)! (n-m)! m!} x^m. \quad (\text{B.6})$$

Alternatively, the associated Laguerre polynomials can be written as [240]

$$L_n^l(x) = \frac{e^x}{n! x^l} \frac{d^n}{dx^n} x^{n+l} e^{-x}. \quad (\text{B.7})$$

### **Sturm-Liouville form and orthogonality.**

Every second order differential equation of the form

$$p(x)y''(x) + r(x)y'(x) + q(x)y(x) = -\lambda \rho(x)y(x) \quad (\text{B.8})$$

with  $\rho(x)$  non-negative on the domain of interest can be put in Sturm-Liouville form using an integrating factor  $F(x)$  such that one obtains

$$-(F(x)p(x)y'(x))' - F(x)q(x)y(x) = \lambda F(x)\rho(x)y(x) \quad (\text{B.9})$$

yielding the integrating factor  $F(x) = e^{\int x \frac{p'(x)-r(x)}{p(x)} dx}$ . Going through this calculation for the differential equation for the associated Laguerre polynomials yields the Sturm-Liouville equation

$$-(x^{l+1} e^{-x} L_n^{l'}(x))' = nx^l e^{-x} L_n^l. \quad (\text{B.10})$$

Using the hermiticity of Sturm-Liouville operators implies that Laguerre polynomials with different  $n$  and the same  $l$  are orthogonal under an appropriately defined scalar product, which can be found from the Sturm-Liouville form of their defining differential equation. Taking the integral over  $[0, \infty]$  of the left-hand side, one can integrate by parts and drop the surface terms because  $x^{l+1} e^{-x}|_{x=0} = x^{l+1} e^{-x}|_{x=\infty} = 0$  to find that

$$-\int_0^\infty y^*(x)(x^{l+1} e^{-x} y'(x))' dx = -\int_0^\infty (x^{l+1} e^{-x} y^{*'}(x))' y(x) dx. \quad (\text{B.11})$$

which can be used to get

$$\begin{aligned} & -\int_0^\infty L_{n'}^l(x)(x^{l+1} e^{-x} L_n^{l'}(x))' dx + \int_0^\infty (x^{l+1} e^{-x} L_{n'}^{l'}(x))' L_n^l(x) dx \\ & = (n-n') \int_0^\infty L_{n'}^l(x) x^l e^{-x} L_n^l(x) dx = 0 \implies \int_0^\infty L_{n'}^l(x) x^l e^{-x} L_n^l(x) dx = 0, \quad n \neq n'. \end{aligned} \quad (\text{B.12})$$

To find the value of the scalar product for  $n' = n$ , use eq. (B.7)

$$\frac{1}{n!} \int_0^\infty L_n^l(x) \frac{d^n}{dx^n} x^{l+n} e^{-x} dx = \frac{(-1)^n}{n!} \int_0^\infty \frac{d^n}{dx^n} (L_n^l(x)) x^{l+n} e^{-x} dx. \quad (\text{B.13})$$

The derivative can be computed using the power series definition of the Laguerre polynomials. Only the  $x^n$  term remains after  $n$  differentiations, yielding an easy to integrate expression

$$\frac{1}{n!} \int_0^\infty x^{l+n} e^{-x} dx = \frac{(n+l)!}{n!}. \quad (\text{B.14})$$

## Recurrence relations

In addition to occurring in a variety of problems and possessing useful orthogonality relations, the associated Laguerre polynomials are also a useful mathematical tool because of the recurrence relations that exist between them. We already used one to derive the explicit forms of the  $l \neq 0$  polynomials:

$$L_n^{l'}(x) = -L_{n-1}^{l+1}(x). \quad (\text{B.15})$$

From eq. (B.7) one can obtain a useful relation connecting associated Laguerre polynomials of the  $l$ th and  $l+1$ st kind

$$L_n^{l+1} = \frac{e^x}{x^{l+1}n!} \frac{d^n}{dx^n} x x^{n+l} e^{-x} = \frac{e^x}{x^{l+1}n!} \frac{d^{n-1}}{dx^{n-1}} x^{l+n} e^{-x} + \frac{e^x}{x^l} \frac{d^n}{dx^n} x^{n+l} e^{-x} = L_{n-1}^{l+1}(x) + L_n^l(x) \quad (\text{B.16})$$

or

$$L_n^l(x) = L_n^{l+1} - L_{n-1}^{l+1}. \quad (\text{B.17})$$

This recurrence relation is useful to prove

$$L_n^{l+1}(x) = \sum_{v=0}^n L_v^l(x) \quad (\text{B.18})$$

by induction. This relation is true for  $n=0$ . Assuming it is true for  $n-1$  yields

$$L_n^{l+1}(x) = L_{n-1}^{l+1}(x) + L_n^l(x) = \sum_{v=0}^{n-1} L_v^l(x) + L_n^l(x) = \sum_{v=0}^n L_v^l(x), \quad (\text{B.19})$$

which completes the proof. By repeatedly applying eq. (B.17), one can connect associated Laguerre polynomials more than one  $l$ -index apart.

$$L_n^l(x) = \sum_{v=0}^{\min\{n,\lambda\}} (-1)^v \binom{\lambda}{v} L_{n-v}^{l+\lambda}(x). \quad (\text{B.20})$$

By differentiating eq. (B.7) with respect to  $x$  and then multiplying with  $x$ , one can derive another useful recurrence relation

$$x \frac{d}{dx} \frac{e^x}{n!x^l} \frac{d^n}{dx^n} x^{n+l} e^{-x} = \frac{e^x}{n!x^{l-1}} \frac{d^n}{dx^n} x^{n+l} e^{-x} - l \frac{e^x}{n!x^l} \frac{d^n}{dx^n} x^{n+l} e^{-x} + \frac{e^x}{n!x^{l-1}} \frac{d^{n+1}}{dx^{n+1}} x^{n+1+l-1} e^{-x}$$

$$xL_n^{l'}(x) = xL_n^l(x) - lL_n^l(x) + (n+1)L_{n+1}^{l-1}(x). \quad (\text{B.21})$$

Now using the eqs. (B.15) and (B.17) one can rewrite this

$$xL_n^{l+1}(x) - l \left( L_n^{l+1}(x) - L_{n-1}^{l+1}(x) \right) + (n+1) \left( L_{n+1}^{l+1}(x) - 2L_n^{l+1}(x) + L_{n-1}^{l+1}(x) \right) = 0. \quad (\text{B.22})$$

Shifting the  $l$ -index and rearranging gives<sup>1</sup>

$$xL_n^l(x) = -(n+1)L_{n+1}^l(x) + (2n+l+1)L_n^l(x) - (n+l)L_{n-1}^l(x). \quad (\text{B.23})$$

There is one more useful recurrence relation which can be found by combining eqs. (B.15), (B.17) and (B.23):

$$xL_{n+1}^{l-1}(x) = (n+1) \left( L_{n+1}^l(x) - L_n^l(x) \right) - (n+l) \left( L_n^l(x) - L_{n-1}^l(x) \right) \iff \\ xL_n^l(x) = nL_n^l(x) - (n+l)L_{n-1}^l(x). \quad (\text{B.24})$$

## B.2 Laguerre-Gauß functions.

The Laguerre-Gauß functions are complex functions on  $\mathbb{R}^2$  defined in polar coordinates

$$LG_n^l(r, \phi) = r^{|l|} L_n^{|l|}(r^2) e^{-\frac{r^2}{2}} e^{il\phi} \equiv Lg_n^l(r) e^{il\phi}, \quad n \in \mathbb{N}_0, l \in \mathbb{Z}. \quad (\text{B.25})$$

The Laguerre-Gauß functions form an orthogonal basis on  $\mathbb{R}^2$ , as can be verified using eqs. (B.12) and (B.13):

$$\int_0^\infty \int_0^{2\pi} LG_{n'}^{l'}(r) LG_n^l(r) r d\phi dr = \pi \frac{(n+l)!}{n!} \delta_{l'l'} \delta_{nn'}. \quad (\text{B.26})$$

### The Hankel transforms of Laguerre-Gauß functions

The order  $l$  Hankel appears when Fourier transforming a function in polar coordinates. It is defined by

$$F_l(\kappa) = \int_0^\infty f(r) J_l(\kappa r) r dr. \quad (\text{B.27})$$

With  $J_l$  the order  $l$  Bessel function. The Laguerre Gauß functions have the property that they Hankel transform to themselves (up to a sign) (eq. (7.421.4) in [241])

$$\int_0^\infty Lg_n^l(r) J_{|l|}(\kappa r) r dr = (-1)^n Lg_n^l(\kappa). \quad (\text{B.28})$$

This can be proven in three steps. First consider  $Lg_0^0(r)$ , which is a simple Gaußian. Consider that the Fourier transform of a radially symmetric function can be written in polar coordinates

$$\int_0^\infty \int_0^{2\pi} f(r) e^{i\kappa r \cos(\theta)} r d\theta dr = \int_0^\infty f(r) J_0(\kappa r) r dr \quad (\text{B.29})$$

and the Gaußian Fourier transforms to itself, implying

$$\int_0^\infty Lg_0^0(r) J_0(\kappa r) r dr = Lg_0^0(\kappa). \quad (\text{B.30})$$

Now writing out eq. (B.28) explicitly for  $n = 0, l > 0$ , one has

$$\int_0^\infty r^{|l|} e^{-\frac{r^2}{2}} J_{|l|}(\kappa r) r dr = \kappa^{|l|} \int_0^\infty e^{-\frac{r^2}{2}} J_0(\kappa r) r dr = \kappa^{|l|} e^{-\frac{\kappa^2}{2}} = Lg_0^l(\kappa), \quad (\text{B.31})$$

<sup>1</sup>As nothing forbids one from choosing  $l = -1$  in eq. (B.7), this result applies for  $l = 0$  too.

where the intermediate step follows from repeated integration by parts and the relation  $\frac{d}{dr}r^{|l|}J_l(\kappa r) = \kappa r^{|l|}J_{l-1}(\kappa r)$ . Having proven eq (B.28) for  $n = 0$ , the cases  $n > 0$  follow by induction, assuming eq (B.28) is true for  $n$ . Using eq. (B.23) one gets

$$(n+1) \int_0^\infty Lg_{n+1}^l(r)J_l(\kappa r)rdr = \int_0^\infty (-r^2Lg_n^l(r) + (2n+l+1)Lg_n^l(r) - (n+l)Lg_{n-1}^l(r))J_l(\kappa r)rdr \quad (\text{B.32})$$

then one can use the identity

$$\int_0^\infty -r^2f(r)J_l(\kappa r)rdr = \left( \frac{d^2}{d\kappa^2} + \frac{1}{\kappa} \frac{d}{d\kappa} - \frac{l^2}{\kappa^2} \right) F_l(\kappa). \quad (\text{B.33})$$

An identity that can be proven by noticing that the Hankel transform is its own inverse and integrating the right hand side by parts. Then using

$$\begin{aligned} \frac{d}{d\kappa}Lg_n^l(\kappa) &= \left( |l|\kappa^{|l|-1}L_n^{|l|}(\kappa^2) - \kappa^{|l|+1}L_n^{|l|}(\kappa^2) + 2\kappa^{|l|+1}L_n^{|l|'}(\kappa^2) \right) e^{-\frac{\kappa^2}{2}} \\ \frac{d^2}{d\kappa^2}Lg_n^l(\kappa) &= \left( |l|(|l|-1)\kappa^{|l|-2}L_n^{|l|}(\kappa^2) - (2|l|+1)\kappa^{|l|}L_n^{|l|}(\kappa^2) + (4|l|+2)\kappa^{|l|}L_n^{|l|'}(\kappa^2) \right) e^{-\frac{\kappa^2}{2}} \\ &\quad + \left( L_n^{|l|}(\kappa^2) - 4L_n^{|l|'}(\kappa^2) + 4L_n^{|l|''}(\kappa^2) \right) \kappa^{|l|+2}e^{-\frac{\kappa^2}{2}} \end{aligned} \quad (\text{B.34})$$

one finds

$$\begin{aligned} \int_0^\infty -r^2Lg_n^l(r)J_{|l|}(\kappa r)rdr &= (-1)^n \left( -2(|l|+1)\kappa^{|l|}L_n^{|l|}(\kappa^2) + 4(l+1)\kappa^{|l|}L_n^{|l|'}(\kappa^2) \right) e^{-\frac{\kappa^2}{2}} \\ &\quad + (-1)^n \left( L_n^{|l|}(\kappa^2) - 4L_n^{|l|'}(\kappa^2) + 4L_n^{|l|''}(\kappa^2) \right) \kappa^{|l|+2}e^{-\frac{\kappa^2}{2}}. \end{aligned} \quad (\text{B.35})$$

Using eq. (B.1) one can simplify this to

$$\int_0^\infty -r^2Lg_n^l(r)J_{|l|}(\kappa r)rdr = (-1)^n \left( -2(|l|+1)Lg_n^l(\kappa) - 4nLg_n^l(\kappa) + \kappa^2Lg_n^l(\kappa) \right). \quad (\text{B.36})$$

from which one obtains

$$\begin{aligned} (n+1) \int_0^\infty Lg_{n+1}^l(r)J_{|l|}(\kappa r)rdr &= (-1)^n \kappa^2Lg_n^l(\kappa) - (-1)^n (2n+l+1)Lg_n^l(\kappa) \\ &\quad - (-1)^{n-1} (n+l)Lg_{n-1}^l(\kappa) \\ &= (-1)^{n+1} (n+1)Lg_{n+1}^l(\kappa), \end{aligned} \quad (\text{B.37})$$

which completes the proof.

Another useful Hankel transform identity involving Laguerre polynomials times a Gaussian functions is (eq. (6.631.10)) in [241])

$$\int_0^\infty r^{2n+l}e^{-r^2}J_l(\kappa r)rdr = \frac{n!}{2} \left( \frac{\kappa}{2} \right)^l L_n^l \left( \frac{\kappa^2}{4} \right) e^{-\frac{\kappa^2}{4}}, \quad (\text{B.38})$$

Which can again be proven by induction. The  $n = 0$  cases are similar to eq. (B.31) and can be verified in the same way. Now assuming the identity is true for  $n$  and using eq. (B.33) one finds (after some algebra)

$$\begin{aligned} \int_0^\infty r^{2(n+1)+l} e^{-r^2} J_l(\kappa r) r dr &= -\frac{n!}{2} \left( (l+1)L_n^{l'} \left( \frac{\kappa^2}{4} \right) - (l+1)L_n^l \left( \frac{\kappa^2}{4} \right) \right) \left( \frac{\kappa}{2} \right)^l e^{-\frac{\kappa^2}{4}} \\ &\quad - \frac{n!}{2} \left( L_n^l \left( \frac{\kappa^2}{4} \right) - 2L_n^{l'} \left( \frac{\kappa^2}{4} \right) + L_n^{l''} \left( \frac{\kappa^2}{4} \right) \right) \left( \frac{\kappa}{2} \right)^{l+2} e^{-\frac{\kappa^2}{4}} \end{aligned} \quad (\text{B.39})$$

Using eq. (B.1) to simplify gives

$$\begin{aligned} \int_0^\infty r^{2(n+1)+l} e^{-r^2} J_l(\kappa r) r dr &= \\ \frac{n!}{2} \left( (n+l+1)L_n^l \left( \frac{\kappa^2}{4} \right) - \frac{\kappa^2}{4} L_n^l \left( \frac{\kappa^2}{4} \right) + \frac{\kappa^2}{4} L_n^{l'} \left( \frac{\kappa^2}{4} \right) \right) \left( \frac{\kappa}{2} \right)^l e^{-\frac{\kappa^2}{4}} \end{aligned} \quad (\text{B.40})$$

Now one can use eq. (B.24) to further simplify

$$\begin{aligned} \int_0^\infty r^{2(n+1)+l} e^{-r^2} J_l(\kappa r) r dr &= \\ \frac{n!}{2} \left( (2n+l+1)L_n^l \left( \frac{\kappa^2}{4} \right) - (n+l)L_{n-1}^l \left( \frac{\kappa^2}{4} \right) - \frac{\kappa^2}{4} L_n^l \left( \frac{\kappa^2}{4} \right) \right) \left( \frac{\kappa}{2} \right)^l e^{-\frac{\kappa^2}{4}}, \end{aligned} \quad (\text{B.41})$$

which reduces to (using eq. (B.23))

$$\int_0^\infty r^{2(n+1)+l} e^{-r^2} J_l(\kappa r) r dr = \frac{(n+1)!}{2} \left( \frac{\kappa}{2} \right)^l L_{n+1}^l \left( \frac{\kappa^2}{4} \right) e^{-\frac{\kappa^2}{4}}, \quad (\text{B.42})$$

completing the proof.

## The relation to Hermite-Gauß functions

The Laguerre Gauß functions can be expressed as linear combinations of Hermite-Gauß functions expressed in cartesian coordinates, an identity due to [10]. This simple relation was used to construct twisted Laguerre-Gauß light beams from Hermite-Gauß laser beams [242] and it has been employed for electrons as well [48]. To find the expansion of a Laguerre-Gauß beam in terms of Hermite-Gauß beams we introduce the coordinate  $\rho = re^{i\phi}$  and consider

$$\begin{aligned} \frac{d}{d\rho^*} \rho^l L_n^l(\rho\rho^*) e^{-\rho\rho^*} &= \left( L_n^{l'}(\rho\rho^*) - L_n^l(\rho\rho^*) \right) \rho^{l+1} e^{-\rho\rho^*} = -\rho^{l+1} L_{n+1}^{l+1}(\rho\rho^*) e^{-\rho\rho^*}, \\ \frac{d}{d\rho} \rho^l L_n^l(\rho\rho^*) e^{-\rho\rho^*} &= \left( L_n^{l'}(\rho\rho^*) - L_n^l(\rho\rho^*) \right) \rho^{l+1} \rho^* e^{-\rho\rho^*} + l\rho^{l-1} L_n^l(\rho\rho^*) e^{-\rho\rho^*} \\ &= (n+1)\rho^{l-1} L_{n+1}^{l-1}(\rho\rho^*) e^{-\rho\rho^*}. \end{aligned} \quad (\text{B.43})$$

One gets the first line by using eqs. (B.15) and (B.17) and the second line by using eqs. (B.23) and (B.24). There are two similar equations for  $\rho \leftrightarrow \rho^*$ . Using these one



finds

$$\begin{aligned} \left(\frac{d}{d\rho^*}\right)^l \left(\frac{d}{d\rho^*} \frac{d}{d\rho}\right)^n e^{-\rho\rho^*} &= (-1)^{n+l} n! \rho^l L_n^l(\rho\rho^*) e^{-\rho\rho^*}, \\ \left(\frac{d}{d\rho}\right)^l \left(\frac{d}{d\rho^*} \frac{d}{d\rho}\right)^n e^{-\rho\rho^*} &= (-1)^{n+l} n! \rho^{*l} L_n^l(\rho\rho^*) e^{-\rho\rho^*}. \end{aligned} \quad (\text{B.44})$$

writing the left hand sides in cartesian coordinates gives ( $\rho = x + iy$ )

$$\begin{aligned} 2^{-2n-l} \left(\frac{d}{dx} + i \frac{d}{dy}\right)^{l+n} \left(\frac{d}{dx} - i \frac{d}{dy}\right)^n e^{-x^2-y^2} &= \\ (-2)^{-2n-l} \sum_{\lambda=0}^{l+n} \sum_{\nu=0}^n \binom{l+n}{\lambda} \binom{n}{\nu} i^{\lambda-\nu} H_{2n+l-\lambda-\nu}(x) H_{\lambda+\nu}(y) e^{-x^2-y^2} \\ 2^{-2n-l} \left(\frac{d}{dx} - i \frac{d}{dy}\right)^{l+n} \left(\frac{d}{dx} + i \frac{d}{dy}\right)^n e^{-x^2-y^2} &= \\ (-2)^{-2n-l} \sum_{\lambda=0}^{l+n} \sum_{\nu=0}^n \binom{l+n}{\lambda} \binom{n}{\nu} i^{\nu-\lambda} H_{2n+l-\lambda-\nu}(x) H_{\lambda+\nu}(y) e^{-x^2-y^2}. \end{aligned} \quad (\text{B.45})$$

these expressions are identical up to the complex phase factors of the different terms. Introducing  $\Lambda = \lambda + \nu$ , one can write these as

$$(-2)^{-2n-l} \sum_{\Lambda=0}^{2n+l} \sum_{\nu=0}^{\min(n,\Lambda)} \frac{1}{\Lambda!} \binom{\Lambda}{\nu} \frac{(l+n)!}{(l+n-\Lambda+\nu)!} \frac{n!}{(n-\nu)!} i^{\Lambda-2\nu} H_{2n+l-\Lambda}(x) H_{\Lambda}(y) e^{-x^2-y^2}, \quad (\text{B.46})$$

$$(-2)^{-2n-l} \sum_{\Lambda=0}^{2n+l} \sum_{\nu=0}^{\min(n,\Lambda)} \frac{1}{\Lambda!} \binom{\Lambda}{\nu} \frac{(l+n)!}{(l+n-\Lambda+\nu)!} \frac{n!}{(n-\nu)!} i^{2\nu-\Lambda} H_{2n+l-\Lambda}(x) H_{\Lambda}(y) e^{-x^2-y^2}.$$

Equating these expressions in terms of Hermite and Laguerre polynomials ( $l \geq 0$ ) yields the relations

$$2^{-2n-l} \sum_{\Lambda=0}^{2n+l} \sum_{\nu=0}^{\min(n,\Lambda)} \frac{1}{\Lambda!} \binom{\Lambda}{\nu} \frac{(l+n)!}{(l+n-\Lambda+\nu)!} \frac{n!}{(n-\nu)!} i^{\Lambda-2\nu} H_{2n+l-\Lambda}(x) H_{\Lambda}(y) = (-1)^n n! r^l e^{i\phi} L_n^l(r^2), \quad (\text{B.47})$$

$$2^{-2n-l} \sum_{\Lambda=0}^{2n+l} \sum_{\nu=0}^{\min(n,\Lambda)} \frac{1}{\Lambda!} \binom{\Lambda}{\nu} \frac{(l+n)!}{(l+n-\Lambda+\nu)!} \frac{n!}{(n-\nu)!} i^{2\nu-\Lambda} H_{2n+l-\Lambda}(x) H_{\Lambda}(y) = (-1)^n n! r^l e^{-i\phi} L_n^l(r^2).$$



## Appendix C

# Integrating complex exponentials

In this appendix we will prove

$$\int_{-\infty}^{\infty} e^{i(\omega-\omega')t} dt = 2\pi\delta(\omega-\omega'). \quad (\text{C.1})$$

first we write

$$\int_{-\infty}^{\infty} e^{i(\omega-\omega')t} dt = \lim_{T \rightarrow \infty} \int_{-T}^T e^{i(\omega-\omega')t} dt = \lim_{T \rightarrow \infty} 2 \frac{\sin((\omega-\omega')T)}{\omega-\omega'}. \quad (\text{C.2})$$

This is the limit of a sinc function whose height goes to infinity as its width goes to zero. To prove that this is  $2\pi\delta(\omega-\omega')$  we need to prove that the area of this expression integrated over  $\omega-\omega'$  converges to  $2\pi$  for  $T \rightarrow \infty$ . using the substitution  $(\omega-\omega')T = \xi$ , we have

$$2 \int_{-\infty}^{\infty} \frac{\sin((\omega-\omega')T)}{\omega-\omega'} d\omega-\omega' = 2 \int_{-\infty}^{\infty} \frac{\sin(\xi)}{\xi} d\xi = 4 \int_0^{\infty} \frac{\sin(\xi)}{\xi} d\xi. \quad (\text{C.3})$$

Now we use  $1/\xi = \int_0^{\infty} e^{-x\xi} dx$  and change the order of integration

$$\begin{aligned} 4 \int_0^{\infty} \frac{\sin(\xi)}{\xi} d\xi &= \frac{2}{i} \int_0^{\infty} \int_0^{\infty} e^{-x\xi+i\xi} - e^{-x\xi-i\xi} d\xi dx = \\ &= \frac{2}{i} \int_0^{\infty} \left[ \frac{1}{-x-i} - \frac{1}{-x+i} \right] dx = 4 \int_0^{\infty} \frac{1}{1+x^2} dx = 4[\text{arctg}(x)]_0^{\infty} = 2\pi, \end{aligned} \quad (\text{C.4})$$

which completes the proof.



## Appendix D

# Kinematics of two-particle decay

When a particle decays into two other particles, the magnitudes of the energy and momentum of the outgoing particles are fixed by their respective conservation laws. In this respect two-particle decays are much simpler than three- or more particle decays where the decay energy can be distributed in different ways over the decay products. Here we compute the energies and momenta of the decay products in the rest frame of the parent particle as functions of the three particles masses. These calculations can be found in several textbooks (they are given as an exercise in [243]).

Consider a particle with mass  $m_A$  decaying into two particles with masses  $m_B$  and  $m_C$  ( $m_A > m_B + m_C$ ). In the rest frame of  $A$ , the decay products have exactly opposite momenta, thus conservation of four momentum can be written as

$$\begin{bmatrix} m_A \\ 0 \end{bmatrix} = \begin{bmatrix} \mathcal{E}_B \\ \mathbf{p} \end{bmatrix} + \begin{bmatrix} \mathcal{E}_C \\ -\mathbf{p} \end{bmatrix}. \quad (\text{D.1})$$

Moving the four-momentum of particle  $B$  to the left hand side and squaring both sides yields (recall  $p_\mu p^\mu = m^2$ )

$$m_A^2 + m_B^2 - 2\mathcal{E}_B m_A = m_C^2 \implies \mathcal{E}_B = \frac{m_A^2 + m_B^2 - m_C^2}{2m_A}. \quad (\text{D.2})$$

the expression for the energy of particle  $C$  is the same with  $B$  and  $C$  interchanged. squaring eq. (D.1) without moving any terms gives

$$m_A^2 = m_B^2 + m_C^2 + 2\mathcal{E}_B \mathcal{E}_C + 2|\mathbf{p}|^2. \quad (\text{D.3})$$

Using the expressions for  $\mathcal{E}_B$  and  $\mathcal{E}_C$  this equation can be written as

$$m_A^2 = m_B^2 + m_C^2 + \frac{(m_A^2 + m_B^2 - m_C^2)(m_A^2 + m_C^2 - m_B^2)}{2m_A^2} + 2|\mathbf{p}|^2. \quad (\text{D.4})$$

From this expression one can find

$$|\mathbf{p}| = \frac{\sqrt{m_A^4 + m_B^4 + m_C^4 - 2m_A^2 m_B^2 - 2m_A^2 m_C^2 - 2m_B^2 m_C^2}}{2m_A}. \quad (\text{D.5})$$



## Appendix E

# A two-population model for equilibration times

To estimate the time scales over which an electron in a magnetic field approaches its equilibrium spin polarisation, we construct a simplified two-population model that captures the essentials. Consider a population of  $N$  electrons that undergo random spin flips at the rates  $\Gamma_{\uparrow\downarrow}$  from spin up to spin down and  $\Gamma_{\downarrow\uparrow}$ . We furthermore assume that the times at which different electrons undergo spin flips are uncorrelated as are the times at which one electron undergoes a series of spin flips. The expected spin occupation fractions of spin up electrons  $n_{\uparrow} = N_{\uparrow}/N$  and spin down electrons  $n_{\downarrow} = N_{\downarrow}/N$  are then given by two coupled first order differential equations.

$$\dot{n}_{\uparrow} = \Gamma_{\downarrow\uparrow}n_{\downarrow} - \Gamma_{\uparrow\downarrow}n_{\uparrow}, \quad \dot{n}_{\downarrow} = \Gamma_{\uparrow\downarrow}n_{\uparrow} - \Gamma_{\downarrow\uparrow}n_{\downarrow}. \quad (\text{E.1})$$

Obviously the total number of electrons is conserved,  $\dot{N} = N(\dot{n}_{\uparrow} + \dot{n}_{\downarrow}) = 0$ . By requiring that the right hand sides of eqs. (E.1) are zero one can find the equilibrium values of the spin occupation fractions and the spin polarisation

$$n_{\uparrow} = \frac{\Gamma_{\downarrow\uparrow}}{\Gamma_{\uparrow\downarrow} + \Gamma_{\downarrow\uparrow}}, \quad n_{\downarrow} = \frac{\Gamma_{\uparrow\downarrow}}{\Gamma_{\uparrow\downarrow} + \Gamma_{\downarrow\uparrow}}, \quad n_{\downarrow} - n_{\uparrow} = \frac{\Gamma_{\uparrow\downarrow} - \Gamma_{\downarrow\uparrow}}{\Gamma_{\uparrow\downarrow} + \Gamma_{\downarrow\uparrow}} \quad (\text{E.2})$$

To find the rate at which the spin polarisation approaches its equilibrium value, we introduce the quantity  $\delta n_{eq}$  which is zero when the spin polarisation achieves its equilibrium and is defined as

$$\delta n_{eq} = \frac{\Gamma_{\downarrow\uparrow}n_{\downarrow} - \Gamma_{\uparrow\downarrow}n_{\uparrow}}{\Gamma_{\uparrow\downarrow} + \Gamma_{\downarrow\uparrow}} \implies \delta \dot{n}_{eq} = -(\Gamma_{\uparrow\downarrow} + \Gamma_{\downarrow\uparrow})\delta n_{eq} \implies \delta n_{eq} \propto e^{-(\Gamma_{\uparrow\downarrow} + \Gamma_{\downarrow\uparrow})t}. \quad (\text{E.3})$$

One can write  $\delta n_{eq}$  in the form  $n_0 e^{-t/\tau_{eq}}$  with  $\tau_{eq}$  the equilibration time which is in our case is  $1/(\Gamma_{\uparrow\downarrow} + \Gamma_{\downarrow\uparrow})$ . It is interesting to note that the rate at which the electron spin equilibrates increases monotonically with both spin flip rates in this model.





# Summaries

## English summary

Waves are some of the most studied and most ubiquitous physical phenomena. Well known types of waves, each of which has its own subdiscipline devoted to them are water waves, sound waves and light waves. Thanks to quantum mechanics, we know that every object can display wavelike traits. Sound waves in air are among a very simple class of waves which can be characterised by giving the value of a single quantity everywhere. In the case of sound this quantity is the pressure which will vary in an undulating pattern whenever sound passes through air. Such waves are called scalar waves.

Light is described by electric and magnetic fields which oscillate and there is not a single quantity that can be used to fully describe the wave. The electric and magnetic fields do not only have a magnitude (like pressure had), but a direction too. The dynamics of the electric and magnetic fields are closely connected to each other and by specifying only the electric field one can fully characterise a light wave. As a light wave passes by, the electric field can oscillates back and forth, this is called linearly polarised light. There are more possibilities, however, the electric and magnetic fields can rotate as they move past, but maintain the same magnitude, this is called circular polarisation. The electric and magnetic fields can also oscillate in a manner intermediate between circularly and linearly polarised, where the electric and magnetic fields rotate and change their amplitudes, this is called elliptic polarisation. The electric field is, however, constrained to point in a direction perpendicular to the local propagation direction of the wave at all times. This implies that if you warp the wave front, the *orientation* of the electric field has to be warped accordingly and it is generally impossible to have the orientation of the electric field the same everywhere across the wave front. This phenomenon occurs for other non-scalar waves and it will be important for electrons too.

It is intuitive to understand that circularly polarised light can set things into rotation. Consider a small dumbbell with two opposite charges on either end. If a circularly polarised wave passes by, the positive charge gets pulled in the direction of the electric field and the negative charge against it<sup>1</sup>. The dumbbell thus will align with the electric field and starts to rotate along with it. Therefore circularly polarised light is said to carry *spin*.

A useful quantity in relation to the spin is the helicity, which is the circular polarisation along the local propagation direction of the wave. If, for an observer looking at the oncoming wave, the electric field rotates counterclockwise the helicity is positive, and if the field rotates clockwise, the helicity is negative. Linearly polarised light has helicity 0, circularly

---

<sup>1</sup>The law that like charges repel and opposite charges attract is a consequence of electric field pulling opposite charges in opposite directions

polarised light has helicity  $\pm 1$  and elliptically polarised light falls somewhere in between. The usefulness of helicity lies therein that it can be defined even if the light's wave front is not flat. For in empty space the helicity does not change as the light travels. In chapter 1 of this dissertation, we will investigate in how far helicity does not change when light travels from one transparent material to another.

A fundamental property of waves is interference. If two wave crests or wave troughs overlap, they resulting wave will be twice as high, if a crest and a trough overlap, they will extinguish each other. For scalar waves, interference occurs whenever one superpose multiple waves. For light waves, one can choose the polarisations such that they do not interfere. Chapter 2 investigates how many light waves can be superposed without interference between the electric fields occurring. The helicity density of these noninterfering superpositions shows a large variety of crystal-like patterns of which we will show many examples.

Electrons are in many ways the simplest particles of matter. They do not decay to lighter particles, are not known to be made of smaller constituents, and unlike the particles that make up the atomic nucleus, they are not affected by the strong nuclear force. They are affected by the weak nuclear force, which is weak for any situation we consider here and can be ignored. Thus to a very good approximation the electron can be described as being affected by the electromagnetic force, which is the most accurately studied of the fundamental forces, only. This makes the electron a useful model system for investigating the wave nature of matter. They were the first particles of matter of which the wave nature has been demonstrated and electron wavefront shaping is nowadays an active research area in electron microscopy.

Electrons do carry spin, just like light, although the mathematics of the quantum mechanics of the electron are such that one can not intuitively grasp the electron spin's ability to set objects into rotation. In the relativistic quantum theory of the electron, the electron spin configuration is constrained by the shape of the wavefront, like the polarisation for light, although the cause is different. The relativistic quantum theory of the electron predicts that the electron has an antiparticle, the positron, which is identical in every way except having the opposite electric charge. When an electron and a positron meet they annihilate each other and emit gamma rays. Half of the electron's spin configurations are reserved for positron states which imposes a restriction on the electron spin similar to the restriction imposed on the polarisation of light, although from a different underlying cause.

In chapter 3 we study the effects of the wavefront shape on the electron's spin structure for an electron in a magnetic field. The magnetic field confines the electrons to form a narrow beam, narrower than a laser beam, giving a strong warping of the wavefront. The force of the magnetic field on the electrons makes them circulate counterclockwise (looking against the magnetic field lines). The effect of the electron spin is that it creates narrow rings where the electron rotation is clockwise.

In chapter 4 we bring together light and electrons, considering interacting wave theories. Just as sound waves can make ripples in water and water waves can make sound, light and electron waves can interact with each other too. The theoretical framework used for describing interacting waves is quantum field theory, a theory developed to unify quantum mechanics with the special theory of relativity<sup>2</sup>, describe how particles are created and

---

<sup>2</sup>There is an important distinction between the special and the general theory of relativity. The special theory of relativity is the general theory of relativity without gravity and it has been unified with quantum mechanics already by the end of the 1920's, yielding quantum field theory. Unifying the general theory of relativity with quantum field theory is still an unsolved problem.

annihilated (something ordinary quantum mechanics cannot.) and reconcile the wave and particle nature of light and matter. In quantum field theory every wave is quantised, requiring its energy is an integer multiple of its frequency, thus imparting a particle-like nature on each wave phenomenon. We use quantum field theory to study the simplest process with an electron in a magnetic field, the creation of a ‘particle of light’, a photon, by the electron. The photon production rate can be computed by summing the photon production rate for a physically allowed transition of the electron from one waveform to another over all physically allowed electron waves. This sum can be separated into two parts with different electron spins after the emission of a photon and by comparing the rates of these two parts, the final average spin of the electron can be computed. It turns out that for the right initial electron wave forms, the spin of the electron tends to point itself against the magnetic field in a much stronger manner than expected from previous calculations on this problem.

## Nederlandse samenvatting

Golven behoren tot de meest bestudeerde en alomtegenwoordigste fysische verschijnselen. Bekende soorten golven, die allemaal een eigen onderzoekdiscipline aan zich hebben gewijd, zijn watergolven, geluidsgolven en lichtgolven. Geluidsgolven in lucht behoren tot een simpele klasse van golven die kunnen worden gekarakteriseerd door overal één enkele grootheid te specificeren. In het geval van geluid is deze grootheid de luchtdruk die in een golvend patroon varieert als geluid de lucht doorkruist. Zulke golven heten scalaire golven.

Licht wordt beschreven door oscillerende elektrische en magnetische velden en er is niet één enkele grootheid die de golf volledig beschrijft. De elektrische en magnetische velden hebben niet alleen een grootte (zoals de luchtdruk), maar ook een richting. De dynamica van de elektrische en magnetische velden zijn nauw verweven en het specificeren van alleen het elektrische veld volstaat om de volledige lichtgolf te karakteriseren. Als een lichtgolf voorbijkomt kunnen de elektrische en magnetische velden heen en weer bewegen, dit heet lineair gepolariseerd licht. Er zijn echter meer mogelijkheden. De elektrische en magnetische velden kunnen ronddraaien zonder van grootte te veranderen, dit heet circulaire polarisatie. De elektrische en magnetische velden kunnen ook bewegen op een manier die tussen lineaire en circulaire polarisatie in ligt, waarbij de elektrische en magnetische velden ronddraaien en van grootte veranderen, dit heet elliptische polarisatie. Het elektrische veld moet altijd wijzen in een richting loodrecht op de lokale voortplantingsrichting van de lichtgolf. Dit impliceert dat als je het golffront vervormt, de *richting* waarin het elektrische veld wijst moet meevormen en het in het algemeen onmogelijk is dat het elektrische veld overal op een golffront in dezelfde richting wijst. Dit fenomeen treedt ook op voor andere niet-scalaire golven en is ook relevant voor elektronen.

Het kan intuïtief worden begrepen dat circulair gepolariseerd licht voorwerpen kan doen draaien. Stel je een halteretje voor met tegengestelde elektrische ladingen op beide uiteinden. Als een circulair gepolariseerde lichtgolf voorbijkomt wordt de positieve lading in de richting van het elektrische veld getrokken en de negatieve lading ertegenin.<sup>3</sup> Het halteretje zal zich dus naar het elektrische veld richten en meedraaien. Daarom wordt gezegd dat circulair gepolariseerd licht *spin* bezit.

Een bruikbare aan de spin gerelateerde grootheid is de heliceiteit, de circulaire polarisatie gezien in de lokale voortplantingsrichting van de golf. Als, voor een waarnemer die tegen de aankomende golf in kijkt, het elektrische veld tegen de klok in draait, is de heliceiteit positief, als het met de klok meedraait, is de heliceiteit negatief. Lineair gepolariseerd licht heeft een heliceiteit van 0, circulair gepolariseerd licht heeft een heliceiteit van  $\pm 1$  en elliptisch gepolariseerd licht zit daartussenin. Heliceiteit is bruikbaar, omdat het kan worden gedefinieerd als het golffront van het licht niet vlak is. Voor licht dat zich door lege ruimte voortplant verandert de totale heliceiteit niet. In hoofdstuk 1 van dit proefschrift gaan we na in hoeverre heliceiteit niet verandert als het van het ene doorzichtige materiaal naar het andere gaat.

Een fundamentele golfeigenschap is interferentie. Als twee golftoppen of twee golfdalen over elkaar heen vallen versteken ze elkaar. Als een top en een dal over elkaar heen vallen doven ze elkaar uit. Voor scalaire golven treedt interferentie altijd op wanneer men meerdere golven superponeert. Voor lichtgolven kunnen de polarisaties zo worden gekozen dat ze niet interfereren. Hoofdstuk 2 onderzoekt hoe veel lichtgolven kunnen worden gesuperponeerd zonder dat hun elektrische velden interfereren. De heliceiteitsdichtheid van deze

<sup>3</sup>De wet dat gelijke ladingen elkaar afstoten en tegengestelde ladingen elkaar aantrekken is een gevolg van het feit dat een elektrisch veld tegengestelde ladingen in tegengestelde richtingen trekt.

superposities vertoont een grote diversiteit aan regelmatige patronen, waarvan we een groot aantal voorbeelden tonen.

Elektronen zijn in veel opzichten de eenvoudigste materiedeeltjes. Ze vervallen niet tot lichtere deeltjes, bestaan voor zover bekend niet uit kleinere bouwstenen en in tegenstelling tot de deeltjes waaruit atoomkernen bestaan ondervinden ze niet de sterke kernkracht. Ze ondervinden de zwakke kernkracht, maar die is zwak en kan voor alle situaties die we hier beschouwen worden genegeerd. Het elektron kan dus in een zeer goede benadering worden beschreven met uitsluitend de interacties met de elektromagnetische kracht, de nauwkeurigst bestudeerde aller natuurkrachten. Dit maakt elektronen een goed model-systeem voor het onderzoeken van het golfkarakter van materie. Ze waren de eerste materiedeeltjes waarvoor het golfkarakter werd aangetoond en elektrongolffrontvervorming is tegenwoordig een actief onderzoeksgebied in de elektronenmicroscopie.

Elektronen bezitten spin, net zoals licht, alleen kan men uit de wiskunde van de quantummechanica van het elektron niet intuïtief zien dat de elektronspin voorwerpen kan doen draaien. In de relativistische quantumtheorie van het elektron is de elektronspinconfiguratie ingeperkt door de vorm van het golffront, zoals de polarisatie van licht, hoewel de achterliggende oorzaak anders is. De relativistische quantumtheorie van het elektron voorspelt dat het elektron een antideeltje heeft, het positron, dat identiek is afgezien van een tegengestelde lading. Als een elektron en een positron samenkomen verdwijnen ze en zenden ze gammastraling uit. De helft van de elektronspinconfiguraties zijn gereserveerd voor positronen, wat een beperking oplegt aan de mogelijke elektronspin, soortgelijk aan de beperking opgelegd aan de polarisatie van licht, alleen met een andere achterliggende oorzaak.

In hoofdstuk 3 onderzoeken we de effecten van golffrontvervorming op de elektronspinstructuur voor een elektron in een magnetisch veld. Het magnetische veld sluit elektronen op in een smalle bundel, smaller dan een laserstraal, wat een sterke vervorming van het golffront geeft. De magnetische kracht op de elektronen doet ze tegen de klok in draaien (gezien tegen de richting van het magnetische veld in). Het effect van de elektronspin is dat er in de elektronenbundel smalle ringen ontstaan waarin de elektrondraaiing met de klok mee is.

In hoofdstuk 4 komen licht en elektronen samen in een golftheorie met interacties. Net zoals geluidsgolven rimpelingen op een wateroppervlak kunnen maken en watergolven geluid kunnen maken, kunnen licht- en elektrongolven interacties met elkaar hebben. Het theoretische raamwerk voor het beschrijven van de intracterende golven is quantumveldentheorie, een theorie ontwikkeld om de quantummechanica met de speciale relativiteitstheorie te verenigen<sup>4</sup>, te beschrijven hoe deeltjes worden gemaakt en vernietigd en het verzoeken van de golf- en deeltjeseigenschappen van licht en materie. In de quantumveldentheorie, kan de energie van een golf alleen een heeltallig veelvoud van diens frequentie zijn, wat een deeltjeskarakter geeft aan elk golfverschijnsel. We gebruiken quantumveldentheorie om het eenvoudigste proces te beschrijven dat kan plaatsvinden als een elektron in een magnetisch veld beweegt, de creatie van een lichtdeeltje, een foton. Het fotonproductietempo kan worden berekend door het fotonproductietempo te berekenen voor elke toegestane overgang van het elektron van één golfvorm naar een andere en deze bij elkaar op te tellen. Deze som kan worden opgedeeld in twee delen alnaargelang de elektronspin

<sup>4</sup>Er is een belangrijk onderscheid tussen de speciale en de algemene relativiteitstheorie. De speciale relativiteitstheorie is de algemene relativiteitstheorie zonder zwaartekracht en ze werd al aan het eind van de jaren '20 met de quantummechanica verenigd, wat quantumveldentheorie opleverde. Het verenigen van quantumveldentheorie met de algemene relativiteitstheorie is nog steeds een onopgelost probleem.

na het uitzenden van het foton en door de grootte van deze twee delen te vergelijken kan de gemiddelde elektronspin na uitzending van een foton worden berekend. Het blijkt dat de elektronspin zich voor de juiste aanvangsgolfvormen veel sterker tegen het magneetveld richt dan uit eerdere berekeningen werd verwacht.

## Deutsche Zusammenfassung

Wellen gehören zu den allgegenwärtigsten und meist studierten physikalischen Erscheinungen. Bekannte Wellenarten, die alle ihr eigenes Forschungsgebiet haben, sind Wasserwellen, Schallwellen und Lichtwellen. Schallwellen in Luft gehören zu einer einfachen Klasse Wellen die können werden beschrieben mittels Spezifizierung einer Größe. Für Schallwellen ist das der Luftdruck der ein Wellenmuster formt wenn Schall die Luft durchquert.

Licht wird beschrieben durch oszillierende elektrische und magnetische Felder und es gibt nicht eine Größe die die Welle im ganzen beschreibt. Die elektrische und magnetische Felder haben nicht nur eine Größe (wie Luftdruck), sondern auch eine Richtung. Die Dynamik der elektrischen und magnetischen Felder ist eng verknüpft und für eine vollständige Beschreibung des Lichts reicht es nur das elektrische Feld zu spezifizieren. Wenn eine Lichtwelle vorbeikommt können die elektrische und magnetische Felder hin und her schwingen, dies heißt linear polarisiertes Licht. Aber es gibt mehr Möglichkeiten. Die elektrische und magnetische Felder können runderdrehen ohne ihre Größe zu verändern, dies heißt zirkulare Polarisierung. Die elektrische und magnetische Felder können auch bewegen auf einer Weise die zwischen linearer und zirkularer Polarisierung liegt, wobei die elektrische und magnetische Felder runderdrehen und ihre Größe verändert. Dies heißt elliptische Polarisierung. Das elektrische Feld muss immer in eine Richtung senkrecht auf die Fortpflanzungsrichtung der Welle zeigen. Dies impliziert daß wenn das Wellenfront verformt, die *Richtung* des elektrischen Felds muss mitverformen und es generell unmöglich ist daß das elektrische Feld überall auf der Wellenfront in dieselbe Richtung zeigt. Dieses Phänomän tritt auch auf für andere nicht-skalare Wellen und wird für Elektronen relevant.

Es ist intuitiv zu verstehen daß zirkular polarisiertes Licht Gegenstände zum Drehen kann bringen. Stelle dich eine Hantel vor mit gegengestellten Ladungen an beiden Enden. Käme eine zirkular polarisierte Lichtwelle vorbei, wird die positive Ladung in die Richtung des elektrischen Felds gezogen und die negative Ladung in die gegengestellte Richtung<sup>5</sup>. Die Hantel richtet sich dann entlang das elektrische Feld und fängt an zu drehen. Deswegen wird gesagt zirkular polarisiertes Licht habe *Spin*.

Eine nützliche dem Spin verwandte Größe ist die Helizität, die zirkulare Polarisierung entlang die lokale Fortpflanzungsrichtung der Welle gesehen. Wenn, für einen Wahrnehmer die gegen die ankommende Welle schaut, das elektrische Feld gegen den Uhrzeigersinn dreht, ist die Helizität positiv, dreht das elektrische Feld in die Uhrzeigersinn, ist die Helizität negativ. Linear polarisiertes Licht hat eine Helizität von 0, zirkular polarisiertes Licht hat eine Helizität von  $\pm 1$  und die Helizität von elliptisch polarisiertes Licht liegt irgendwo dazwischen. Helizität ist nützlich weil es kann werden definiert wenn die Wellenfront nicht flach ist. Für Licht das durch den leeren Raum bewegt verändert die Helizität nicht. Inwiefern Helizität nicht verändert für Licht das von einem durchsichtigen Material ins anderen geht untersuchen wir in Kapitel 1 dieser Dissertation.

Interferenz ist eine fundamentale Welleneigenschaft. Wenn zwei Wellengipfel oder -Tale übereinander liegen, verstärken sie einander, wenn ein Gipfel einer Welle über einem Tal einer anderen Welle liegt tauben sie einander aus. Für skalare Wellen tritt Interferenz immer auf wenn man mehrere Wellen superponiert. Für Lichtwellen können die Polarisierungen so werden gewählt daß sie nicht interferieren. Kapitel 2 untersucht wie viele Lichtwellen können werden superponiert ohne daß Interferenz auftritt. Die Helizitätsdichte

---

<sup>5</sup>Das Gesetz daß gegengestellte Ladungen einander anziehen ist eine Folge davon daß ein elektrisches Feld gegengestellte Ladungen in gegengestellte Richtungen zieht.

dieser Superpositionen zeigt eine große Diversität regelmäßiger Patrone, wovon wir eine große Anzahl Beispiele zeigen.

Elektrone sind in vielen Hinsichten die einfachste Materieteilchen. Sie zerfallen nicht zu leichteren Teilchen, sind nicht, insofern bekannt, aus kleineren Bausteinen aufgebaut und, im Gegensatz zu den Teilchen woraus Atomkernen sind aufgebaut, empfinden sie die starke Kernkraft nicht. Sie empfinden die schwache Kernkraft, aber die ist schwach und kann in allen von uns betrachteten Fällen werden ignoriert. Das Elektron kann deswegen in sehr guter Näherung angesehen werden als beeinflusst von nur der elektromagnetischen Kraft, die genau erforscht aller Naturkräfte. Das macht elektrone ein gutes Modellsystem für die Forschung des Wellencharakters der Materie. Wellenfrontverformung der Elektronenwellen ist außerdem ein aktives Forschungsgebiet in der Elektronenmikroskopie.

Elektronen haben spin, genauso wie Licht, aber man kann aus der Mathematik der Quantenmechanik der Elektronen nicht intuitiv sehen daß der Elektronspin Gegenstände zum Drehen kann bringen. In der relativistischen Quantentheorie des Elektrons schränkt die Wellenfront die Spinkonfiguration des Elektrons ein, wie die Polarisierung des Lichts, obwohl die unterliegende Ursache anders ist. Die relativistische Quantentheorie des Elektrons sagt vorher daß das Elektron ein Antiteilchen, das Positron, hat das in allen Eigenschaften identisch ist, abgesehen von einer gegengestellten Ladung. Begegnen ein Elektron und ein Positron einander, dann heben sie einander auf unter Aussendung von Gammastrahlung. Die Hälfte der Elektronspinkonfigurationen sind für Positronen reserviert, was den Elektronspin einschränkt. Dies ist der Einschränkung der Polarisierung ähnlich, obwohl mit einer anderen unterliegenden Ursache.

In Kapitel 3 untersuchen wir die Effekte der Wellenfrontverformung auf die Elektronspinstruktur für ein Elektron in einem Magnetfeld. Das Magnetfeld schließt die Elektronen in einen schmalen Bundel ein, schmaler als ein Laserstrahl, was eine starke Wellenfrontverformung gibt. Die magnetische Kraft läßt die Elektronen gegen den Uhrzeigersinn (gegen die Richtung des Magnetfelds gesehen) drehen. Der Effekt des Elektronspins ist daß schmale Ringe entstehen worin die Elektronendrehung in den Uhrzeigersinn ist.

In Kapitel 4 kommen Licht und Elektronen zusammen in einer wechselwirkenden Wellentheorie. Wie Schallwellen eine Wasseroberfläche können runzeln und Wasserwellen Schall können produzieren, können Licht und Elektronenwellen mit einander wechselwirken. Der theoretische Rahmen der Beschreibung wechselwirkender Wellen ist Quantenfeldtheorie, eine Theorie entwickelt um die Quantenmechanik mit der speziellen Relativitätstheorie zu vereinigen<sup>6</sup>, zu beschreiben wie Teilchen entstehen und werden vernichtet und zum Versöhnen des Wellen- und Teilchencharakters des Lichts und Materie. In der Quantenfeldtheorie kann die Energie einer Welle nur eine ganzzahlige Vielfache seiner Frequenz sein, was jeder Wellenerscheinung einen Teilchencharakter gibt. Wir nutzen Quantenfeldtheorie zur Beschreibung der einfachsten Wechselwirkung eines Elektrons in einem Magnetfeld, die Ausstrahlung eines Lichtteilchens oder Photons. Die Photonproduktionsrate kann berechnet werden für jeden einzelnen erlaubten Übergang des Elektrons von einer Wellenform in eine andere die Photonproduktionsrate zu berechnen und diese aufzuzählen. Diese Summe kann werden aufgeteilt in zwei Teile je nachdem der Spin des Elektrons nach Aussendung des Photons und durch die Größe dieser zwei Teile zu vergleichen kann den gemittelten Elektronspin nach Aussendung eines Photons werden berechnet.

---

<sup>6</sup>Der Unterschied zwischen spezieller und allgemeiner Relativitätstheorie ist wichtig hier. Die spezielle Relativitätstheorie ist die allgemeine Relativitätstheorie ohne Gravitation und sie wurde schon Ende der '20er Jahre mit der Quantenmechanik vereinigt, was die Quantenfeldtheorie ergab. Das Vereinigen der Quantenfeldtheorie und der allgemeinen Relativitätstheorie ist bis heute ein ungelöstes Problem.



Für bestimmte Anfangswellenformel zeigt sich daß der Elektronspin sich stärker gegen das Magnetfeld richtet als aus ältere Berechnungen war zu erwarten.



# Acknowledgements

First and foremost, I want to thank my supervisor, Jörg Götze, for introducing me to the topic of waves carrying vortices the first time we met and for being a great supervisor throughout. Your office door was always open and you were always willing to look into what I came up with, even though in the end, I did none of the projects you wanted me to do, and even when I thought light could not travel through an optical fibre because there were too many boundary conditions. Then you had to leave the institute and perhaps the best testimony to your skill as a supervisor is how you managed to keep me on track from afar (Glasgow), very afar (Nanjing) and afar (Glasgow again). Your English and writing skills were a great help, too, both when you were proof-reading the draft of an article we were working on and in the correspondence with journal editors and other scientists, your suggestions always hit exactly the right note. And there is no need to be modest about it, whenever you said ‘I am not sure, maybe you should ask a native speaker’, you were invariably right.

Then I want to thank my co-workers whom I worked with on various projects.

First: Armen Hayrapetyan, I enjoyed working with you on electron vortices with spin. Your suggestion to compute the electron current gave substance to the whole project.

Second: Rob Cameron, expert on the chirality of molecules and dinosaurs. Apart from a lot of discussions about science, we had some great times together, both in Dresden and in Glasgow. It’s a shame that open air Shakespeare performance we wanted to attend was cancelled due to ‘adverse weather’ (drizzle; in Glasgow). As for the science, I think we have found a treasure trove with these noninterfering superpositions and I am looking forward to working with you on them in the future.

Third: Felix Mackenroth, thanks to you I finally understood quantum electrodynamics, something I have to admit I struggled with ever since my first quantum field theory courses. You were always there to support me when my motivation was low again and I don’t believe I could have finished the last project without your support. Thanks.

Then I wish to thank the coordinators of the international Max Planck research school who were very helpful with such various things as helping me get settled in Dresden, organising the IMPRS seminar and helping PhD students figure out all the paperwork for their promotions. Michael Genkin, Anatole Kenfack and Paul McClarty (Even the coordinators have a high turnover rate here), thank you.

Of course I should not forget the go-to person in the finite systems division for anything you don’t know whom to ask, Gabriele Makolies. You were always there to make things run smoothly.

Then I want to thank the people at the quantum theory group of the university of Glasgow for their hospitality during my two weeks stay there, in particular Stephen Barnett and Rob Cameron.

Then I want to thank all the people with whom I shared an office the past four years (I'll switch to first names only). Günes, Nikolaj, Niladri, Philipp, Ghassan and Ji-Yen, you were all great office mates. Of course I won't forget you Marc, with whom I shared this office almost from the beginning until the end. There was always something interesting to discuss with you, thanks to which I now know who Axel Stoll was.

Then the Max Planck institute does not end at my office door. There are many more people at the institute who made my time in Dresden pleasant and memorable, so in no particular order Abraham, Karsten, David, Alan, Callum, Mehrdad, Valentin, Andreas, Mozhdeh, Wildan, Laura, Rick, Adrian, Talia, Omar, Chris, Perttu, Stephan, Lisa, Cornelia, Soumi, Kieran, Andrew and Fermin, thanks to all of you.

Finally I want to thank my parents, Nynke and Corstiano and my sister Emma and brother in law Viktor for their unwavering support and for putting up with me being so far from home for four years.

# Bibliography

- [1] J. H. Poynting, *The wave motion of a revolving shaft, and a suggestion as to the angular momentum in a beam of circularly polarised light*, Proc. R. Soc. Lond. A **82**, 560 (1909), ISSN 09501207.
- [2] R. A. Beth, *Mechanical detection and measurement of the angular momentum of light*, Phys. Rev. **50**, 115 (1936).
- [3] L. Allen, M. W. Beijersbergen, R. J. C. Spreeuw, and J. P. Woerdman, *Orbital angular momentum of light and the transformation of Laguerre-Gaussian modes*, Phys. Rev. A **45**, 8185 (1992).
- [4] C. G. Darwin, *Notes on the theory of radiation*, Proc. R. Soc. Lond. A **136**, 36 (1932).
- [5] J. F. Nye and M. V. Berry, *Dislocations in wave trains*, Proc. R. Soc. Lond. A **336**, 165 (1974).
- [6] J. Durnin, *Exact solutions for nondiffracting beams. I. the scalar theory*, J. Opt. Soc. Am A **4**, 651 (1986).
- [7] J. Durnin, J. J. Miceli, and J. H. Eberly, *Diffraction-free beams*, Phys. Rev. Lett. **58**, 1499 (1987).
- [8] S. Knitter, S. F. Lui, W. Xiong, M. I. Guy, G. S. Solomon, and H. Cao, *Topological defect lasers*, J. Opt. **18**, 014005 (2016).
- [9] C. Tamm and C. O. Weiß, *Bistability and optical switching of spatial patterns in a laser*, J. Opt. Soc. Am. B **7**, 1034 (1990).
- [10] E. Abramochkin and V. Volostnikov, *Beam transformations and nontransformed beams*, Opt. Comm. **83**, 123 (1991), ISSN 0030-4018.
- [11] H. He, M. E. J. Friese, N. R. Heckenberg, and H. Rubinsztein-Dunlop, *Direct observation of transfer of angular momentum to absorptive particles from a laser beam with a phase singularity*, Phys. Rev. Lett. **75**, 826 (1995).
- [12] M. E. J. Friese, J. Enger, H. Rubinsztein-Dunlop, and N. R. Heckenberg, *Optical angular-momentum transfer to trapped absorbing particles*, Phys. Rev. A **54**, 1593 (1996).
- [13] M. P. MacDonald, L. Paterson, K. Volke-Sepulveda, J. Arlt, W. Sibbett, and K. Dholakia, *Creation and manipulation of three-dimensional optically trapped structures*, Science **296**, 1101 (2002), ISSN 0036-8075.
- [14] A. T. O’Neil, I. MacVicar, L. Allen, and M. J. Padgett, *Intrinsic and extrinsic nature of the orbital angular momentum of a light beam*, Phys. Rev. Lett. **88**, 053601 (2002).
- [15] J. Courtial, K. Dholakia, D. A. Robertson, L. Allen, and M. J. Padgett, *Measurement of the rotational frequency shift imparted to a rotating light beam possessing orbital angular momentum*, Phys. Rev. Lett. **80**, 3217 (1998).

- [16] M. P. J. Lavery, F. C. Speirits, S. M. Barnett, and M. J. Padgett, *Detection of a spinning object using light's orbital angular momentum*, Science **341**, 537 (2013), ISSN 0036-8075.
- [17] M. P. J. Lavery, S. M. Barnett, F. C. Speirits, and M. J. Padgett, *Observation of the rotational doppler shift of a white-light, orbital-angular-momentum-carrying beam backscattered from a rotating body*, Optica **1**, 1 (2014).
- [18] V. Westphal and S. W. Hell, *Nanoscale resolution in the focal plane of an optical microscope*, Phys. Rev. Lett. **94**, 143903 (2005).
- [19] J. Keller, A. Schönle, and S. W. Hell, *Efficient fluorescence inhibition patterns for resolt microscopy*, Opt. Express **15**, 3361 (2007).
- [20] M. Dyba and S. W. Hell, *Focal spots of size  $\lambda/23$  open up far-field florescence microscopy at 33 nm axial resolution*, Phys. Rev. Lett. **88**, 163901 (2002).
- [21] S. Fürhapter, A. Jesacher, S. Bernet, and M. Ritsch-Marte, *Spiral phase contrast imaging in microscopy*, Opt. Express **13**, 689 (2005).
- [22] A. Jesacher, S. Fürhapter, S. Bernet, and M. Ritsch-Marte, *Shadow effects in spiral phase contrast microscopy*, Phys. Rev. Lett. **94**, 233902 (2005).
- [23] S. Bernet, A. Jesacher, S. Fürhapter, C. Maurer, and M. Ritsch-Marte, *Quantitative imaging of complex samples by spiral phase contrast microscopy*, Opt. Express **14**, 3792 (2006).
- [24] G. Foo, D. M. Palacios, and G. A. Swartzlander, *Optical vortex coronagraph*, Opt. Lett. **30**, 3308 (2005).
- [25] G. A. Swartzlander, E. L. Ford, R. S. Abdul-Malik, L. M. Close, M. A. Peters, D. M. Palacios, and D. W. Wilson, *Astronomical demonstration of an optical vortex coronagraph*, Opt. Express **16**, 10200 (2008).
- [26] F. Tamburini, B. Thidé, G. Molina-Terriza, and G. Anzolin, *Twisting of light around rotating black holes*, Nat. Phys. **7**, 195 (2011).
- [27] G. Gibson, J. Courtial, M. J. Padgett, M. Vasnetsov, V. Pas'ko, S. M. Barnett, and S. Franke-Arnold, *Free-space information transfer using light beams carrying orbital angular momentum*, Opt. Express **12**, 5448 (2004).
- [28] C. Paterson, *Atmospheric turbulence and orbital angular momentum of single photons for optical communication*, Phys. Rev. Lett. **94**, 153901 (2005).
- [29] T.-C. Wei, J. T. Barreiro, and P. G. Kwiat, *Hyperentangled bell-state analysis*, Phys. Rev. A **75**, 060305 (2007).
- [30] J. T. Barreiro, T.-C. Wei, and P. G. Kwiat, *Beating the channel capacity limit for linear photonic superdense coding*, Nat. Phys. **4**, 282 (2008).
- [31] F. Tamburini, E. Mari, A. Sponselli, B. Thidé, A. Bianchini, and F. Romanato, *Encoding many channels on the same frequency through radio vorticity: first experimental test*, New J. Phys. **14**, 033001 (2012).
- [32] J. Wang, J.-Y. Yang, I. M. Fazal, N. Ahmed, Y. Yan, H. Huang, Y. Ren, Y. Yue, S. Dolinar, M. Tur, et al., *Terabit free-space data transmission employing orbital angular momentum multiplexing*, Nat. Phot. **6**, 488 (2012).
- [33] N. K. Fontaine, R. Ryf, J. Bland-Hawthorn, and S. G. Leon-Saval, *Geometric requirements for photonic lanterns in space-division multiplexing*, Opt. express **20**, 27123 (2012).
- [34] B. Huang, N. K. Fontaine, R. Ryf, B. Guan, S. G. Leon-Saval, R. Shubochkin, Y. Sun, R. Lingle, and G. Li, *All-fiber mode-group-selective photonic lantern using graded-index multimode fibers*, Opt. express **23**, 224 (2015).
- [35] M. Krenn, R. Fickler, M. Fink, J. Handsteiner, M. Malik, T. Scheidl, R. Ursin, and

- A. Zeilinger, *Communication with spatially modulated light through turbulent air across vienna*, New J. Phys. **16**, 113028 (2014).
- [36] S. Restuccia, D. Giovannini, G. Gibson, and M. Padgett, *Comparing the information capacity of Laguerre-Gaussian and Hermite-Gaussian modal sets in a finite-aperture system*, Opt. Express **24**, 27127 (2016).
- [37] A. Mair, A. Vazari, G. Wiehs, and A. Zeilinger, *Entanglement of the orbital angular momentum states of photons*, Nature **412**, 313 (2001).
- [38] S. S. R. Oemrawsingh, A. Aiello, E. R. Eliel, G. Nienhuis, and J. P. Woerdman, *How to observe high-dimensional two-photon entanglement with only two detectors*, Phys. Rev. Lett. **92**, 217901 (2004).
- [39] S. S. R. Oemrawsingh, X. Ma, D. Voigt, A. Aiello, E. R. Eliel, G. W. 't Hooft, and J. P. Woerdman, *Experimental demonstration of fractional orbital angular momentum entanglement of two photons*, Phys. Rev. Lett. **95**, 240501 (2005).
- [40] J. Romero, J. Leach, B. Jack, S. M. Barnett, M. J. Padgett, and S. Franke-Arnold, *Violation of leggett inequalities in orbital angular momentum subspaces*, New J. Phys. **12**, 123007 (2010).
- [41] B. T. Hefner and P. L. Marston, *An acoustical helicoidal wave transducer with applications for the alignment of ultrasonic and underwater systems*, J. Acous. Soc. Am. A **106**, 3313 (1999).
- [42] M. W. Beijersbergen, R. P. C. Coerwinkel, M. Kristensen, and J. P. Woerdman, *Helical-wavefront laser beams produced with a spiral phaseplate*, Opt. Comm. **112**, 321 (1994).
- [43] K. Y. Bliokh, Y. P. Bliokh, S. Savel'ev, and F. Nori, *Semiclassical dynamics of electrons wave packet states with phase vortices*, Phys. Rev. Lett. **99**, 190404 (2007).
- [44] M. Uchida and A. Tonomura, *Generation of electron beams carrying orbital angular momentum*, Nature **464**, 737 (2010).
- [45] J. Verbeeck, H. Tian, and P. Schattschneider, *Production and application of electron vortex beams*, Nature **467**, 301 (2010).
- [46] B. J. McMorran, A. Agrawal, I. M. Anderson, A. A. Herzing, H. J. Lezec, J. J. McClelland, and J. Unguris, *Electron vortex beams with high quanta of orbital angular momentum*, Science **331**, 192 (2011), ISSN 0036-8075.
- [47] J. Verbeeck, P. Schattschneider, S. Lazar, M. Stöger-Pollach, S. Löffler, A. Steiger-Thirsfeld, and G. V. Tendeloo, *Atomic scale electron vortices for nanoresearch*, Appl. Phys. Lett. **99**, 203109 (2011).
- [48] P. Schattschneider, M. Stöger-Pollach, and J. Verbeeck, *Novel vortex generator and mode converter for electron beams*, Phys. Rev. Lett. **109**, 084801 (2012).
- [49] J. Verbeeck, H. Tian, and A. Béché, *A new way of producing electron vortex probes for stem*, Ultramicroscopy **113**, 83 (2012), ISSN 0304-3991.
- [50] T. Niermann, J. Verbeeck, and M. Lehmann, *Creating arrays of electron vortices*, Ultramicroscopy **136**, 165 (2014), ISSN 0304-3991.
- [51] V. Grillo, G. C. Gazzadi, E. Karimi, E. Mafakheri, R. W. Boyd, and S. Frabboni, *Highly efficient electron vortex beams generated by nanofabricated phase holograms*, Appl. Phys. Lett. **104**, 043109 (2014).
- [52] V. Grillo, E. Karimi, G. C. Gazzadi, S. Frabboni, M. R. Dennis, and R. W. Boyd, *Generation of nondiffracting electron Bessel beams*, Phys. Rev. X **4**, 011013 (2014).
- [53] V. Grillo, G. C. Gazzadi, E. Mafakheri, S. Frabboni, E. Karimi, and R. W. Boyd, *Holographic generation of highly twisted electron beams*, Phys. Rev. Lett. **114**, 034801 (2015).

- [54] I. P. Ivanov, *Colliding particles carrying nonzero orbital angular momentum*, Phys. Rev. D **83**, 093001 (2011).
- [55] I. P. Ivanov and V. G. Serbo, *Scattering of twisted particles: Extension to wave packets and orbital helicity*, Phys. Rev. A **84**, 033804 (2011).
- [56] I. P. Ivanov, *Measuring the phase of the scattering amplitude with vortex beams*, Phys. Rev. D **85**, 076001 (2012).
- [57] O. Matula, A. G. Hayrapetyan, V. G. Serbo, A. Surzhikov, and S. Fritzsche, *Radiative capture of twisted electrons by bare ions*, New. J. Phys. **16**, 053024 (2014).
- [58] V. G. Serbo, I. P. Ivanov, S. Fritzsche, D. Seipt, and A. Surzhikov, *Scattering of twisted relativistic electrons by atoms*, Phys. Rev. A **92**, 012705 (2015).
- [59] I. P. Ivanov, D. Seipt, A. Surzhikov, and S. Fritzsche, *Elastic scattering of vortex electrons provides direct access to the coulomb phase*, Phys. Rev. D **94**, 076001 (2016).
- [60] P. Schattschneider, S. Löffler, M. Stöger-Pollach, and J. Verbeeck, *Is magnetic chiral dichroism feasible with electron vortices?*, Ultramicroscopy **136**, 81 (2014), ISSN 0304-3991.
- [61] R. Juchtmans, A. Béché, A. Abakumov, M. Batuk, and J. Verbeeck, *Using electron vortex beams to determine chirality of crystals in transmission electron microscopy*, Phys. Rev. B **91**, 094112 (2015).
- [62] R. Juchtmans and J. Verbeeck, *Orbital angular momentum in electron diffraction and its use to determine chiral crystal symmetries*, Phys. Rev. B **92**, 134108 (2015).
- [63] P. Schattschneider, V. Grillo, and D. Aubry, *Spin polarisation with electron Bessel beams*, Ultramicroscopy **176**, 188 (2017), ISSN 0304-3991.
- [64] I. I. Rabi, *Das freie Elektron im homogenen Magnetfeld nach der Diracschen Theorie*, Z. Phys. **49**, 507 (1928), ISSN 0044-3328.
- [65] L. D. Landau and J. M. Lifshitz, *Quantum mechanics (non-relativistic theory)*, vol. 3 of *Course of theoretical physics* (Butterworth-Heinemann, 1991), 3rd ed.
- [66] P. A. M. Dirac, *The quantum theory of the electron*, Proc. R. Soc. Lond. A **117**, 610 (1928).
- [67] E. Hecht, *Optics* (Pearson, 2002), 4th ed.
- [68] Y. Tang and A. E. Cohen, *Optical chirality and its interaction with matter*, Phys. Rev. Lett. **104**, 163901 (2010).
- [69] Y. Tang and A. E. Cohen, *Enhanced enantioselectivity in excitation of chiral molecules by superchiral light*, Science **332**, 333 (2011), ISSN 0036-8075.
- [70] E. Hendry, T. Carpy, J. Johnston, M. Popland, R. V. Michailovski, A. J. Lapthorn, S. M. Kelly, L. D. Barron, N. Gadegaard, and M. Kadowala, *Ultrasensitive detection and characterization of biomolecules using superchiral fields*, Nat. Nanotech. **5**, 783 (2010).
- [71] A. Canaguier-Durand, J. A. Hutchison, C. Genet, and T. W. Ebbesen, *Mechanical separation of chiral dipoles by chiral light*, New J. Phys. **15**, 123037 (2013).
- [72] R. P. Cameron, S. M. Barnett, and A. M. Yao, *Discriminatory optical force for chiral molecules*, New. J. Phys. **16**, 013020 (2014).
- [73] R. P. Cameron, A. M. Yao, and S. M. Barnett, *Diffraction gratings for chiral molecules and their applications*, J. Phys. Chem. A **118**, 3472 (2014).
- [74] M. Born and E. Wolf, *Principles of optics* (Cambridge university press, 1999), 7th ed.
- [75] J. D. Jackson, *Classical electrodynamics* (Wiley, 1998), 3rd ed.
- [76] M. G. Calkin, *An invariance property of the free electromagnetic field*, Am. J. Phys.



- 33**, 958 (1965).
- [77] G. N. Afanasiev and Y. P. Stepanovski, *The helicity of the free electromagnetic field and its physical meaning*, Nuovo Cim. A (1965-1970) **109**, 271 (1996), ISSN 1826-9869.
- [78] J. L. Trueba and A. F. Rañada, *The electromagnetic helicity*, Eur. J. Phys. **17**, 141 (1996).
- [79] R. P. Cameron, S. M. Barnett, and A. M. Yao, *Optical helicity, optical spin and related quantities in electromagnetic theory*, New. J. Phys. **14**, 053050 (2012).
- [80] R. P. Cameron and S. M. Barnett, *Electric-Magnetic symmetry and Noether's theorem*, New. J. Phys. **14**, 123019 (2012).
- [81] K. Y. Bliokh, A. Y. Bekshaev, and F. Nori, *Dual electromagnetism: helicity, spin, momentum and angular momentum*, New. J. Phys. **15**, 033026 (2013).
- [82] L. D. Landau, J. M. Lifshitz, and L. P. Pitajevski, *The classical theory of fields*, vol. 2 of *Course of theoretical physics* (Butterworth Heineman, 1994), 4th ed.
- [83] E. Noether, *Invarianten beliebiger Differentialausdrücke*, Nachr. Gesellschaft Wiss. Gött. **1918**, 37 (1918).
- [84] E. Noether, *Invariante variationsprobleme*, Nachr. Gesellschaft Wiss. Gött. **1918**, 235 (1918).
- [85] L. Woltjer, *A theorem on force-free magnetic fields*, PNAS **44**, 289 (1958).
- [86] A. F. Rañada, *On the magnetic helicity*, Eur. J. Phys. **13**, 70 (1992).
- [87] M. A. Berger, *Introduction to magnetic helicity*, Plas. Phys. Contr. Fusion **41**, B167 (1999).
- [88] G. Nienhuis, *Conservation laws and symmetry transformations on the electromagnetic field with sources*, Phys. Rev. A **93**, 023840 (2016).
- [89] D. J. Griffiths, *Introduction to electrodynamics* (Pearson, 1999), 3rd ed.
- [90] L. D. Landau and J. M. Lifshitz, *Elektrodynamik der Kontinua*, vol. 8 of *Lehrbuch der theoretischen Physik* (Akademie-Verlag Berlin, 1967), 1st ed.
- [91] I. Fernandez-Corbaton, X. Zambrana-Puyalto, N. Tischler, X. Vidal, M. L. Juan, and G. Molina-Terriza, *Electromagnetic duality symmetry and helicity conservation for the macroscopic Maxwell's equations*, Phys. Rev. Lett. **111**, 060401 (2013).
- [92] K. Y. Bliokh, Y. S. Kivshar, and F. Nori, *Magnetolectric effect in local light-matter interaction*, Phys. Rev. Lett. **113**, 033601 (2014).
- [93] B. D. H. Tellegen, , Philips Res. Rept. **3**, 81 (1948).
- [94] I. E. Dzialoshinski, *On the magneto-electrical effect in antiferromagnets*, Sov. Phys. JETP **37**, 881 (1959).
- [95] D. N. Astrov, *The magnetolectric effect in antiferromagnets*, Sov. Phys. JETP **11**, 708 (1960).
- [96] V. J. Folen, G. T. Rado, and E. W. Stalder, *Anisotropy of the magnetolectric effect in  $\text{Cr}_2\text{O}_3$* , Phys. Rev. Lett. **6**, 607 (1961).
- [97] G. T. Rado, *Mechanism of the magnetolectric effect in an antiferromagnet*, Phys. Rev. Lett. **6**, 609 (1961).
- [98] K. Y. Bliokh and F. Nori, *Characterizing optical chirality*, Phys. Rev. A **83**, 021803 (2011).
- [99] R.-L. Chern, *Wave propagation in chiral media: composite Fresnel equations*, J. Opt. **15**, 075702 (2013).
- [100] R. Kronig, B. S. Blaisse, and J. J. van der Sande, *Optical impedance and surface coating*, Appl. Sci. Res. **B1**, 63 (1947).
- [101] L. Silberstein, *Elektromagnetische grundgleichungen in bivectorieller behandlung*,

- Ann. Phys. **327**, 579 (1907), ISSN 1521-3889.
- [102] L. Silberstein, *Quaternionic form of relativity*, Phil. Mag. **23**, 790 (1912).
- [103] I. Bialynicki-Birula and Z. Bialynicka-Birula, *The role of the Riemann-Silberstein vector in classical and quantum theories of electromagnetism*, J. Phys. A. **46**, 053001 (2013).
- [104] J. Dressel, K. Y. Bliokh, and F. Nori, *Spacetime algebra as a powerful tool for electromagnetism*, Phys. Repts. **589**, 1 (2015).
- [105] M. Ricci, N. Orloff, and S. M. Anlage, *Superconducting metamaterials*, Appl. Phys. Lett. **87**, 034102 (2005).
- [106] M. C. Ricci, H. Xu, R. Prozorov, A. P. Zhuravel, A. V. Ustinov, and S. M. Anlage, *Tunability of superconducting metamaterials*, IEEE Trans. Appl. Supercond. **17**, 918 (2007).
- [107] C. Kurter, J. Abrahams, and S. M. Anlage, *Miniaturized superconducting metamaterials for radio frequencies*, Appl. Phys. Lett. **96**, 253504 (2010).
- [108] J. B. Pendry, A. J. Holden, W. J. Stewart, and I. Youngs, *Extremely low frequency plasmons in metallic mesostructures*, Phys. Rev. Lett. **76**, 4773 (1996).
- [109] J. B. Pendry, A. J. Holden, D. J. Robbins, and W. J. Stewart, *Low frequency plasmons in thin-wire structures*, J. Phys. Cond. Mat. **10**, 4785 (1998).
- [110] J. B. Pendry, A. J. Holden, D. J. Robbins, and W. J. Stewart, *Magnetism from conductors and enhanced nonlinear phenomena*, IEEE Trans. Microwave Theor. Techn. **47**, 2075 (1999), ISSN 0018-9480.
- [111] J. B. Pendry, *A chiral route to negative refraction*, Science **306**, 1353 (2004), ISSN 0036-8075.
- [112] D. R. Smith, W. J. Padilla, D. C. Vier, S. C. Nemat-Nasser, and S. Schultz, *Composite medium with simultaneously negative permeability and permittivity*, Phys. Rev. Lett. **84**, 4184 (2000).
- [113] R. A. Shelby, D. R. Smith, S. C. Nemat-Nasser, and S. Schultz, *Microwave transmission through a two-dimensional, isotropic, left-handed metamaterial*, Appl. Phys. Lett. **78**, 489 (2001).
- [114] R. A. Shelby, D. R. Smith, and S. Schultz, *Experimental verification of a negative index of refraction*, Science **292**, 77 (2001), ISSN 0036-8075.
- [115] T. Young, *An account on some cases of the production of colours, not hitherto described*, Phil. Trans. R. Soc **92**, 387 (1802).
- [116] T. Young, *Experiments and calculations relative to physical optics*, Phil. Trans R. Soc **94**, 1 (1804).
- [117] D. F. J. Arago and A. J. Fresnel, *Mémoire sur l'action que les rayons lumière polarisée exercent les uns sur les autres*, Ann. Chim. Phys. (1819).
- [118] R. P. Cameron, S. M. Barnett, and A. M. Yao, *Optical helicity of interfering waves*, J. Mod. opt. **61**, 25 (2013).
- [119] C. Rosales-Guzmán, K. Volke-Sepulveda, and J. P. Torres, *Light with enhanced optical chirality*, Opt. Lett. **37**, 3486 (2012).
- [120] M. Schäferling, X. Yin, and H. Giessen, *Formation of chiral fields in a symmetric environment*, Opt. Express **20**, 26326 (2012).
- [121] M. Schäferling, X. Yin, N. Engheta, and H. Giessen, *Helical plasmonic nanostructures as prototypical chiral near-field sources*, ACS Phot. **1**, 530 (2014).
- [122] X. Tian, Y. Fang, and M. Sun, *Formation of Enhanced Uniform Chiral Fields in Symmetric Dimer Nanostructures*, Sci. Repts. **5**, 17534 (2015).
- [123] M. Schäferling, N. Engheta, H. Giessen, and T. Weiss, *Reducing the complexity:*

- enantioselective chiral near-fields by diagonal slit and mirror configuration*, ACS Phot. **3**, 1076 (2016).
- [124] C. Kramer, M. Schäferling, T. Weiss, H. Giessen, and T. Brixner, *Analytic optimization of near-field optical chirality enhancement*, ACS Phot. **4**, 396 (2017).
- [125] S. K. Mohanty, K. D. Rao, and P. K. Gupta, *Optical trap with spatially varying polarization: application in controlled orientation of birefringent microscopic particle(s)*, Appl. Phys. B **80**, 631 (2005), ISSN 1432-0649.
- [126] G. Cipparrone, I. Ricardez-Vargas, P. Pagliusi, and C. Provenzano, *Polarization gradient: exploring an original route for optical trapping and manipulation*, Opt. Express **18**, 6008 (2010).
- [127] K. Hornberger, S. Gerlich, H. Ulbricht, L. Hackermüller, S. Nimmrichter, I. V. Goldt, O. Botalina, and M. Arndt, *Theory and experimental verification of Kapitza-Dirac-Talbot-Lau interferometry*, New. J. Phys. **11**, 043032 (2009).
- [128] S. Eibenberger, S. Gerlich, M. Arndt, M. Mayor, and J. Tüxen, *Matter-wave interference of particles selected from a molecular library with masses exceeding 10 000 amu*, Phys. Chem. Chem. Phys. **15**, 14696 (2013).
- [129] R. P. Cameron, J. B. Götte, S. M. Barnett, and J. P. Cotter, *Matter-wave grating distinguishing conservative and dissipative interactions*, Phys. Rev. A **94**, 013604 (2016).
- [130] L. Nikolova, T. Todorov, M. Ivanov, F. Andruzzi, S. Hvilsted, and P. Ramanujam, *Photoinduced circular anisotropy in side-chain azobenzene polyesters*, Opt. Mater. **8**, 255 (1997), ISSN 0925-3467.
- [131] L. Nikolova, L. Nedelchev, T. Todorov, T. Petrova, N. Tomova, V. Dragostinova, P. S. Ramanujam, and S. Hvilsted, *Self-induced light polarization rotation in azobenzene-containing polymers*, Appl. Phys. Lett. **77**, 657 (2000).
- [132] G. Iftime, F. L. Labarthe, A. Natansohn, and P. Rochon, *Control of Chirality of an Azobenzene Liquid Crystalline Polymer with Circularly Polarized Light*, J. Am. Chem. Soc **122**, 12646 (2000).
- [133] S.-W. Choi, T. Izumi, Y. Hoshino, Y. Takanishi, K. Ishikawa, J. Watanabe, and H. Takezoe, *Circular-polarization-induced enantiomeric excess in liquid crystals of an achiral, bent-shaped mesogen*, Angew. Chem. Int. Ed. **45**, 1382 (2006), ISSN 1521-3773.
- [134] R. M. Tejedor, L. Oriol, J. L. Serrano, F. Partal Ureña, and J. J. López González, *Photoinduced chiral nematic organization in an achiral glassy nematic azopolymer*, Adv. Funct. Mater. **17**, 3486 (2007), ISSN 1616-3028.
- [135] F. Vera, R. M. Tejedor, P. Romero, J. Barberá, M. B. Ros, J. L. Serrano, and T. Sierra, *Light-driven supramolecular chirality in propeller-like hydrogen-bonded complexes that show columnar mesomorphism*, Angew. Chem. Int. Ed. **46**, 1873 (2007), ISSN 1521-3773.
- [136] J. d. Barrio, R. M. Tejedor, and L. Oriol, *Thermal and light control of the chiral order of azopolymers*, Eur. Polym. J. **48**, 384 (2012), ISSN 0014-3057.
- [137] L. de Vega, S. van Cleuvenbergen, G. Depotter, E. M. García-Frutos, B. Gómez-Lor, A. Omenat, R. M. Tejedor, J. L. Serrano, G. Hennrich, and K. Clays, *Nonlinear optical thin film device from a chiral octopolar phenylacetylene liquid crystal*, J. Org. Chem. **77**, 10891 (2012), PMID: 23126464.
- [138] J. Kim, J. Lee, W. Y. Kim, H. Kim, S. Lee, H. C. Lee, Y. S. Lee, M. Seo, and S. Y. Kim, *Induction and control of supramolecular chirality by light in self-assembled helical nanostructures*, nat. comm. **6**, 6959 (2014).

- [139] G. Martínez-Ponce, C. Solano, R. J. Rodríguez González, L. Larios-López, D. Navarro-Rodríguez, and L. Nikolova, *All-optical switching using supramolecular chiral structures in azopolymers*, *J. Opt. A* **10**, 115006 (2008).
- [140] C. J. Davisson and L. H. Germer, *Reflection of electrons by a crystal of nickel*, *PNAS* **14**, 317 (1928), ISSN 0027-8424.
- [141] G. P. Thomson, *The waves of an electron*, *Nature* **122**, 279 (1928).
- [142] H. Kurz and H. Rauch, *Beugung thermischer neutronen an einem strichgitter*, *Z. Phys. A* **220**, 419 (1969), ISSN 0939-7922.
- [143] W. Bauspiess, U. Bonse, H. Rauch, and W. Treimer, *Test measurements with a perfect crystal neutron interferometer*, *Z. Phys.* **271**, 177 (1974), ISSN 0044-3328.
- [144] A. Zeilinger, R. Gaehler, C. G. Shull, and W. Treimer, *Experimental status and recent results of neutron interference optics*, in *AIP Conference Proceedings* (1982), vol. 89, pp. 93–100.
- [145] O. Carnal and J. Mlynek, *Young's double-slit experiment with atoms: A simple atom interferometer*, *Phys. Rev. Lett.* **66**, 2689 (1991).
- [146] M. Arndt, O. Nairz, J. Vos-Andreae, C. Keller, G. van der Zouw, and A. Zeilinger, *Wave-Particle duality of C60 molecules*, *Nature* **401**, 680 (1999).
- [147] M. R. Andrews, C. G. Townsend, H.-J. Miesner, D. S. Durfee, D. M. Kurn, and W. Ketterle, *Observation of interference between two bose condensates*, *Science* **275**, 637 (1997), ISSN 0036-8075.
- [148] A. Tonomura, J. Endo, T. Matsuda, T. Kawasaki, and H. Ezawa, *Demonstration of single-electron buildup of an interference pattern*, *Am. J. Phys.* **57**, 117 (1989).
- [149] S. Frabboni, A. Gabrielli, G. C. Gazzadi, F. Giorgi, G. Matteucci, G. Pozzi, N. S. Cesari, M. Villa, and A. Zoccoli, *The young-feynman two-slits experiment with single electrons: build-up of the interference pattern and arrival-time distribution using a fast-readout pixel detector*, *Ultramicroscopy* **116**, 73 (2012), ISSN 0304-3991.
- [150] R. Bach, D. Pope, S.-H. Liou, and H. Batelaan, *Controlled double-slit electron diffraction*, *New. J. Phys.* **15**, 033018 (2013).
- [151] T. Juffmann, A. Milic, M. Mülleritsch, P. Asenbaum, A. Tsukernik, J. Tüxen, M. Mayor, O. Cheshnovsky, and M. Arndt, *Real-time single molecule imaging of quantum interference*, *Nat. Nanotech.* **7**, 297 (2012).
- [152] C. W. Clark, R. Barankov, M. G. Huber, M. Arif, D. G. Cory, and D. A. Pushin, *Controlling neutron orbital angular momentum*, *Nature* **525**, 504 (2015).
- [153] K. Y. Bliokh, P. Schattschneider, J. Verbeeck, and F. Nori, *Electron vortex in a magnetic field: a new twist on Landau levels and Aharonov-Bohm states*, *Phys. Rev. X* **2**, 041011 (2012).
- [154] I. P. Ivanov and D. V. Karlovets, *Detecting transition radiation from a magnetic moment*, *Phys. Rev. Lett.* **110**, 264801 (2013).
- [155] A. S. Konkov, A. P. Potylitsyn, and M. S. Polonskaja, *Transition radiation of electrons with a nonzero orbital angular momentum*, *JETP Lett.* **100**, 421 (2014), ISSN 1090-6487.
- [156] K. Y. Bliokh, M. R. Dennis, and F. Nori, *Relativistic electron vortex beams: angular momentum and spin-orbit interaction*, *Phys. Rev. Lett.* **107**, 174802 (2011).
- [157] D. V. Karlovets, *Electron with orbital angular momentum in a strong laser wave*, *Phys. Rev. A* **86**, 062102 (2012).
- [158] R. van Boxem, J. Verbeeck, and B. Partoens, *Spin effects in electron vortex states*, *Europhys. Lett.* **102**, 40010 (2013).
- [159] A. G. Hayrapetyan, O. Matula, A. Aiello, A. Surzhikov, and S. Fritzsche, *Interaction*

- of relativistic electron-vortex beams with few-cycle laser pulses*, Phys. Rev. Lett. **112**, 134801 (2014).
- [160] G. Guzzinati, P. Schattschneider, K. Y. Bliokh, F. Nori, and J. Verbeeck, *Observation of the Larmor and Gouy rotations with electron vortex beams*, Phys. Rev. Lett. **110**, 093601 (2013).
- [161] P. Schattschneider, T. Schachinger, M. Stöger-Pollach, S. Löffler, A. Steiger-Thirsfeld, K. Y. Bliokh, and F. Nori, *Imaging the dynamics of free-electron Landau states*, Nat. Comm. **5**, 4586 (2014).
- [162] C. Greenshields, R. L. Stamps, and S. Franke-Arnold, *Vacuum Faraday effect for electrons*, New J. Phys. **14**, 103040 (2012).
- [163] C. R. Greenshields, S. Franke-Arnold, and R. L. Stamps, *Parallel axis theorem for free-space electron wavefunctions*, New J. Phys. **17**, 093015 (2015).
- [164] G. Nienhuis, *Doppler effect induced by rotating lenses*, Opt. Comm. **132**, 8 (1996).
- [165] S. Franke-Arnold, G. Gibson, R. W. Boyd, and M. J. Padgett, *Rotary photon drag enhanced by a slow-light medium*, Science **333**, 65 (2011), ISSN 0036-8075.
- [166] J. M. Lifshitz, L. P. Pitajevski, and W. B. Berestetskii, *Quantenelektrodynamik*, vol. 4 of *Lehrbuch der Theoretischen Physik* (Harri Deutsch, 1991), 7th ed.
- [167] L. S. Brown and G. Gabrielse, *Precision spectroscopy of a charged particle in an imperfect penning trap*, Phys. Rev. A **25**, 2423 (1982).
- [168] D. Hanneke, S. Fogwell Hoogerheide, and G. Gabrielse, *Cavity control of a single-electron quantum cyclotron: Measuring the electron magnetic moment*, Phys. Rev. A **83**, 052122 (2011).
- [169] E. Karimi, L. Marrucci, V. Grillo, and E. Santamato, *Spin-to-orbital angular momentum conversion and spin-polarization filtering in electron beams*, Phys. Rev. Lett. **108**, 044801 (2012).
- [170] J. Nsofini, D. Sarenac, C. J. Wood, D. G. Cory, M. Arif, C. W. Clark, M. G. Huber, and D. A. Pushin, *Spin-orbit states of neutron wave packets*, Phys. Rev. A **94**, 013605 (2016).
- [171] M. M. Dellweg and C. Müller, *Controlling electron spin dynamics in bichromatic Kapitza-Dirac scattering by the laser field polarization*, Phys. Rev. A **95**, 042124 (2017).
- [172] M. M. Dellweg and C. Müller, *Spin-polarizing interferometric beam splitter for free electrons*, Phys. Rev. Lett. **118**, 070403 (2017).
- [173] H. C. Ohanian, *What is spin?*, Am. J. Phys. **54**, 500 (1986).
- [174] K. Y. Bliokh and F. Nori, *Transverse spin of a surface polariton*, Phys. Rev. A **85**, 061801 (2012).
- [175] K. Y. Bliokh, A. Y. Bekshaev, and F. Nori, *Extraordinary momentum and spin in evanescent waves*, Nat. Comm. **5**, 3300 (2014).
- [176] A. Y. Bekshaev, K. Y. Bliokh, and F. Nori, *Transverse spin and momentum in two wave interference*, Phys. Rev. X **5**, 011039 (2015).
- [177] M. Neugebauer, T. Bauer, A. Aiello, and P. Banzer, *Measuring the transverse spin density of light*, Phys. Rev. Lett. **114**, 063901 (2015).
- [178] M. Antognozzi, C. R. Berminham, R. I. Harniman, S. Simpson, J. Senior, R. Hayward, H. Hoerber, M. R. Dennis, Y. Bekshaev, Alexandr, K. Y. Bliokh, et al., *Direct measurements of the extraordinary optical momentum and transverse spin-dependent force using a nano-cantilever*, Nat. Phys. **12**, 731 (2016).
- [179] F. L. Kien and K. Hakuta, *Cooperative enhancement of channeling emission from atoms into a nanofiber*, Phys. Rev. A **77**, 013801 (2008).

- [180] F. L. Kien and A. Rauschenbeutel, *Anisotropy in scattering of light from an atom into the guided modes of a nanofiber*, Phys. Rev. A **90**, 023805 (2014).
- [181] C. Junge, D. O'Shea, J. Volz, and A. Rauschenbeutel, *Strong coupling between single atoms and nontransversal photons*, Phys. Rev. Lett. **110**, 213604 (2013).
- [182] J. Petersen, J. Volz, and A. Rauschenbeutel, *Chiral nanophotonic waveguide interface based on spin-orbit interaction of light*, Science **346**, 67 (2014), ISSN 0036-8075.
- [183] R. Mitsch, C. Sayrin, B. Albrecht, P. Schneeweiß, and A. Rauschenbeutel, *Quantum state-controlled directional spontaneous emission of photons into a nanophotonic waveguide*, Nat. Comm. **5**, 5713 (2014).
- [184] C. Sayrin, C. Junge, R. Mitsch, B. Albrecht, D. O'Shea, P. Schneeweiss, J. Volz, and A. Rauschenbeutel, *Nanophotonic optical isolator controlled by the internal state of cold atoms*, Phys. Rev. X **5**, 041036 (2015).
- [185] T. Ramos, H. Pichler, A. J. Daley, and P. Zoller, *Quantum spin dimers from chiral dissipation in cold-atom chains*, Phys. Rev. Lett. **113**, 237203 (2014).
- [186] H. Pichler, T. Ramos, A. J. Daley, and P. Zoller, *Quantum optics of chiral spin networks*, Phys. Rev. A **91**, 042116 (2015).
- [187] T. Ramos, B. Vermersch, P. Hauke, H. Pichler, and P. Zoller, *Non-markovian dynamics in chiral quantum networks with spins and photons*, Phys. Rev. A **93**, 062104 (2016).
- [188] B. Vermersch, T. Ramos, P. Hauke, and P. Zoller, *Implementation of chiral quantum optics with Rydberg and trapped-ion setups*, Phys. Rev. A **93**, 063830 (2016).
- [189] I. Söllner, S. Mahmoodian, S. L. Hansen, L. Lidolo, A. Javadi, G. Kirsanske, T. Pregolato, H. El-Ella, E. H. Lee, J. D. Song, et al., *Deterministic photon-emitter coupling in chiral photonic circuits*, Nat. Nanotech. **10**, 775 (2015).
- [190] W. Gordon, *Der strom der Diracschen elektronentheorie*, Z. Phys. **50**, 630 (1928), ISSN 0044-3328.
- [191] J. Leach, M. J. Padgett, S. M. Barnett, S. Franke-Arnold, and J. Courtial, *Measuring the orbital angular momentum of a single photon*, Phys. Rev. Lett. **88**, 257901 (2002).
- [192] L. S. Brown and T. W. B. Kibble, *Interaction of intense laser beams with electrons*, Phys. Rev. **133**, A705 (1964).
- [193] T. W. B. Kibble, *Frequency shift in high-intensity compton scattering*, Phys. Rev. **138**, B740 (1965).
- [194] T. W. B. Kibble, *Mutual refraction of electrons and photons*, Phys. Rev. **150**, 1060 (1966).
- [195] L. M. Frantz, *Compton scattering of an intense photon beam*, Phys. Rev. **139**, B1326 (1965).
- [196] F. Sauter, *Über das verhalten eines elektrons im homogenen elektrischen feld nach der relativistischen theorie diracs*, Z. Phys. **69**, 742 (1931), ISSN 0044-3328.
- [197] J. Schwinger, *On gauge invariance and vacuum polarization*, Phys. Rev. **82**, 664 (1951).
- [198] A. I. Nikishov, *Pair production by a constant external field*, Zh. Eksp. Teor. Fiz. **57**, 1210 (1969).
- [199] N. B. Narozhnyi and A. I. Nikishov, *Solutions of the klein-gordon and dirac equations for a particle in a constant electric field and a plane electromagnetic wave propagating along the field*, Theor. Math. Phys. **26**, 9 (1976), ISSN 1573-9333.
- [200] H. Herold, *Compton and Thomson scattering in strong magnetic fields*, Phys. Rev.

- D **19**, 2868 (1979).
- [201] V. Ritus, *Quantum effects of the interaction of elementary particles with an intense electromagnetic field*, J. Sov. Laser Res. **6**, 497 (1985).
- [202] F. Mackenroth and A. Di Piazza, *Nonlinear Compton scattering in ultrashort laser pulses*, Phys. Rev. A **83**, 032106 (2011).
- [203] C. Bamber, S. J. Boege, T. Koffas, T. Kotseroglou, A. C. Melissinos, D. D. Meyerhofer, D. A. Reis, W. Ragg, C. Bula, K. T. McDonald, et al., *Studies of nonlinear QED in collisions of 46.6 GeV electrons with intense laser pulses*, Phys. Rev. D **60**, 092004 (1999).
- [204] S. Sturm, A. Wagner, M. Kretschmar, W. Quint, G. Werth, and K. Blaum, *g-factor measurement of hydrogenlike  $^{28}\text{Si}^{13+}$  as a challenge to QED calculations*, Phys. Rev. A **87**, 030501 (2013).
- [205] A. Minguzzi, *Non-linear effects in the vacuum polarization*, Nuovo. Cim. **4**, 476 (1956), ISSN 1827-6121.
- [206] D. Constantinescu, *Vacuum polarization in magnetic field*, Nucl. Phys. B **36**, 121 (1972), ISSN 0550-3213.
- [207] D. Constantinescu, *Electron self-energy in a magnetic field*, Nucl. Phys. B **44**, 288 (1972), ISSN 0550-3213.
- [208] A. J. Parle, *Quantum Electrodynamics in Strong Magnetic Fields. IV. Electron Self-energy*, Aust. J. Phys. **40**, 1 (1987).
- [209] R. Geprägs, H. Riffert, H. Herold, H. Ruder, and G. Wunner, *Electron self-energy in a homogeneous magnetic field*, Phys. Rev. D **49**, 5582 (1994).
- [210] M. Neuman, *The radiation of a high energy electron in a constant magnetic field*, Phys. Rev. **90**, 682 (1953).
- [211] A. A. Sokolov and I. M. Ternov, *on polarization effects in the radiation of an accelerated electron*, JETP **4**, 396 (1957).
- [212] A. A. Sokolov and I. M. Ternov, *On polarization and spin effects in the theory of synchrotron radiation*, Sov. Phys. Dokl **8**, 1203 (1964).
- [213] H. Herold, H. Ruder, and G. Wunner, *Cyclotron emission in strongly magnetized plasmas*, Astron. Astrophys. **115**, 90 (1982).
- [214] M. G. Baring, P. L. Gonthier, and A. K. Harding, *Spin-dependent cyclotron decay rates in strong magnetic fields*, Astrophys. J. **630**, 430 (2005).
- [215] Z. Léczy, I. V. Konopolev, A. Serji, and A. Andrejev, *GigaGauss solenoidal magnetic field inside bubbles excited in under-dense plasma*, Sci. Repts. **6**, 36139 (2016).
- [216] D. J. Stark, T. Toncian, and A. V. Arefiev, *Enhanced multi-MeV photon emission by a laser-driven electron beam in a self-generated magnetic field*, Phys. Rev. Lett. **116**, 185003 (2016).
- [217] J. R. Sims, D. G. Rickel, C. A. Swenson, J. B. Schillig, G. W. Ellis, and C. N. Ammerman, *Assembly, commissioning and operation of the nfmfl 100 tesla multipulse magnet system*, IEEE Trans. Appl. Supercond. **18**, 587 (2008), ISSN 1051-8223.
- [218] B. Paczynskiy, *GB 790305 as a very strongly magnetized neutron star*, Act. Astr. **42**, 145 (1992).
- [219] C. Thompson and R. C. Duncan, *The soft gamma repeaters as very strongly magnetized neutron stars - i. radiative mechanism for outbursts*, Mon. Not. R. Astr. Soc. **275**, 255 (1995).
- [220] C. Thompson and R. C. Duncan, *The soft gamma repeaters as very strongly magnetized neutron stars. ii. quiescent neutrino, x-ray, and Alfvén wave emission*, Astro-

- phys. J. **473**, 322 (1996).
- [221] G. Vasisht and E. V. Gotthelf, *The discovery of an anomalous x-ray pulsar in the supernova remnant kes 73*, *Astrophys. J. Lett.* **486**, L129 (1997).
- [222] C. Kouveliotou, S. Dieters, T. Strohmayer, J. van Paradijs, G. J. Fishman, C. A. Meegan, K. Hurley, J. Kommers, I. Smith, D. Frail, et al., *An X-ray pulsar with a superstrong magnetic field in the soft gamma-ray repeater SGR1806 - 20*, *Nature* **393**, 295 (1998).
- [223] W. H. Furry, *On bound states and scattering in positron theory*, *Phys. Rev.* **81**, 115 (1951).
- [224] D. B. Melrose and A. J. Parle, *quantum electrodynamics in strong magnetic fields I electron states*, *Aust. J. Phys* **36**, 755 (1983).
- [225] F. Mackenroth, N. Neitz, and A. D. Piazza, *Novel aspects of radiation reaction in the ultrarelativistic quantum regime*, *Plasma Phys. Contr. Fusion* **55**, 124018 (2013).
- [226] A. Angioi, F. Mackenroth, and A. Di Piazza, *Nonlinear single compton scattering of an electron wave packet*, *Phys. Rev. A* **93**, 052102 (2016).
- [227] V. A. Zaytsev, V. G. Serbo, and V. M. Shabajev, *Radiative recombination of twisted electrons with bare nuclei: Going beyond the born approximation*, *Phys. Rev. A* **95**, 012702 (2017).
- [228] M. E. Peskin and D. V. Schroeder, *An introduction to quantum field theory* (Westview press, 1995).
- [229] S. N. Gupta, *Theory of longitudinal photons in quantum electrodynamics*, *Proc. Phys. Soc.* **63**, 681 (1950).
- [230] R. Loudon, *The Quantum theory of light* (Oxford niversity press, 2000), 3rd ed.
- [231] S. M. Barnett and M. V. Berry, *Superweak momentum transfer near optical vortices*, *J. Opt.* **15**, 125701 (2013).
- [232] P. H. van Cittert, *Die wahrscheinliche Schwingungsverteilung in einer von einer Lichtquelle direkt oder mittels einer Linse beleuchteten Ebene*, *Physica* **1**, 201 (1934).
- [233] F. Zernike, *The concept of degree of coherence and its application to optical problems*, *Physica* **5**, 785 (1938), ISSN 0031-8914.
- [234] A. A. Michelson, *On the application of interference methods to astronomical measurements*, *Phil. Mag.* **30**, 1 (1890).
- [235] A. A. Michelson and F. G. Pease, *Measurement of the diameter of alpha orionis with the interferometer*, *Astrophys. J.* **53**, 429 (1921).
- [236] A. N. Kolmogorov, *The Local Structure of Turbulence in Incompressible Viscous Fluid for Very Large Reynolds Numbers*, *Dokl. Akad. Nauk SSSR* **30** (1941).
- [237] A. N. Kolmogorov, *Dissipation of Energy in the Locally Isotropic Turbulence*, *Dokl. Akad. Nauk. SSSR* **32** (1941).
- [238] D. L. Fried, *Statistics of a geometric representation of wavefront distortion*, *J. Opt. Soc. Am.* **55**, 1427 (1965).
- [239] D. L. Fried, *Optical resolution through a randomly inhomogeneous medium for very long and very short exposures*, *J. Opt. Soc. Am.* **56**, 1372 (1966).
- [240] K. F. Riley, M. P. Hobson, and S. J. Bence, *Mathematical methods for physics and engineering* (Cambridge university press, 2006), 3rd ed.
- [241] I. S. Gradshteyn and I. M. Ryzhik, *Table of integrals, series and products* (Elsevier, 2007), 7th ed.
- [242] M. W. Beijersbergen, L. Allen, H. E. L. O. van der Veen, and J. P. Woerdman, *Astigmatic laser mode converters and transfer of orbital angular momentum*, *Opt.*



- Comm. **96**, 123 (1993).  
[243] D. J. Griffiths, *Introduction to elementary particles* (Wiley, 2008), 2nd ed.